Robust Eye Coding Mechanisms in Humans during Face Detection

Fei Yi

Submitted in fulfillment of the requirements for the
Degree of Doctor of Philosophy

July 2018

School of Psychology
Institute of Neuroscience and Psychology
College of Medical, Veterinary and Life Sciences
University of Glasgow

Summary

We can detect faces more rapidly and efficiently compared to non-face object categories (Bell et al., 2008; Crouzet, 2011), even when only partial information is visible (Tang et al., 2014).

Face inversion impairs our ability to recognise faces. The key to understand this effect is to determine what special face features are processed and how coding of these features is affected by face inversion. Previous studies from our lab showed coding of the contralateral eye in an upright face detection task, which was maximal around the N170 recorded at posterior-lateral electrodes (Ince et al., 2016b; Rousselet et al., 2014). In chapter 2, we used the Bubble technique to determine whether brain responses also reflect the processing of eyes in inverted faces and how it does so in a simple face detection task. The results suggest that in upright and inverted faces alike the N170 reflects coding of the contralateral eye, but face inversion quantitatively weakens the early processing of the contralateral eye, specifically in the transition between the P1 and the N170 and delays this local feature coding.

Group and individual results support this claim. First, regardless of face orientation, the N170 coded the eyes contralateral to the posterior-lateral electrodes, which was the case in all participants. Second, face inversion delayed coding of contralateral eye information. Third, time course analysis of contralateral eye coding revealed weaker contralateral eye coding for inverted compared to upright faces in the transition between the P1 and the N170. Fourth, single-trial EEG responses were driven by the corresponding single-trial visibility of the left eye. The N170 amplitude was larger and latency shorter as the left eye visibility increased in upright and upside-down faces for the majority of participants.

However, for images of faces, eye position and face orientation were confounded, i.e., the upper visual field usually contains eyes in upright faces; in upside-down faces lower visual field contains eyes. Thus, the impaired processing of the contralateral eye by inversion might be simply attributed to that face inversion removes the eyes away from upper visual filed.

In chapter 3, we manipulated three vertical locations of images in which eyes are presented in upper, centre and lower visual field relative to fixation cross (the centre of the screen) so that in upright and inverted faces the eyes can shift from the upper to the lower visual field. We used the similar technique as in chapter 2 during a face detection task. First, we found

that regardless of face orientation and position, the modulations of ERPs recorded at the posterior-lateral electrodes were associated with the contralateral eye. This suggests that coding of the contralateral eye underlying the N170. Second, face inversion delayed processing of the contralateral eye when the eyes of faces were presented in the same position, *Above*, *Below* or at the *Centre* of the screen. Also, in the early N170, most of our participants showed weakened contralateral eye sensitivity by inversion of faces, of which the eyes appeared in the same position. The results suggest that face inversion related changes in processing of the contralateral eye cannot be simply considered as the results of differences of eye position.

The scan-paths traced by human eye movements are similar to the low-level computation saliency maps produced by contrast based computer vision algorithms (Itti et al., 1998). This evidence leads us to a question of whether the coding function to encode the eyes is due to the significance in the eye regions. In chapter 4, we aim to answer the question. We introduced two altered version of original faces: normalised and reversed contrast faces in a face detection task - removing eye saliency (Simoncelli and Olshausen, 2001) and reversing face contrast polarity (Gilad et al., 2009) in a simple face detection task. In each face condition, we observed ERPs, that recorded at contralateral posterior lateral electrodes, were sensitive to eye regions. Both contrast manipulations delayed and reduced eye sensitivity during the rising part of the N170, roughly 120 – 160 ms post-stimulus onset. Also, there were no such differences between two contrast-manipulated faces. These results were observed in the majority of participants. They suggest that the processing of contralateral eye is due partially to low-level factors and may reflect feature processing in the early N170.

Table of Contents

Table of Figures

Acknowledgement

First and foremost, I would like to thank my supervisors, Dr Guillaume Rousselet, for patient guidance and advice he has provided throughout my PhD study and for teaching me to critically think. I would never have been able to finish my thesis without enormous knowledge, enthusiasm he shared with me.

Thanks also to Prof. Philippe Schyns for insightful comments, Dr Robin Ince for sharing his immense technical knowledge, Hannah for sharing tough and fun times with me, Vicky and Michalina for help with data collection.

To Kasia and Chaona, thank you for all you have done for me. Words cannot express my appreciation. Without your kindness and help I cannot imagine how my life would be.

Special thanks should go to my family and best friends, Weijun, for his trust, patience, knowledge and love.

Finally, I would like to thank China Scholarship Council (CSC) for providing the financial support for my PhD study.

List of Publications

Yi, F., Jaworska, K., Ince, R.A.A., Schyns, P.G., & Rousselet, G.A. (in prep). Face inversion does not affect the information content coded during N170. Manuscript in preparation

Yi, F., Nicholls V., Jakubczak M., Ince, R.A.A., Schyns, P.G., & Rousselet, G.A. (in prep). Low Eye Saliency and Contrast Polarity Reversal Impair Contralateral Eye Coding In A Face Detection Task. Manuscript in preparation

Ma, R., Jia, H., **Yi, F.**, Ming, Q., Wang, X., Gao, Y., ... & Yao, S. (2016). Electrophysiological responses of feedback processing are modulated by MAOA genotype in healthy male adolescents. Neuroscience letters, 610, 144-149.

Chapter 1: Introduction

Faces contain invariant structural information with two eyes positioned above nose and mouth, and changeable information that can convey emotion and direct attention. Detecting a face in a scene and assess this face's identity, emotion, sex, age, and several other characteristics are easy and essential daily tasks. The brain contains specialized cells and network that support face processing.

Core network in face processing (human)

In classical distributed face model, the processing of the static and dynamic face information occurs in two separate but interacting pathways, ventral and dorsal streams (Freiwald et al., 2016; Turk-Browne et al., 2010). ventral pathway includes the lateral surface of the inferior occipital gyrus (occipital face area, OFA), the middle fusiform gyrus (fusiform face area, FFA). The dorsal core system resides in the posterior section of the superior temporal sulcus (pSTS). The three regions form the core system of face processing, all of which exhibit preferences for faces over non-face objects (for a review, see Haxby et al., 2000).

Previous evidence from transcranial magnetic stimulation (TMS, Pitcher et al., 2014, 2007) and intracerebral electrical stimulation (Jonas et al., 2014) has revealed a causal role of the OFA in face recognition. The function of the OFA has been investigated by a series of fMRI and TMS studies, showing that OFA is highly involved in the processing of local properties of face, especially eye features (Arcurio et al., 2012; Liu et al., 2010 for fMRI studies; Pitcher et al., 2011, 2009, 2007 for TMS studies). For example, Arcurio et al. (2012) reported that the OFA responses more to a single face part than combinations of at least two face parts. In addition to the feature-based analysis, the OFA is also sensitive to the physical properties of faces (Rotshtein et al., 2005; Tanskanen et al., 2005) and position (Hemond et al., 2007; Schwarzlose et al., 2008; Kay et al., 2015).

The FFA is also activated specifically by faces, which is supported by a number of fMRI studies. Additionally, an intracranial electrophysiological study has reported a causal link between face selective neural responses of the FFA and face perception (Parvizi et al., 2012). However, the debate that concerns domain-specificity of the FFA is still on. Previous evidence has revealed that the activity of the FFA is also selective to non-face

objects (Gauthier, 2000; Hanson and Schmidt, 2011; Haxby et al., 2001) and that adaptation to nonfaces in this area (Dricot et al., 2008; Schiltz and Rossion, 2006), but because this evidence comes from fMRI data with limited spatial resolution, it is possible that some cells in the fMRI-defined FFA may not be face-selective. The functional roles of the FFA have also received much debate. For instance, the FFA preferentially represent the invariant aspects of faces, including identity and gender (Duchaine and Yovel, 2015; Grill-Spector et al., 2004; for a review, see Duchaine and Yovel, 2015), but may also contribute to the processing of changeable information such as expression (for a review, see Bernstein and Yovel, 2015). Past studies have reported that the FFA is not activated by the low-level stimulus features usually present in faces (Rotshtein et al., 2005). However, Rossion et al. (2012) reported larger FFA response to scrambled faces than scrambled cars, suggesting FFA face-sensitivity may be partly accounted for by low-level visual cues (amplitude spectrum and colour). Although the FFA is believed to involve in face configural processing (Kanwisher and Yovel, 2006; Liu et al., 2010; Parvizi et al., 2012), several studies have also reported that the FFA is sensitive to both whole faces and face components (Harris and Aguirre, 2010; Tong et al., 2000; Arcurio et al. 2012).

The pSTS is thought to involve in representing dynamic changes in the faces that are important for social interactions, such as expression, eye-gaze (Baseler et al., 2014; Engell and Haxby, 2007; Harris et al., 2012, 2014).

According to the hierarchical model, the OFA is the first stage of hierarchical face network that receives inputs from the retinotopic cortex (Pitcher et al., 2011b, 2014). This most posterior ventral area, the OFA, represents single part of a face and shows less invariance to position than the FFA. After receiving inputs from the OFA, The two downstream regions the FFA and the pSTS further analyses faces (Pitcher 2014). The FFA and the pSTS process a wide range of features for face identity and ongoing social interactions. Thus, the face system along a posterior-anterior axis analyzes face properties in a series of stages in which increasing complexity of stimulus features are processed (DiCarlo and Cox, 2007, Haxby et al., 2000).

However the hierarchical view is contrast to results from several patients that indicated multiple pathways into the face system (Delvenne et al., 2004; Gschwind et al., 2012; Rossion, 2009; Sorger et al., 2007; Steeves et al., 2006; Weiner et al., 2016; Yang et al., 2016). For instance, Weiner et al. (2016) measured the face network before and after a surgical resection of the IOG/OFA in a patient. They found that after the resection of the IOG, downstream regions remained functionally intact. Additionally, there are multiple

white matter connections from retinotopic regions to the face-selective regions including FG and STS, suggesting that these connections served as alternate routes may contribute to the resiliency of the face network after resection.

Timing of activity in face-selective regions

Of crucial importance is to determine the timing of neural activation in the three distinct face-selective regions. The timing of face-specific brain processes has been investigated through many studies using TMS, Electroencephalography (EEG) and fMRI combined, Magnetoencephalography (MEG), as well as in intracranial recordings. Approximately 100 ms and 170 ms are thought to be the important periods of neural activation in the three distinct brain regions that contribute to face processing.

Two TMS studies reported that accuracy was selectively dropped when pulse was delivered to the OFA 60 and 100 ms after stimulus onset (Pitcher et al., 2007, 2008). A later study more precisely identified the timing of face-selective activity in the OFA by using pulse pairs that were separated by only 10 ms (Pitcher et al., 2012). They found that TMS to the OFA disrupted face performance at 100/110 ms rather than the neighbouring time windows. Studies using correlations between EEG and BOLD signals suggest activity in the fusiform gyrus (Horovitz et al., 2004) and STS (Nguyen and Cunnington, 2014) correlated with neural activity measured at 170 ms after stimulus onset. A study with acquired prosopagnosia patients reported that both right FFA and STS might be necessary to generate the face-sensitive neural activity at 170 ms (Prieto, 2011). In addition, a simultaneous EEG-fMRI study found that face selectivity in the OFA was correlated with the EEG response at 110 ms and high correlations between face selectivity measured with EEG at 170 ms and BOLD activity related to faces in the FFA and pSTS (Sadeh et al., 2010). However, fMRI does not measure direct sources of brain activity. Intracerebral recordings of electrophysiological responses can provide more information for localising the generators of electrical currents. An intracerebral study with depth electrodes supports right OFA contribution as a source of the N170 recorded on the scalp (Jonas et al., 2012). Thus, it has been suggested that the face preferential N170 is not a marker of a single cortical component alone, but the product of an integrated activity from core face-network, the OFA, the FFA and pSTS (Dalrymple et al., 2011).

Eye coding

In human faces, eyes are inherently more salient compared to other parts of the face, on the basis of the physical properties of faces (i.e. contrast). Visual attention is directed to regions of natural scenes which are of higher significance (Parkhurst, Law, & Niebur, 2002). The scan-paths traced by human eye movements are similar to the low-level computation saliency maps produced by the contrast based computer vision algorithms (Itti et al., 1998). Eye tracking studies revealed that the initial fixation is directed to or close to the eye regions across task (Arizpe et al., 2012; Peterson and Eckstein, 2012). In fact, after the first one or two fixations face identification performance saturates (Hsiao & Cottrell, 2008). The preference for the eye regions has been replicated robustly across studies using reverse correlation (Gaspar, Bennett, & Sekuler, 2008; Sekuler et al., 2004) and Bubble technique (Schyns et al., 2002). This preference is also seen in infants (Oakes and Ellis, 2013) (Haith, Bergman, & Moore, 1977), with an ability to detect eyes and gaze direction in faces (Batki et al., 2000; Farroni et al., 2002). Gathering information around the eye regions approaches optimality for face recognition across common face-related tasks (Peterson and Eckstein, 2012), but, this capability is impaired in acquired prosopagnosic patients (Bukach et al., 2008; Caldara et al., 2005; Rossion et al., 2009) and in Autism Spectrum Disorder (Jones et al., 2008).

Neurophysiological studies step further by shedding light on how the human visual system transformed the visual information including the eyes. They revealed that face encoding starts with processing of the eyes, and followed the integration of task-relevant features (for a review, see Schyns et al., 2009). In their experiments, during a face detection or a discrimination task, the images of faces appearing one at a time on the screen are sampled with randomly Gaussian apertures. Since randomly sampling the input image changes the visibility of local information, they determined how the visibility of this information affected measurements of brain activity (Ince et al., 2016b). A series of studies consistently reported that regardless of the task the information about the contralateral eye is associated with the single-trial EEG activity in the N170 time window (Ince et al., 2016b; Rousselet et al., 2014; Schyns et al., 2011, 2007, 2003, Smith et al., 2007, 2004) In the same window, brain activity is also sensitive to other diagnostic features, for instance the smiling mouth to categorise ‘happy’ faces (Schyns et al., 2007; Smith et al., 2004, 2007). Further, the information integration follows a default order that scans from the eyes downward to task-related information.

Growing fMRI and TMS studies also found that the feature-based analysis was processed in OFA (Arcurio et al., 2012; Pitcher et al., 2007, 2009, 2011a). In addition, a MEG study

showing that sensitivity to face parts including eye regions occurred in lateral cortical areas in the time window of the M170 (Smith et al., 2009).

The feature-based coding has also been found in monkey studies. Nonhuman primates studies demonstrated that inferior temporal (IT) cortex neurons were sensitive to object parts that are diagnostic for behaviours (Kovács et al., 1995; Sigala and Logothetis 2002). Nielsen et al., (2006) further examined that those diagnostic object parts are first encoded in posterior IT cortex. For face detection, early responses in monkey most posterior face patch (PL) were strongly driven by the presence of the contralateral eye in the early response window, 60 – 100 ms following image onset (Issa and DiCarlo 2012). They also found that the early PL responses (0 – 40 ms after response onset) to the combinations of face features were well matched to the linear sum of the responses to the individual features. Their results suggested independent processing of local feature in the initial steps of face processing, which argues against holistic face processing (Maurer et al., 2002). While the homologies between monkey and human face processing systems are unclear, the occipital face area (OFA), the earliest face selective region, could be comparable with the monkey posterior lateral patches (Yovel and Freiwald, 2013). Those studies consistently pointed to that faces are analyzed in the occipito-temporal direction, which starts with local feature coding.

Methods

In visual research, behavioural responses are the outputs of a series stage of processing spanning from visual inputs filtered in the retina to motor execution controlled by neural impulses. But the processing stages at which visual cortex encodes the visual inputs is fleeting and still elusive.

Scalp EEG

The visual perceptual processes can be continuously sampled as a discrete set of voltage by the scalp electroencephalogram (EEG). To avoid misinterpretation of ERP data, it's important to understand what the EEG measures.

Scalp EEG records the summed activity in a large population of cortical neurons, by placing non-invasive electrodes along the scalp (Lopes da Silva, 2010, for reviews). There are two main types of electrical activity produced by neurons, action potentials and postsynaptic potentials (Luck, 2005). No single brain-imaging technique can record most of the events in the brain, so dose EEG (Cohen, 2014). Because of the timing of the action

potentials and the physical arrangement of axons, action potentials are too fast to sum up to produce measurable EEG signal. Thus, there is general agreement on the primary source of the EEG signal: the summation of excitatory and inhibitory postsynaptic potentials in pyramidal neurons of the cortex are thought to produce the most EEG signal.

Depending on the synapse and neurotransmitter involved, postsynaptic potential can be excitatory or inhibitory. When an excitatory neurotransmitter is released from the presynaptic terminals at the apical dendrite, a negative extracellular voltage is yielded near the apical dendrites, and a net positivity is created near the cell body and basal dendrites. This situation is referred to as a dipole. If the postsynaptic potential is inhibitory, this reverses the polarity (Luck, 2005; Jackson and Bolger, 2014)

EEG recordings are sensitive to dipoles that are perpendicular or parallel to the surface of the head. However, an electrode can only detect dipoles when the electrode is closer to either the positive or negative end of the dipole. If an electrode is equidistant from the positive and negative end of the dipole, the electrode will measure a net neutral (Ahlfors et al., 2010).

A single dipole is too small to be recorded from a scalp electrode. To produce measurable activity on the scalp, the following conditions must be met: thousands, or even millions, of neurons must be arranged in a parallel fashion, active at the same time and most of them have the same direction of current flow to avoid canceling each other out. In addition, because the strength of voltage field gradients drop off rapidly with distance, activity from deep brain structures is difficult to detect by scalp EEG. Altogether, EEG is a high-temporal-resolution technique but with low spatial resolution.

Bubble technique

With a very high temporal resolution, non-invasively scalp EEG can precisely track the time course of task-related neural activity. Then, what information modulates brain activity? And how is visual information transformed by the visual system that operates en route to recognition? To solve these issues, understanding a detailed relationship between input information content and behaviour and ERP modulations is a necessary prerequisite (Schyns et al., 2009).

Gosselin and Schyns (2001) developed a variant of reverse correlation methods, which is called Bubbles. This method manipulates the visibility of the selected regions through randomly Gaussian apertures on images. In the region of interest (i.e. face oval in our case), the location of all Bubbles changes randomly across trials. Thus, it is criticized by

Murray and Gold, (2004). They suggest that strategies observers used with a few small pieces of the stimulus might differ from when the whole stimulus is presented. Under natural viewing conditions, for example, faces are perceived as a whole, but processing is forced to be featural when using the Bubble method (Macke and Wichmann, 2010; Neath and Itier, 2013).

However, because of limited viewing angles, low luminosity, occlusion, visual inputs is not always complete under natural viewing conditions (Gosselin and Schyns, 2004; Sekuler et al., 2000; Tang et al., 2014). Behavioural (Sekuler et al., 2000) and human intracranial studies (Tang et al., 2017, 2014) suggested that partly occluded objects seems to be effectively treated as functionally complete by the visual system, although recognition of occluded objects require additional time compared to the whole counterparts. Additionally, observers' strategies were similar on expression and gender discrimination tasks compared with reverse correlation technique using Gaussian white noise (Gosselin and Schyns, 2004). Altogether, Bubble technique has proven to be an effective method to tease out specific stimuli content that associated responses and is widely used in fMRI, EEG, MEG, and monkey studies (Schyns et al., 2007; Schyns et al., 2009; (van Rijsbergen and Schyns, 2009; Issa and DiCarlo, 2012; Smith et al., 2009).

Information theoretic analyses

Since randomly manipulating the characteristic of each pixel in stimuli leads to a vector that is Gaussian distribution, we can use information theoretic analyses (Ince et al., 2016a, 2016b; Rousselet et al., 2014) to an un-biasedly estimate of each pixel's importance in driving behaviour responses and ERP. Bubble technique coupled with information theoretic analyses can translate the measurements of brain activity into the successive information processing states (Schyns et al., 2009).

Given two random variables X and Y, the amount of uncertainty in X that is reduced by knowing Y is the mutual information (MI). It thus can be used to quantify reduction in the uncertainty about the responses after stimuli were observed. For example, imagine two people John and Bob living in Norway and UK. John works whenever it is not raining strongly as a fish man. Bob works no matter what the weather is like as a writer. Bob's actions give no weather information in the UK. But John's actions and the weather in Norway are both random and correlated. John's behaviour gives information about the weather in Norway. The uncertainty could be removed from the weather in Norway by knowing John's actions. But the uncertainty of weather in the UK is kept when knowing Bob's actions. Thus, the MI between John's actions and weather in Norway is larger than

that between Bob's actions and UK's weather. Mutual information is considered as one way to quantify the uncertainty, which is given by (Cover and Thomas, 1991)

$$I(X;\ Y) = h(X) + h(Y) - h(X, Y).$$

where $h(X)$ or $h(Y)$ is the entropy measured the uncertainty in X or Y. The joint entropy $h(X, Y)$ measures how much uncertainty in the two random variables X and Y taken together.

In this thesis, we calculated MI using a bin-less rank approach based on Gaussian copulas (Ince et al., 2016a, 2016b). This method greatly reduces the statistical bias that is generally inherent to direct information theoretic estimates and is robust to outliers in the EEG data because it relies on ranked rather than raw data values. We used MI to measure directly how much information gained about the set of responses from stimuli (Schneidman et al., 2003), which has been used to study the selectivity of neural and behavioural responses to external stimuli (Schyns et al., 2011; Magri et al., 2009; Ince et al., 2009).

Reverse analyses

To further determine how the presence of the eye modulates behaviour and single-trial ERPs, we used reverse analyses. Because randomly sampling the input image changes the visibility of the eye across trials, we can bin distributions of behavioural responses according to the availability of eye information. We created ten equi-populated bins of eye information, and then computed mean accuracy and median RT and mean ERPs of the trials in each bin. The difference between bin 1 and bin 10 provides a good indication of how eye visibility affected behaviour and brain activity.

Aims of the thesis

Face detection in humans is rapid and efficient (Bell et al., 2008; Crouzet, 2011), even when only partial information is visible (Bentin et al., 2002; Jiang et al., 2011; Rousselet et al., 2008; Tang et al., 2014). Thus, the whole of the face is not necessarily involved in face detection (Ullman et al., 2002). A key question is what specific image properties enable us to perceive faces so efficiently. Previous ERP, MEG, intracranial and monkey studies revealed that the eye is the main contributor to optimize face processing, and early brain activity to faces is strongly modulated by the presence of the contralateral eye across tasks and species (Rousselet et al., 2014; Schyns et al., 2011, 2007, 2007, 2003, Smith et al., 2009, 2007, 2004; Issa and DiCarlo, 2012; Tang et al., 2014). It suggests eye coding

mechanisms underlying early brain responses to faces. The present thesis attempts to shed light on how face manipulations drive changes of the eye coding function during face detection. We used the Bubble technique coupled with information-theoretic analyses similar to Rousselet et al., (2014) and Ince et al., (2016). In detail, we presented randomly sampled contiguous image pixels with Gaussian apertures as Bubble stimulus. Since group analyses are an abstraction that might hide inter-participant variability (Rousselet, 2011; Rousselet and Pernet, 2011), in this thesis we detailed individual and group results.

Inversion dramatically impairs our special ability to recognise faces efficiently. This impairment is more prominent for faces than objects, which is known as the face inversion effect (FIE) (Yin, 1969; Garrido et al., 2008; Rousselet et al., 2003). Previous behaviour studies explain the FIE as a result of less efficient extraction of the same information in inverted compared to upright faces (C. Gaspar et al., 2008; Goffaux, 2010; Willenbockel et al., 2010), i.e. information around the eye regions (Sekuler et al., 2004). Only one monkey study revealed that regardless of face orientation cells in the most posterior face patch were selective to the eye-like feature in earliest neuronal responses (60 – 100 ms time window following image onset). To our knowledge, the study in chapter 2 is the first ERP study to determine whether brain responses also reflect the processing of eyes in inverted faces and how it does so in a simple face detection task in humans.

We first replicated previous findings that reported, for upright faces, eye sensitivity contralateral to posterior-lateral electrodes in the N170 time window. Also, we extended this eye coding function to inverted faces. The evidence points to that independent of face orientation, face processing starts with the coding of one local feature, the contralateral eye, in the time window of the N170. However, the eye coding function in the early N170 time window was weakened and delayed by ~ 15 – 19 ms in both hemispheres by face inversion.

In chapter 2, for the stimulus we used, eye position and face orientation were confounded, i.e., the upper visual field contains the eyes in upright faces; in upside-down faces lower visual field contains the eyes. In chapter 3, we aim to answer a question of whether impaired eye coding mechanism for inverted faces is simply due to that face inversion removes the eyes away from upper visual field. We manipulated three vertical locations of images in which the eyes were presented in upper, centre and lower visual field relative to fixation cross (the centre of the screen) so that in upright and inverted faces the eyes can shift from the upper to the lower visual field. We found that face inversion delayed the eye coding and weakened it in the N170 time window, when the eyes of upright and inverted

faces were presented in the same position. Thus, face inversion related changes in processing of the contralateral eye cannot be simply considered as the results of differences of eye position.

Visual attention is directed to salient areas that based on the basic information of an input image such as intensity (Itti et al., 1998, p. 1; Itti and Koch, 2000; Parkhurst et al., 2002). In human faces, eyes are inherently more salient compared to other parts of the face, on the basis of the physical properties of faces, such as local contrast and luminance (Zerouali et al., 2013). Therefore, in chapter 4, we aim to answer a question of whether the coding function to encode the eyes is due to a low-level factor: local contrast. We introduced two altered version of original faces: normalised and reversed contrast faces. For normalised contrast faces, we equalised the local contrast across a face so that the eyes were not standing out. Reversed contrast faces were generated by reversing the contrast polarity of faces.

We observed that removing the saliency of the eyes decreased the association between the contralateral eye region and brain activity ~ 100 – 160 ms post-stimulus. It seems eye saliency is the explanation for this contralateral eye sensitivity. If higher local contrast in eye region is the only explanation, we should obverse higher contralateral eye sensitivity in reversed compared to normalised contrast faces ~ 100 – 160 ms since reversed contrast faces still keep the eye saliency. In contrast, we found that contralateral eye sensitivity was comparable between normalised and reversed contrast faces. Thus, besides eye saliency, feature-specificity might also be crucial for contralateral eye sensitivity. It was further evidenced by the result that compared to original faces there was impaired eye sensitivity ~ 100 – 160 ms for reversed contrast faces in which eye feature per se was influenced. Thus, contralateral eye sensitivity might be attributed to the low-level properties, local contrast in our case, and high-level visual feature in combination in ~ 100 – 160 ms.

Chapter 2: The influence of inversion on eye coding mechanisms

Introduction

We can detect faces more rapidly and efficiently compared to non-face object categories (Bell et al., 2008; Crouzet, 2011), even when only partial information is visible (Tang et al., 2014).

However, inversion can dramatically impair our special ability to perceive faces efficiently. This impairment is more prominent for faces than objects, which is known as the face inversion effect (FIE) (Yin, 1969; Garrido et al., 2008; Rousselet et al., 2003). These impairments in performance are interesting because face inversion preserves physical information. A classical view claims that the FIE is due to the disruption of simultaneous integration of facial features as a whole, leading to qualitative differences in upright and inverted face processing (i.e., holistic vs. feature based) (Rossion, 2013; Tanaka and Farah, 1993).

In contrast, psychophysical evidence suggests an alternative view that considers quantitative processing differences as an explanation for FIE (Gold et al., 2012; Ince et al., 2016b; Rousselet et al., 2014). For example, Gold et al. (2012) suggested that regardless of face orientation face processing is feature-based. They showed that, for both upright and inverted faces, the information observers used to perceive a whole face was no more than the sum of the information in its individual parts, arguing against the holistic processing (Gold et al., 2012). Sekuler et al. (2004) reported that pixels near the eyes and eyebrows were used to discriminate faces regardless of their orientation. Since eyes and eyebrows contain different patterns of spatial frequency (SF), it remains possible that qualitative processing differences can be found in SF domain. However, so far studies have found that the lower performance for inverted faces is due to less efficient processing of the same SF compared to upright faces (C. Gaspar et al., 2008; Goffaux, 2010; Willenbockel et al., 2010). These behavioural studies converge to explain the FIE as a result of less efficient extraction of the same information in inverted compared to upright faces.

However, the evidence above is based on behavioural measures that represent the output of a sequence of processing. Neurophysiological studies shed light on the neural mechanisms involved in face processing. In human scalp electrophysiological studies, a face

preferential ERP component has been originally described as a negative potential peaking approximately 170 ms following stimulus onset (Bentin et al., 1996). This face-sensitive N170 is consistently found to be of later latency for upside-down faces than upright faces, termed as the N170 FIE (Jacques et al., 2007; Rousselet et al., 2004; Bentin et al., 1996; Caharel et al., 2006; Eimer, 2000; Rossion et al., 2000).

Accumulating evidence points to a link between early brain responses and eye information during upright face processing. Bubble studies reported that early brain activity to upright faces is strongly modulated by the presence of the contralateral eye across tasks, and the strongest effects are observed in the time window of the N170 (Schyns et al., 2007, 2011, Smith et al., 2004, 2007, 2009; van Rijsbergen and Schyns, 2009). In a simple face detection task, the rising part of the N170 has been proposed to reflect the product of the contralateral eye coding mechanisms (Ince et al., 2016; Rousselet et al., 2014). Similarly, a macaque study revealed that presenting an eye alone was sufficient to elicit earliest neuronal responses (60 – 100 ms time window following image onset) in the posterior and middle face patches (PL and ML) similar to those for the whole face (Issa and DiCarlo, 2012). These studies suggest the early responses to upright faces reflect processing of the eye.

To understand the neural mechanisms underlying the N170 FIE, a key question is how inverted faces drive changes of the eye coding function. To answer this question, in this chapter, we take advantage of the Bubble technique coupled with reverse analyses similar to Rousselet et al., (2014) and Ince et al., (2016) to test the quantitative/qualitative dissociation in a face detection task. If the FIE is due to quantitative differences, we should observe that the same face features, the eyes, are processed in a less efficient way for inverted compared to upright faces. On the contrary, if qualitative differences, we should observe face features are represented in distinct ways for inverted faces compared to upright. For instance, for inverted faces, a nose or a month is the main contributor to the modulations in behavioural performance and brain activity. In detail, we presented randomly sampled contiguous image pixels with Gaussian apertures as Bubble stimulus. Then we obtained classification images that can depict the association between image pixels and behavioural responses, and also single-trial ERP responses. Following the quantitative view of FIE, we hypothesize that in inverted faces the N170 also reflects information processing mechanisms involving eye coding, but with a weakened and delayed this pattern.

Method

Participants

Ten adults (5 females, median age=23, min=20, max=29) participated in the study. Participants had normal or corrected to normal visual acuity and contrast sensitivity, as assessed using a Colenbrander mixed contrast card set and a Pelli-Robson contrast sensitivity chart. All participants provided written informed consent and filled in a general health questionnaire. Participants did not report history of mental illness, taking psychotropic medications at the time of testing or used to take them, suffering from any neurological condition, diabetes, or having suffered a stroke or a serious head injury. The study was approved by the local ethics committee at the College of Science and Engineering, University of Glasgow (approval no. CSE01361), and conducted in line with the British Psychological Society ethics guidelines. Participants were compensated £6/h.

Stimuli

Face and noise stimuli are illustrated in Figure 2.1. The face stimuli were gray-scale pictures portraying 10 identities (Gold et al., 1999). All stimuli had the same amplitude spectrum, set to the mean across faces, the same mean pixel intensity, 0.2 RMS contrast, and spanned 9.3° x 9.3° of visual angle (256 x 256 pixels, height and width: ~16.3 x 16.3 cm). The face oval was 4.9° x 7.0° of visual angle. A unique image was generated on each trial by introducing phase noise (70% phase coherence) into the face images (Rousselet et al., 2008). Textures had random phase (0% phase coherence). All images were revealed through 10 two-dimensional Gaussian apertures (hereafter Bubbles, sigma=0.36°), with the centre of each aperture always randomly located in the face oval. Stimuli were displayed on a Samsung SyncMaster 1100Mb monitor (85 Hz refresh rate, height and width 600 x 800 pixels, 22° x 28°). We wrote the experiments in MATLAB using the Psychophysics Toolbox extensions (Brainard, 1997; Pelli, 1997; Kleiner et al., 2007).

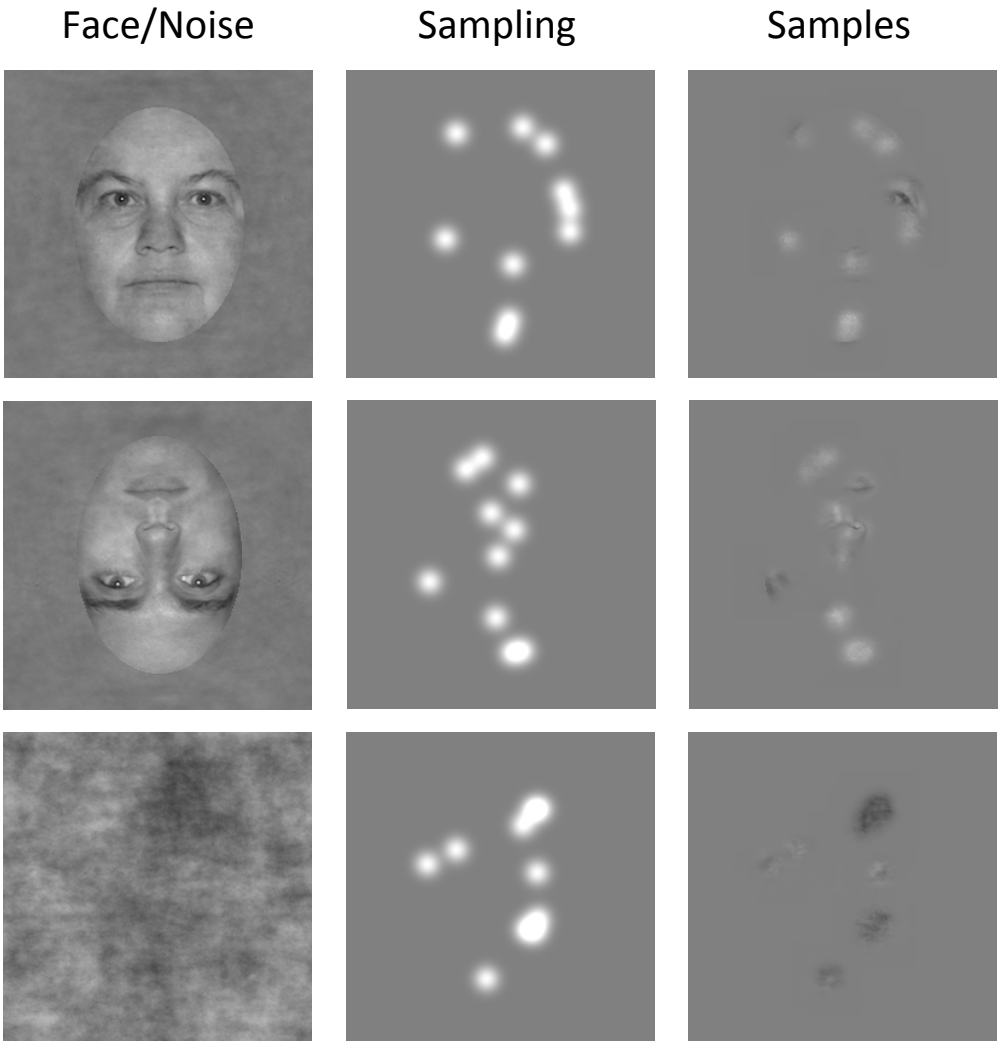

Figure 2.1 Examples of stimuli used in experiment 1

Column 1 shows intact upright and inverted faces and a noise texture. Column 2 shows three examples of Bubble masks, composed of ten Gaussian apertures. Column 3 shows column 1 stimuli masked by column 2 Bubble masks.

Procedure

Participants were tested in four sessions on four separate days. Instead of presenting a series of randomly interleaved upright and inverted faces, face orientation was blocked in each session of this experiment to let participants focus on one face orientation. Additionally, in the intermixed design participants might be biased to the region that is the midway between two eyes of upright and inverted faces, i.e., cheek, which might be the optimal strategy to detect both upright and inverted faces. Two consecutive sessions of upright faces, followed by two sessions of inverted faces, were performed by five participants. The other five participants were tested in the reverse order.

Participants were tested in a sound-attenuated booth, with their head resting on a chinrest 80 cm from the monitor screen. Each trial began with a small black fixation cross (0.4° x 0.4° visual angle) displayed at the centre of the screen for a random time interval of about 500 – 1000 ms, followed by an image of a face or a texture presented for 7 frames (~82 ms). A blank grey screen followed stimulus presentation until participant's response. Participants were asked to respond as fast and accurately as possible by pressing '1' for a face, and '2' for a texture on the numerical pad of a keyboard. At the end of every block they received feedback on their overall performance and, after block 1, on their performance in the previous block: median reaction times and percent correct remained on the screen until participants press a key to move on to the next block. The fixation cross, the stimulus and the blank response screen were all displayed on a uniform grey background with mean luminance ~ 43 cd/m^2. In addition, participants were asked to try not to blink during stimulus presentation and to minimise movements during a block.

Before the main experiment, participants performed a practice block with un-masked images. After that, they performed 11 blocks of images with Bubble masks. Each block consisted of 100 trials, with 10 face identities, each repeated 5 times. Each session lasted ~ 1 hour, with an extra ~ 30 minutes for EEG setup.

EEG recording and pre-processing

EEG data were recorded at 512Hz using an Active Electrode Amplifier System (BIOSEMI) with 128 electrodes mounted on an elastic cap. Two additional electrodes were placed at the outer canthi of the eyes and two below the eyes.

EEG data were pre-processed using Matlab 2013b and the open-source EEGLAB toolbox (Delorme et al., 2004; Delorme et al., 2011). Data were first re-referenced off-line to an average reference. Then we applied a non-causal 4th order Butterworth 1-30 Hz band-pass filter to create non-causal dataset (zero-phase digital filtering, (Acunzo et al., 2012; Rousselet, 2012). To check for timing distortions by the non-causal high-pass filter, we created a causal dataset by applying a 2 Hz high-pass causal filter and a 30 Hz low-pass non-causal filter. Analyses with the two datasets gave very similar results. Both datasets were then resampled at 500 Hz, and epoched between -300 to 1000 ms around stimulus onset. The channel mean was removed from each channel to increase Independent Component Analysis (ICA) reliability in the non-causal dataset (Groppe et al., 2009) (Groppe et al., 2009). Channel baseline means (0 to -300 ms) were removed in the causal dataset. Noisy electrodes and epochs were detected by visual inspection and rejected on a

participant-by-participant basis. We applied Infomax ICA using EEGLAB (Delorme et al., 2004; Delorme et al., 2007). For each participant, ICA was performed on the non-causal dataset and the independent components (IC's) were then applied to the causal dataset. After rejection of components corresponding to horizontal eye movements and blinks (median=11; min=2; max=17), baseline correction was performed. Artifactual data epochs were then removed based on an absolute threshold value larger than 100 μV and an absolute linear trend slope larger than 75 μV per epoch and R^2 larger than 0.3. The median number of Bubble trials accepted for analysis was, out of 1100: face trials = 1046 [min: 1003, max: 1052]; noise trials = 1055 [min: 1009, max: 1063].

Last, single-trial spherical spline current source density waveforms were computed by using the CSD toolbox (Kayser et al., 2009; Tenke and Kayser, 2012). CSD waveforms were computed using parameters 50 iterations, m=4, lambda=10^{-5}. The head radius was arbitrarily set to 10 cm, so that the ERP units in all figures are μV/cm^2. The CSD transformation is a spatial high-pass filtering of the data, which sharpens ERP topographies and reduces the influence of volume-conducted activity.

N170 analysis & electrode selection

For each participant we computed mean ERPs across trials separately for faces and textures without Bubbles. The N170 peak latency and amplitude were measured, at two selected electrodes (LE & RE). The LE was selected based on showing maximum MI(PIX, [ERP, ERP_g]) (details in mutual information section below) across 19 left posterior-lateral electrodes of interest, independently for upright and inverted faces, in a 200 ms time window following stimulus onset. RE was selected from right hemisphere by the same method. Corresponding electrodes are marked in the electrode map in Figure 2.4B. Inversion effects were normalised by computing an inversion index: (upright - inverted) / (inverted + upright).

Mutual information

Mutual information (MI) provides a non-parametric estimation of the linear or nonlinear statistical dependencies between pairs of variables (Magri et al., 2009; Ince et al., 2016b). We used MI to measure in bits the reduction in uncertainty about the response of interest that can be gained from the observation of the stimulus (Cover and Thomas, 1991).

In this study, we calculated MI using a bin-less rank approach based on Gaussian copulas (Ince et al., 2016a, 2016b). This method greatly reduces the statistical bias that is generally inherent to direct information theoretic estimates and is robust to outliers in the EEG data because it relies on ranked rather than raw data values. In addition, Ince et al. (2016a) indicated that the recorded voltage at a single time point is related to nearby time points and their relationship is highly informative. Taking into account changes between two points is a simple way to incorporate information about the shape of the ERP. We thus considered the temporal gradient of the EEG voltage together with raw EEG voltage as a bivariate response for each trial. Ince et al. (2016a) provided a detailed presentation of the method and a tutorial with Matlab and Python code.

Whole stimulus sampling analyses

We applied MI between pairs of variables in single participants to produce classification images that can uncover the image pixels associated with modulations in behavioural performance and brain activity (Figure 2.2):

1. MI(PIX, RT) establishes the relationship, independently at every pixel, between pixel intensities from the Bubble masks and participant's reaction time distribution, separately for face and noise trials.
2. MI(PIX, CORRECT) measures the association between Bubble masks and participant's correct and incorrect responses, separately for face and noise trials.
3. MI(PIX, [ERP, ERP_g]) measures the association between each pixel's intensity distribution and participant's bivariate responses. This analysis was performed independently at every time point and at every electrode using the non-causal and causal filtered dataset.

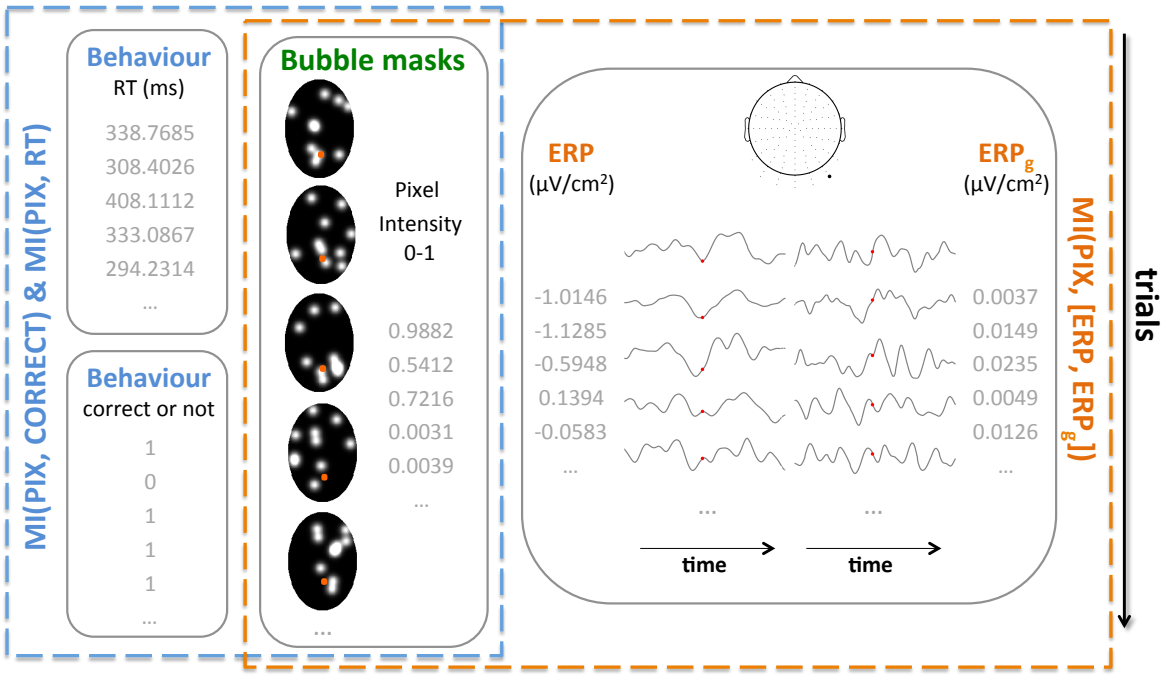

Figure 2.2 MI Computation

On each Bubble trial the stimuli are presented through a randomly generated Bubble mask with ten Gaussian apertures. At the same time behaviour and EEG performance is recorded. Bubble masks take values between 0 and 1, controlling the relative transparency of the mask at each pixel, with 0 being completely opaque and 1 being completely translucent. **Blue frame:** for instance, we can compute MI between two vectors: the distribution of behaviour performance (RT/Correct) and intensity distribution of the pixel marked in red. To obtain classification image that can reveal what information of the image is associated with responses of interest, we repeat MI calculation per each pixel within the face oval. **Orange frame:** similarly, to quantify the dependence between each pixel's intensity from Bubble mask and bivariate responses, we compute MI(PIX, [ERP, ERP_g]) at each time point and electrode.

Eye mask analyses

Previous work from the lab identified a strong association between variability in the eye pixels and behavioural and ERP modulations (Rousselet et al., 2014). To specifically quantify the relationship between eye sampling and our measurements, we performed a region of interest analysis. We created the left eye mask by drawing a circle of 16 pixels radius centred at the maximum MI(PIX, RT) value in the group-averaged classification image for upright faces (Figure 2.3D). Then we horizontally flipped the left eye mask to create the right eye mask. For each Bubble mask, we summed the pixel intensities inside each eye mask, leading to one scalar value per eye mask. Last, we computed MI between

scalar visibility of each eye and the corresponding ERP bivariate responses, thus providing a new quantity: MI(EYE, [ERP, ERP_g]). We repeat the calculation for each time point and electrode, resulting in a 2D MI matrix (time × EEG electrode) for each eye mask. The same approach was applied to behaviour, producing MI(EYE, RT), MI(EYE, CORRECT).

Results

Throughout the chapter, unless stated otherwise, (1) median is the Harrell-Davis estimates of the 0.5 quantile (Harrell & Davis, 1982); (2) 95% confidence intervals (CI) are computed using the percentile bootstrap technique, with 1000 samples; (3) red is used for the upright condition, blue for the inverted condition.

Behavioural diagnostic information: the eye area

Participants were fast and accurate to detect faces from noise textures without Bubbles (upright faces: median RT = 317 [283, 364] ms, mean percent correct = 98.49% [97.67%, 99.82%]; inverted faces: median RT = 322 [291, 355], mean percent correct = 98.05% [96.43%, 99.47%]). There was no evidence for a face inversion effect in practice trials without bubbles ($differences_{upright\ -\ inverted}$: median RT = 2 [-29, 40] ms; mean percent correct = 0.66% [-0.3%, 2%]), probably because of ceiling effects. On bubble trials for upright faces median RT was 394 [347, 444] ms, mean percent correct was 90.43% [85.45%, 91.16%]; for inverted faces median RT was 399 [364, 427] ms and mean percent correct was 85.1% [82.95%, 91%]). There were differences in mean percent correct ($differences_{upright\ -\ inverted}$: 3.62% [0.3%, 6.8%]), but no differences in median RT ($differences_{upright\ -\ inverted}$: 0 [-21, 29] ms).

Participants' behaviour was strongly associated with the eye regions, and in particular the left eye in the picture plane, and no such effects were observed in noise trials (Figure 2.3A). To determine if inversion affected the sensitivity of behaviour responses to eyes, we compared across participants the maximum MI values for upright and inverted faces (Figure 2.3B). We also compared MI values calculated using a left eye region of interest (Figure 2.3C). Both quantities were very similar between upright and inverted faces.

Increased left eye visibility optimized behavioural performances

Because randomly sampling the input image changes the visibility of the eye across trials, we can determine how the presence of the left eye modulates behaviour by using reverse analyses: (Ince et al., 2016b; Rousselet et al., 2014). To do so, we binned distributions of behavioural responses according to the availability of eye information. We created ten equi-populated bins of eye information, and then computed mean accuracy and median RT of the trials in each bin. The difference between bin 1 and bin 10 provides a good

indication of how eye visibility affected behaviour: the presence of the left eye was associated with faster and more accurate responses for upright and inverted faces (Figure 2.3D). Although on average the difference in eye sensitivity between upright and inverted faces was near zero, a few participants (CORRECT: 6/10, RT: 4/10) showed larger left eye sensitivity in inverted compared to upright faces.

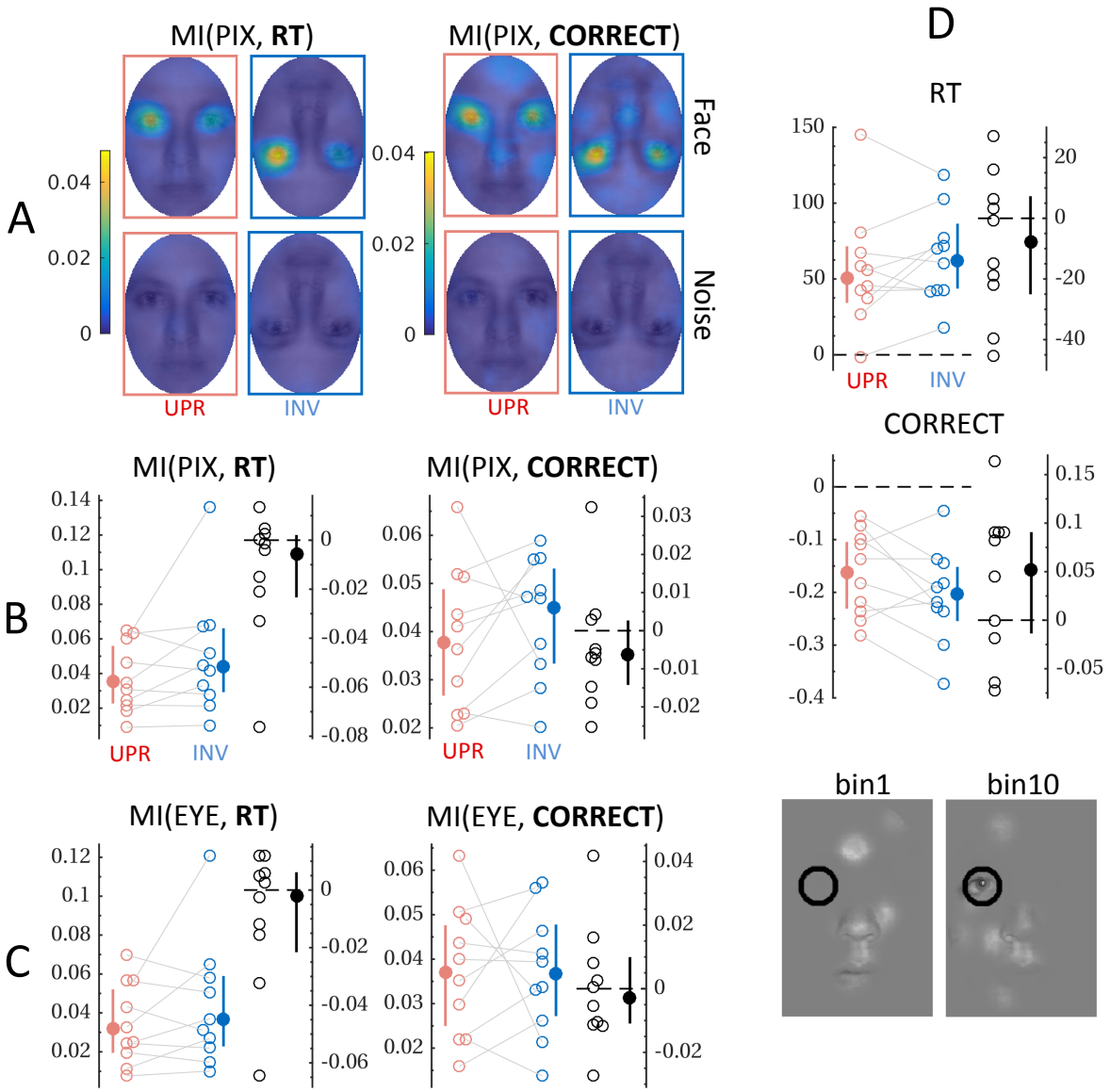

Figure 2.3 Behavioural results

(A) Group-averaged MI classification images, independently for faces (upper) and noise (lower). Left and right panels show results from RT and correct. In addition to eye sensitivity, there was weaker sensitivity to the nose, the forehead and parts of the cheeks in accuracy results, contributed by all participants. **(B)** Scatterplots of maximum MI values (bits) across pixels for each participant (red circles for upright, blue circles for inverted). The coloured disks show the group medians with their 95% CI. The black scatterplot shows the distribution of individual differences (upright - inverted) of maximum MI and the group median with 95% CI (RT: 0 [-0.02, 0] ms, CORRECT: 0

[-0.01, 0]). **(C)** Eye mask results are similar with whole stimulus sampling analysis (upright - inverted: RT, 0 [-0.02 0] ms, CORRECT, 0 [-0.01, 0]) **(D)** Behavioural modulations due to eye visibility. Scatterplots of the behavioural performance differences (bin1 - bin10) for participants (circles) and group medians (disks) with 95% CI, separately for upright (RT: 50.8 [33.81, 71.34] ms, CORRECT: -0.16 [-0.23, -0.1]) and inverted faces (RT: 62.21 [43.30, 82.71] ms, CORRECT: -0.2 [-0.25, -0.15]). The black scatterplot shows the distribution of differences of modulations (bin 1 - bin 10) between upright and inverted faces (upright - inverted, RT: -7.97 [-26.18, 7.89] ms, CORRECT: 0.05 [-0.02, 0.09]). Examples of Bubbles masks weakly (bin 1) and strongly (bin 10) showing the left eye are placed in the bottom.

Face inversion enlarged the N170 amplitude and latency

Using information-theoretic analyses coupled with reverse analyses, we have observed that the visibility of eye regions modulated participants' behaviour in upright and inverted faces to the same extent. We next aim to determine the face inversion-related changes in the N170 waveform (Figure 2.4). We averaged ERPs across practice trials (without Bubbles) per each participant at two selected electrodes (LE & RE), independently for upright and inverted faces. These electrodes recorded the maximum MI(PIX, [ERP, ERP_g]) across left and right posterior-lateral electrodes of interest. Consistent with the literature (Bentin et al., 1996; Caharel et al., 2006; Eimer, 2000), face inversion enlarged and delayed the peak of the N170 in practice trials without Bubbles. As expected, there was no inversion effect for ERPs to textures.

So far, the ERP results were only concerned with the shape of the average response to different image categories. Using the Bubble trials, we asked a different question: how is the association between pixels and single-trial ERP distributions and their temporal gradients affected by inversion?

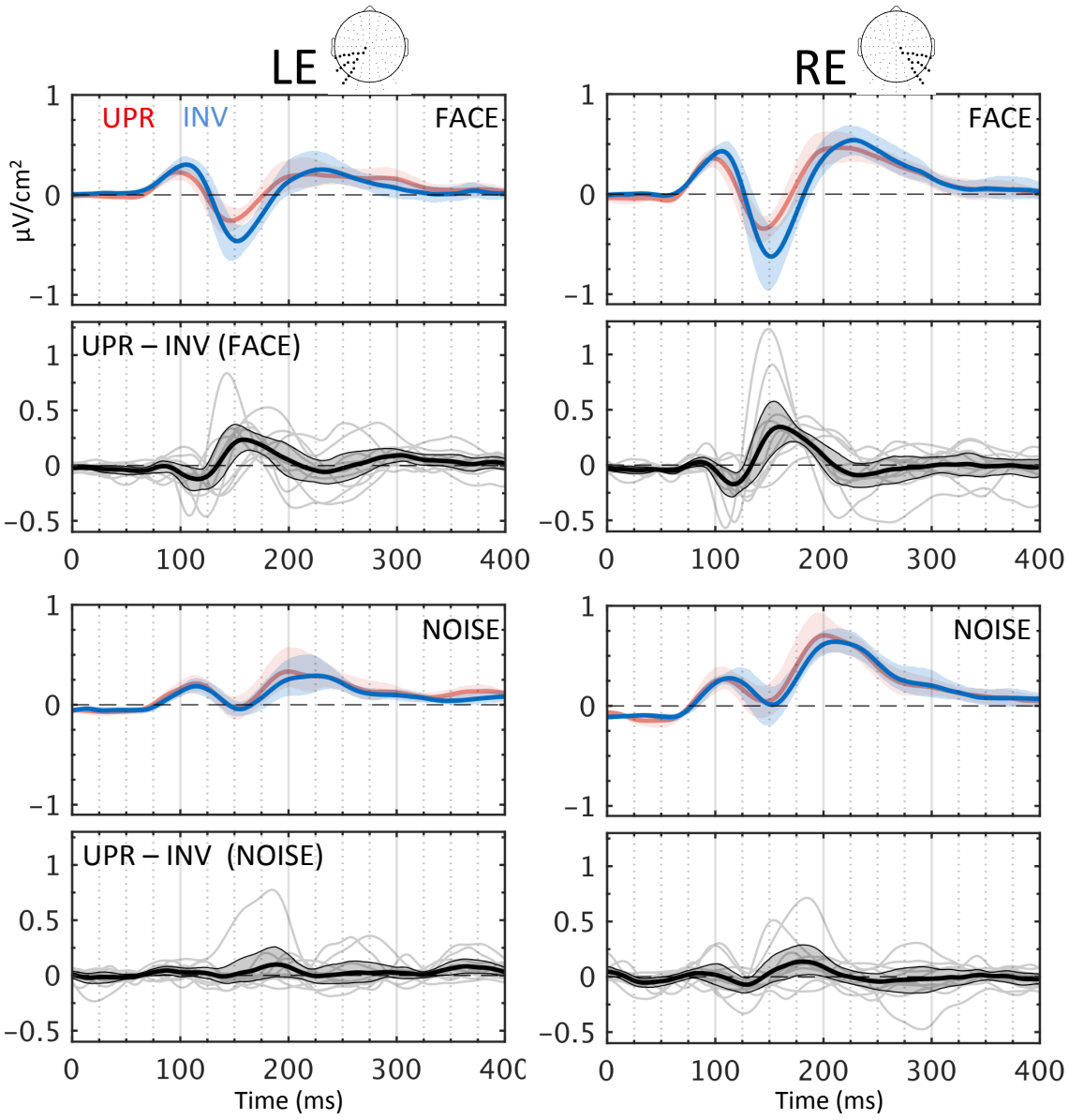

Figure 2.4 Group-averaged ERPs for practise stimuli (without Bubbles)

Left and right columns show results from LE and RE. LE and RE were selected from the left and right electrodes of interest that are highlighted in the electrode maps from the 10/10 system in the top. The first row shows the group averaged ERPs and 95% CI for upright and inverted faces. The thick black line in the second row shows the mean across participants of the differences between upright and inverted faces. The shaded areas show the 95% CI. Thin grey lines show individual results. The last two rows show noise trials in upright and inverted sessions and their differences. At both electrodes, face inversion enhanced the N170 amplitude (LE: -0.23 [-0.39, -0.05] $\mu V/cm^2$, RE: -0.16 [-0.29, -0.08] $\mu V/cm^2$) and delayed its latency (LE: -8.77 [-13.4, -0.34] ms, RE: -7.99 [-9.97, -6] ms). For amplitude, we report the median of the inversion index; for latency we report the median of the differences (upright - inverted) in ms. No inversion effect on noises is observed for

amplitude (LE: -0.08 [-0.24, 0.14] $\mu V/cm^2$, RE: -0.05 [-0.39, 0.28] $\mu V/cm^2$) and latency (LE: -1.78 [-6.62, 24.69] ms, RE: -1.66 [-9.4, 6.23] ms).

Eye sensitivity contralateral to posterior-lateral electrodes

To determine what features were associated with ERP responses, we computed maximum MI(PIX,(ERP, ERP_g]) at each pixel across time points and two regions of interest: left and right posterior-lateral electrodes (see Figure 2.5, corresponding electrodes are highlighted in the electrode map). In upright faces, the classification images reveal the strongest association between pixels in the eye area and bivariate ERPs responses contralateral to the recording electrodes (Figure 2.5A). It is consistent with studies in human and animals showing a strong sensitivity of early visual activity to the eye area (Schyns et al., 2007, 2002; Smith et al., 2007; Issa and DiCarlo 2012; Rousselet et al., 2014; Jaworska et al., in preparation). The contralateral eye pixel area remained the main modulator of brain activity in inverted faces. No such association was observed for noise trials.

Face inversion weakened the contralateral eye sensitivity in the time window of the N170

To quantify how this contralateral eye sensitivity unfolds over time for each participant, we saved maximum MI(PIX,(ERP, ERP_g]) across pixels and electrodes independently for the right and the left hemispheres at every time point. Group-averaged maximum MI peaked around 150 - 200 ms regardless of orientation (figure 2.5B). The time courses of differences between maximum MI for upright and inverted faces revealed larger MI for upright versus inverted faces ~120 - 170 ms at left electrodes, and ~ 130 - 150 ms at right electrodes. Because the association between the contralateral eye area and the single-trial bivariate ERPs was the strongest, we also analysed a quantity with a clearer interpretation: MI(EYE, (ERP, ERP_g]) (figure 2.5C). As expected, the results were very similar to those obtained with MI(PIX, (ERP, ERP_g]), demonstrating that most of the association between pixels and ERPs is carried out by the eye area.

To determine if the majority of participants showed results consistent with those group results, we performed a permutation analysis on single participants independently for upright and inverted faces. For each of 1000 permutations, we randomly shuffled summed pixel intensities within each eye mask (details in *eye mask analysis*) across trials. We then repeated the MI(EYE, (ERP, ERP_g]) calculation for the contralateral posterior-lateral electrodes of interest and time points for each permutation, producing an MI matrix

(electrodes × time points × permutation). We then took the maximum value of MI across electrodes and time points as a permutation distribution and compared the real MI(EYE, (ERP, ERP_g]) against the 95^{th} percentile of the permutation distribution as the statistical threshold separately for the left and right hemisphere. Figures S2.1-2.10 detail, for every participant, how contralateral eye sensitivity unfolded over time, and when it reached significance.

Then we obtained the absolute differences of maximum MI between upright and inverted faces across electrodes of interest, leading to a vector or each permutation and each hemisphere. We computed the maximum of the resulting MI vector for each permutation. For each participant we compared differences of original MI(EYE, (ERP, ERP_g]) between upright and inverted faces against the statistical threshold.

For left electrodes, in ~ 120 - 170 ms time window, out of ten, seven participants showed a statistically significant weaker MI(EYE, (ERP, ERP_g]) in inverted versus upright faces (Figure 2.5D & Figure S2.1-2.10). Two participants showed a stronger effect then a weaker in inverted faces. One participant showed no effects. For right electrodes, in ~ 130 - 150 ms time window, seven participants showed a weaker effect in inverted versus upright faces. One participant showed a weaker then a stronger one in inverted faces. One showed no effect and one showed stronger effect in inverted faces.

Although on right electrodes, ~ 60 – 110ms, six participants showed stronger eye sensitivity in inverted versus upright faces, it might be due to onset distortion by non-causal high-pass filter (Acunzo et al., 2012; Rousselet, 2012; Widmann and Schröger, 2012). We applied the same permutation analysis on the causal dataset. Four out of ten participants showed stronger effects in inverted versus upright faces (Figure S2.11). Additionally, the stronger eye sensitivity ~ 60 – 110ms by face inversion was not replicated in chapter 3. Thus, even though a few participants showed strong eye sensitivity to posterior-lateral electrodes during ~ 60 – 120 ms, the bias might not be reliable.

During ~ 50 - 80 ms we observed group effects at right electrodes. However, statistical analyses of single participants revealed null effects in every participant. It is important to note that group analyses are an abstraction that might hide inter-participant variability (Rousselet, 2011; Rousselet and Pernet, 2011), so to understand brain mechanisms group analyses should be in conjunction with single participant results.

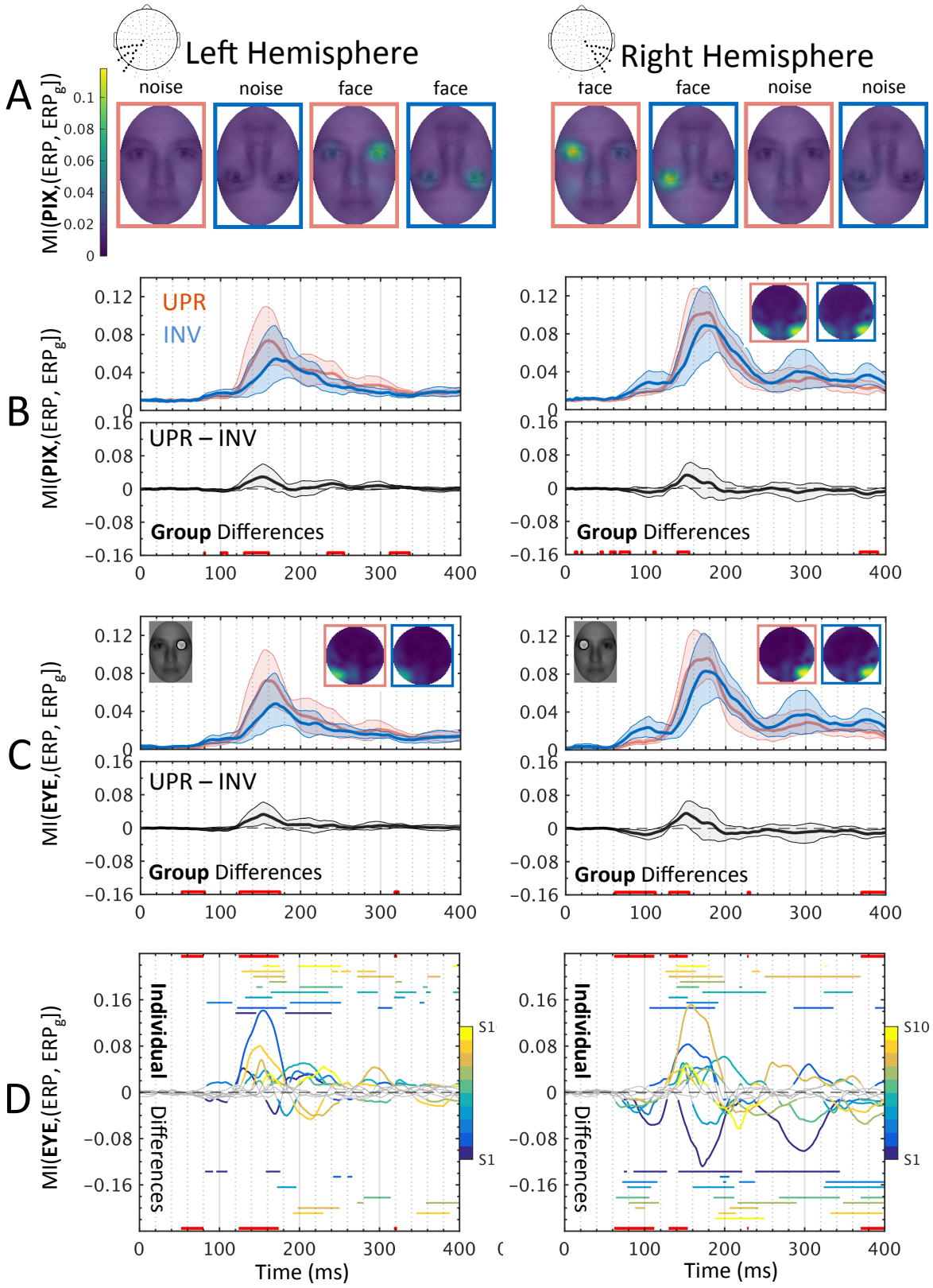

Figure 2.5 MI results for face trials

Left and right electrodes of interest are highlighted in the electrode maps from the 10/10 system at the top. **(A)** Group averaged classification images show contralateral eye hotspots. No clear MI cluster in noise trials. **(B)** MI(PIX, [ERP, ERP_g]). Time course of group averaged maximum MI across electrodes of interest for upright and inverted faces are plotted in curves with 95% CI in first

row. Inset group-averaged topographic maps indicate MI mainly congregate at posterior-lateral electrodes. The econd row showed mean of differences between upright and inverted faces with 95% CI. The red horizontal bar above the x-axis indicates time points of significant group differences. **(C)** MI(EYE, [ERP, ERP_g]). The first row shows the time course of group averaged MI. The insets contain group-averaged topographic maps showing eye sensitivity contralateral to the posterior-lateral electrodes. The second row shows the mean across participants of the differences between upright and inverted faces. **(D)** Individual differences. Colour parts of waves indicate statistically significant differences per participant. Colour-coded horizontal lines above the x-axis show stronger effects in upright versus inverted, and opposite effects are placed below.

Face inversion-related delayed the peak of contralateral eye sensitivity

We next detailed pairwise differences in the peak of MI(EYE, (ERP, ERP_g]). At left electrodes, face inversion prolonged the latency of MI peak and weakened the peak for 8/10 participants, both leading to a statistically significant group effect. At right electrodes there was a significant delay in inverted faces for 9/10 participants. Only 5/10 had a weaker MI and there were no group effects. The comparison analysis of MI(PIX, (ERP, ERP_g]) peak is mostly similar to those obtained with MI(EYE, [ERP, ERP_g]) (Figure S2.12).

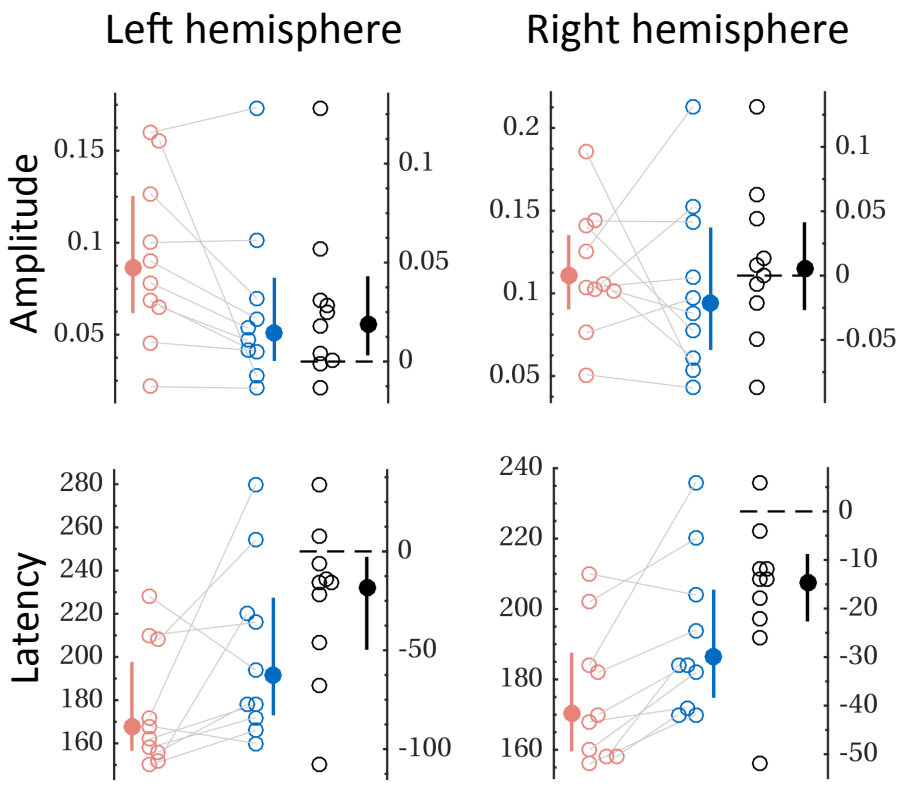

Figure 2.6

Pairwise comparison of the peak of MI(EYE, (ERP, ERP_g]) at LE (value: 0.02 [0 0.04] bit, latency: -18.56 [-49.71, -2.78] ms) and RE (value: 0 [-0.03 0.04] bit, latency: -14.81 [-23.51 -8.53] ms).

Left eye visibility modulated ERPs at RE

To determine how the presence of the left eye affected single-trial ERP distributions at RE, we applied the same reverse approach used previously for behaviour. We measured the mean N170 peak amplitude and latency for trials binned according to the level of left eye visibility. By visual inspection we found one participant had noisy ERPs in trials with lowest right eye visibility (bin1) at RE (Figure S2.3). We removed this participant because the N170 peak cannot be measured. Consistent with previous observations by Rousselet et al. 2014, the N170 latency and amplitude were both modulated by the left eye pixels for upright faces at RE. For inverted faces, the presence of the left eye was associated with the N170 amplitude but not latency (Figure 2.7B).

At RE, in 9/9 participants the N170 tended to get larger with increasing left eye visibility, whether faces were presented upright or upside-down (Figure S2.1-2.2, 2.4-2.10). In 7/9 (~78%) earlier N170 peaks were also associated with increased left eye visibility, but 2/9 showed a later N170 peaks for upright versus inverted faces. For inverted faces, although the presence of the left eye did not influence the N170 latency at the group-level, 6/9 (~67%) showed earlier N170 peaks when the left eye visibility was higher. 2/9 showed opposite effect, and 1/9 had the same latency as left eye visibility increasing. We then tested the face inversion effect on this N170 peak modulation. The differences in the amplitude and latency modulation of the N170 peak by the presence of the left eye between upright and inverted faces were not significant. This suggests the N170 reflects eye coding mechanisms in both upright and inverted faces.

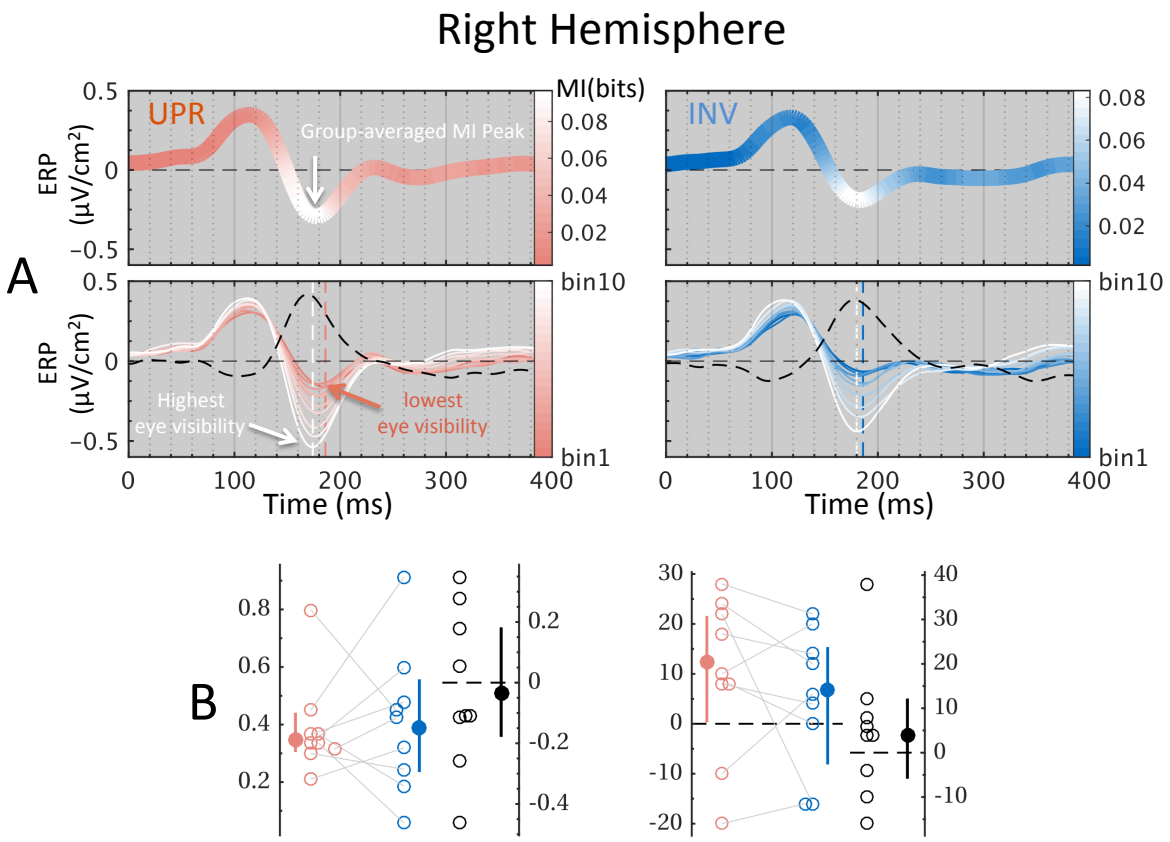

Figure 2.7 ERP modulations due to left eye visibility at RE

(A) The first row shows the mean maximum MI unfolding on the time-course of the group averaged ERPs for Bubble trials at RE. A white arrow refers to the peak of mean maximum MI(EYE, (ERP, ERP_g)). In the second row, averaged ERPs are colour-coded at each level of eye visibility. The red vertical dashed line marks the N170 peak of bin1 (lowest eye visibility) and the white vertical line marks bin10 (highest eye visibility). The black dashed curves represent the differences (bin1 - bin10). **(B)** N170 amplitude (left) and latency (right) modulations. Scatterplots of the ERP differences (bin1 - bin10) show the N170 for upright faces is enlarged (0.35 [0.3, 0.44] $\mu V/cm^2$) and peaks earlier (12.28 [0.26, 21.16] ms) as eye visibility increased at RE. For inverted faces, a significant enlarged N170 can be observed (0.39 [0.23, 0.56] $\mu V/cm^2$), while no changes on latency (6.85 [-8.73,15.84] ms). The black scatterplots show that the amplitude and latency modulations are similar between upright and inverted faces (upright - inverted) (amplitude: -0.01 [-0.12, 0.18] $\mu V/cm^2$, latency: 5.76 [-4.03, 14.59] ms).

Discussion

To address the elusive nature of the FIE, the key step is to understand the information coding function underlying the N170 in upright and inverted faces. Using information theoretic analyses coupled with reverse analyses, we replicated the previous findings for upright faces that the eyes were coded by brain activity recorded at contralateral posterior-lateral electrodes in the N170 time window (Rousselet et al., 2014, Ince, et al., 2016b, Jaworska et al., in prep). We further derived impaired eye information processing mechanisms to inverted faces in the early stage of the N170. First, there was a strong association between variability in the eye pixels and modulations of ERP recorded at contralateral posterior-lateral electrodes whatever the orientation of the face. Second, we found that in the left and right hemisphere the face inversion weakened this association in the early N170 and delayed for inverted compared to upright faces.

Eye regions are diagnostic for face detection

Figure 2.3 detailed that the eye region pixels, predominantly around the left eye, were associated with RT and accuracy in upright and inverted faces to the same extent. These results suggest that the eye information was equally used in upright and inverted faces. It is inconsistent with previous studies that have reported a less effective utilization of common information i.e. eyes, eyebrow or same frequency band in inverted faces compared to upright faces (C. Gaspar et al., 2008; Sekuler et al., 2004; Willenbockel et al., 2010). However, their results cannot be directly compared with ours because of different task requirements (face discrimination vs. face detection), leading to differences in diagnostic information (Schyns, 1998; Schyns et al., 2003). In addition, independent of face orientation, the behavioural results reached ceiling in terms of RT and accuracy in the current study. Thus it should not be a surprise that the eye-dependent strategy used to detect upside-down faces is as efficient as that to detect upright faces.

The behaviourally relevant eyes were coded contralateral to the posterior-lateral electrodes in the N170 time window

Information-theoretic analyses showed that irrespective of face orientation early ERPs were mostly associated with the task relevant eyes (Figure 2.5A) and the strongest association was observed in the time window of the N170 (Figure 2.5, B&C). We also determined how the ERPs are changing with different levels of eye visibility by using

reverse analyses. Figure 2.7A showed that regardless of face orientation higher left eye visibility was associated with larger amplitude and shorter latency of the N170 recorded at RE in most of our participants (Figure 2.7B).

Bubble studies interpreted the N170 as a product of information processing mechanism involving feature coding (Schyns et al., 2003; Schyns et al., 2007; Schyns et al., 2011; Smith et al., 2004, 2007, 2009; van Rijsbergen and Schyns, 2009; Rousselet et al., 2014; Ince et al., 2016b). These studies revealed that the processing of faces starts with eye coding on the rising part of the N170, and followed the integration of task-relevant features. In our study, since independent of face orientation the eyes are diagnostic information in the face detection task, they are sufficient to detect faces, the information integration might end in contralateral eye coding (Rousselet et al., 2014). The feature-based coding in the early responses has also been found in a monkey study, reporting that almost all face-selective cells in PL and, to some extent, ML was modulated by the presence of a single eye in the early response window, 60 – 100 ms following image onset (Issa and DiCarlo, 2012). They also found that the early PL responses (0 – 40 ms after response onset) to the combinations of face features were well matched to the linear sum of the responses to the individual features. Their results suggested independent processing of local feature in the initial steps of face processing, which argues against holistic face processing (Maurer et al., 2002). In line with this monkey study, our data supported that, independent of face orientation, face processing starts with the coding of one local feature, the contralateral eye, in the time window of the N170.

Face inversion weakened and delayed contralateral eye coding in the early N170

In both upright and inverted faces, there was a strong association between variability in the eye pixels and modulations of the N170 amplitude and latency, suggesting the same eye coding mechanism underlying the N170. However, the eye coding function in the early N170 time window was weakened (Figure 2.5) and delayed by ~ 15 – 19 ms (Figure 2.6) in both hemispheres by face inversion.

In line with our data, previous monkey studies have also shown that face-selective neurons decreased (ML and MF, Freiwald et al., 2009; ML, Jessica Taubert et al., 2015; J. Taubert et al., 2015; Taubert et al., 2016) and delayed (MF; Perrett et al., 1985) responses for inverted compared with upright faces in temporal cortex. Issa et al. (2012) reported that the responses of PL face-selective cells were weakened by face inversion, but these cells were tuned to an eye-like region regardless of face orientation. Freiwald et al. (2009) reported

that neural responses in ML to eyebrows were lost entirely under face inversion. Also, ML neurons were profoundly sensitive to eye orientation in upright but not in inverted faces (J. Taubert et al., 2015). These monkey data might suggest that face inversion disrupt the processing of fine structure details around the eye region. Thus, in our case, the impaired eye coding function in the early N170 time window by face inversion might be due to less neural responses to the details of the eye region in inverted compared to upright faces.

While the homologies between monkey and human face processing systems are unclear, the occipital face area (OFA), the earliest face-selective region, could be comparable with the monkey posterior-lateral patches (Yovel and Freiwald, 2013). The ML and the fusiform face area (FFA) may be homologous (Rajimehr et al., 2009; Tsao et al., 2008, 2003; Bell et al., 2009). The functional role of the PL and the ML is similar with the OFA and the FFA. For example, fMRI and TMS studies found that the feature-based analysis was processed in the OFA (Arcurio et al., 2012; Pitcher et al., 2007, 2009, 2011a). Several studies have reported that the FFA is sensitive to both whole faces and face components (Harris and Aguirre, 2010; Tong et al., 2000; Arcurio et al. 2012). A MEG study showed that sensitivity to face parts including eye regions occurred in lateral cortical areas in the time window of the M170 (Smith et al., 2009). In our case, topographic maps indicated that eye sensitivity strongly clustered at contralateral posterior-lateral electrodes, whether faces are presented upright or upside-down (Figure 2.5, B&C). It is in line with previous Bubble studies (Rousselet et al., 2014; Jaworska et al., in prep). These studies consistently pointed to that face processing starts with local feature coding which is involved in posterior-lateral sources. Additionally, the timing of contralateral eye sensitivity for upright faces is much earlier in monkey (started ~ 74 ms and peaked ~ 100 ms, Issa and DiCarlo, 2012) than in humans (started ~ 120 ms and peaked at ~ 160 ms). However, following the 3/5 rule (Kelly et al., 2013), these timings of this sensitivity might be comparable between humans and monkeys.

We found that N170 responses to Bubble faces were delayed (~ 35 ms vs. ~ 28 ms for upright and inverted), with respect to intact faces (Figure S2.13). The longer responses to the occluded or partial objects compared to non-occluded objects have been reported in behavioural (Brown and Koch, 2000; Johnson and Olshausen, 2005), EEG (Rousselet et al., 2014; Jaworska et al., in prep), and monkey studies (Issa and Dicarlo, 2012). The additional time required by partial objects involved horizontal or top-down connections (Tang et al., 2014, 2017).

Therefore, there is a potential explanation for the face inversion-related delays in contralateral eye coding that occlusion from bubbles delays the processing of inverted faces more than that of upright faces. However, there was no group-level interaction between face inversion and occlusion. Even though single-participant analyses showed inter-individual differences, the occlusion-related delay was longer in upright faces than inverted for 6 out of 10 participants, three showed opposite effect, and one had no effect. For these three participants the longer occlusion-related delay in inverted versus upright was ~ 4 ms, which was not matched with the face inversion related delays (~ 20 ms) in eye coding. Thus, occlusion does not seem to affect face inversion-related differences in eye coding speed.

Conclusion

In summary, face inversion weakened contralateral eye coding function in the early N170 and delayed the pattern, but in upright and inverted faces alike brain activity recorded at posterior-lateral electrodes reflect contralateral eye coding in the time window of the N170. Those findings suggest the same mechanism underlying the N170 whatever the orientation of the face. Our results point to a quantitative difference accounted for face inversion effect (Sekuler et al., 2004).

Chapter 3: Inversion-related changes of contralateral eye coding in the same eye location

Introduction

Face inversion impairs our ability to efficiently perceive faces. To address the elusive nature of the face inversion effect (FIE), in chapter 2 we determined what special face features were processed and how coding of these features was affected by face inversion. We used a simple face detection task in which face orientation was blocked. Ten participants were shown images of faces and noises in which contiguous image pixels were sampled by randomly ten Gaussian apertures per Bubble trial. Using information-theoretic analyses, we found strong associations between modulations of the responses of interest (behaviour and brain activity recorded by EEG) and pixel intensities in the eye area regardless of face orientation. Reverse analyses of behaviour revealed that for upright and inverted faces alike the presence of the left eye was associated with faster and more accurate responses, suggesting that participants rely on the presence of the eyes to detect upright and inverted faces to the same extent. Regardless of face orientation, the earlier and larger N170 peaks were also associated with increased left eye visibility for most of our participants, suggesting the same eye coding mechanism underlying the N170. However, the eye coding mechanism in the transition between the P1 and the N170 was weakened and delayed by ~ 15 – 19 ms for inverted compared to upright faces.

In chapter 2, for the stimulus we used, eye position and face orientation were confounded, i.e., the upper visual field contains the eyes in upright faces; in upside-down faces lower visual field contains the eyes. Accumulating evidence suggests a role of feature location in the processing of single face feature (de Haas et al., 2016; Henriksson et al., 2015; Issa and DiCarlo, 2012). In an accurate face identification task, information is extracted within the first one or two fixations (Hsiao and Cottrell, 2008) that are biased to the upper centre region, just below the eyes (Peterson and Eckstein, 2012). A macaque study reported that earliest neuronal responses (60 – 100 ms time window following image onset) of the cells in the most posterior face patch (PL) show a preference for the eyes presented in the upper visual field (Issa and DiCarlo, 2012). This raises the question whether impaired eye coding mechanism for inverted faces is simply due to that face inversion removes the eyes away from upper visual filed.

In chapter 3, to answer this question, we manipulated three vertical locations of images in which the eyes were presented in upper, centre and lower visual field relative to fixation cross (the centre of the screen) so that in upright and inverted faces the eyes can shift from the upper to the lower visual field. We then presented randomly sampled contiguous image pixels with Gaussian apertures as Bubble stimulus. Then we obtained classification images that can depict the association between image pixels and behavioural responses, and also single-trial ERP responses.

Method

Participants

We tested eight adults (5 females, median age=23, min=20, max=29). Participants had normal or corrected to normal visual acuity and contrast sensitivity, as assessed using a Colenbrander mixed contrast card set and a Pelli-Robson contrast sensitivity chart. All participants provided written informed consent and filled in a general health questionnaire. Participants did not report history of mental illness, taking psychotropic medications at the time of testing or used to take them, suffering from any neurological condition, diabetes, or having suffered a stroke or a serious head injury. The study was approved by the local ethics committee at the College of Science and Engineering, University of Glasgow (approval no. CSE01361), and conducted in line with the British Psychological Society ethics guidelines. Participants were compensated £6/h.

Stimuli

The face stimuli were grey-scale pictures portraying ten identities (Gold et al., 1999). All stimuli had the same amplitude spectrum, set to the mean across faces, the same mean pixel intensity, 0.2 RMS contrast, and spanned 9.3° x 9.3° of visual angle (256 x 256 pixels, height and width: ~16.3 x 16.3 cm). The face oval was 4.9° x 7.0° of visual angle. A unique image was generated on each trial by introducing phase noise (70% phase coherence) into the face images (Rousselet et al., 2008). Textures had random phase (0% phase coherence).

The images (faces and noise textures) were presented in three positions, in which the eyes appeared *Above*, *Below* or at the *Centre* of the screen, coinciding with the location of the fixation cross (Figure 3.1). Face stimuli were presented upright or inverted (180° rotation). There were thus six conditions in total (2 face orientations × 3 positions) for face trials. *Above* and *Below* positions were equidistant in visual angle from *Centre*: ~0.78°. Upright faces with the eyes appeared at *Above* (abbr. *UPRabove*), and inverted faces with the eyes were presented at *Below* (abbr. *INVbelow*) correspond to how stimuli presented in chapter 2. All images were revealed through 10 two-dimensional Gaussian apertures (hereafter Bubbles, sigma=0.36°), with the Centre of each aperture always randomly located in the face oval.

Stimuli were displayed on a Samsung SyncMaster 1100Mb monitor (85 Hz refresh rate, height and width 600 x 800 pixels, 22° x 28°). We wrote the experiments in MATLAB

using the Psychophysics Toolbox extensions (Brainard, 1997; Pelli, 1997; Kleiner et al., 2007).

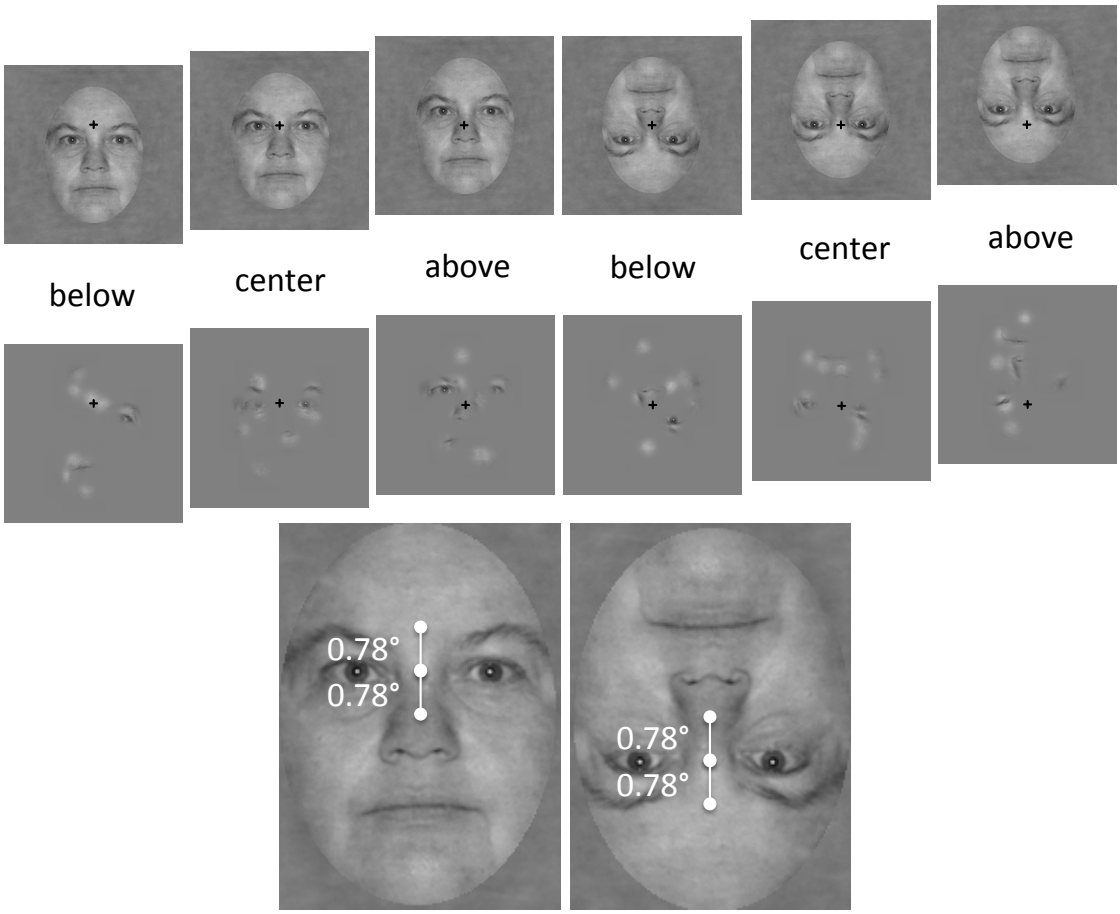

Figure 3.1 Examples of stimuli used in chapter 3

Top panel: examples of face stimuli presented at three positions. *Above*, *Centre* and *Below* refer to the position of the eyes with respect to the fixation cross. Intact faces without bubbles are shown in the top row, faces with bubbles are in the second row. Bottom panel: upright and inverted face examples with angular distance between eye locations.

Procedure

Participants were tested in 6 experimental sessions on 6 separate days. Four of the eight participants did 3 consecutive sessions of upright faces, followed by 3 consecutive sessions of inverted faces. The other 4 participants were tested in the reverse order.

Participants were tested in a sound-attenuated booth, with their head resting on a chinrest 80 cm from the monitor screen. Each trial began with a small black fixation cross (0.4° x 0.4° visual angle) displayed at the Centre of the screen for a random time interval of about 500 – 1000 ms, followed by an image of a face or a texture presented for 7 frames (~ 82

ms). A blank grey screen followed stimulus presentation until participant's response. Participants were asked to try not move their eyes and to indicate as fast and accurately as possible if the image presented on the screen was a face or a texture, regardless of position and orientation, by pressing '1' for face, and '2' for texture. At the end of every block they received feedback on their overall performance and, after block 1, on their performance in the previous block: median reaction times and percent correct remained on the screen until participants press a key to move on to the next block. The fixation cross, the stimulus and the blank response screen were all displayed on a uniform grey background with mean luminance ~ 43 cd/m^2.

Before the main experiment, participants performed a practice block with 90 unmasked images. After that, they performed 12 blocks with Bubble masks. Each block consisted of 90 trials, composed of 60 face trials (10 face identities, each repeated 6 times), and 30 noise trials. There was an equal proportion of each of the three positions. Each session of the experiment lasted ~100 minutes, including EEG setup.

EEG recording and pre-processing

EEG data were recorded at 512Hz using an Active Electrode Amplifier System (BIOSEMI) with 128 electrodes mounted on an elastic cap. Two additional electrodes were placed at the outer canthi of the eyes and two below the eyes.

EEG data were pre-processed using Matlab 2013b and the open-source EEGLAB toolbox (Delorme and Makeig, 2004; Delorme et al., 2011). Data were first re-referenced off-line to an average reference. Then we applied a non-causal 4th order Butterworth 1-30 Hz band-pass filter to create non-causal dataset (zero-phase digital filtering, Rousselet et al., 2012; Acunzo et al., 2012). To check for timing distortions by the non-causal high-pass filter, we created a causal dataset by applying a 2 Hz high-pass causal filter and a 30 Hz low-pass non-causal filter. Analyses with the two datasets gave very similar results. Both datasets were then resampled at 500 Hz, and epoched between -300 to 1000 ms around stimulus onset. The channel mean was removed from each channel to increase Independent Component Analysis (ICA) reliability in the non-causal dataset (Groppe et al., 2009). Channel baseline means (0 to -300 ms) were removed in the causal dataset. Noisy electrodes and epochs were detected by visual inspection and rejected on a participant-by-participant basis. We applied Infomax ICA using EEGLAB (Delorme and Makeig, 2004; Delorme et al., 2007). For each participant, ICA was performed on non-causal dataset and the independent components (IC's) were then applied to causal dataset. After rejection of

components corresponding to horizontal eye movements and blinks (median=3, min=1, max=7), baseline correction was performed. Artifactual data epochs were then removed based on an absolute threshold value larger than 100 μV and an absolute linear trend slope larger than 75 μV per epoch and R^2 larger than 0.3. The median number of Bubble trials accepted for analysis was: face trials = 697 [min: 663, max: 716] out of 720; noise trials = 349 [min: 329, max: 359] out of 360.

Last, single-trial spherical spline current source density waveforms were computed by using the CSD toolbox (Kayser et al., 2009; Tenke et al., 2012). CSD waveforms were computed using parameters 50 iterations, m=4, lambda=10^{-5}. The head radius was arbitrarily set to 10 cm, so that the ERP units in all figures are μV/cm^2. The CSD transformation is a spatial high-pass filtering of the data, which sharpens ERP topographies and reduces the influence of volume-conducted activity.

Mutual information

We used Mutual Information (MI) to measure the reduction of uncertainty about the response of interest (EEG or behaviour) by our knowledge of the stimulus. MI is a statistical quantity that measures the strength of the dependence (linear or non-linear) between two random variables (Panzeri et al., 2010; Magri et al., 2009; (Ince et al., 2010; 2016). In this study, MI was calculated using a bin-less rank-based approach based on Gaussian copulas, which has the advantage of being robust to outliers: a tutorial with Matlab and Python code is available in Ince et al. (2016).

Whole stimulus sampling analyses

To reveal which regions systematically produce an effect on behavioural responses, we calculated several MI quantities in every participant, independently at each pixel: MI(PIX, RT) and MI(PIX, CORRECT) to establish the relationship between each pixel's intensity distribution across trials and distributions of behavioural reaction times (RT) and CORRECT or not responses.

In terms of brain responses, we combined single-trial distributions of EEG responses together with their temporal gradient (ERP_g) into a bivariate response for each trial. This helps to assess how pixel sampling affects both the instantaneous EEG amplitude and the local signal shape (Ince et al. 2016). We then calculate MI(PIX, [ERP, ERP_g]) to establish the relationship between each pixel's intensity distribution and the bivariate responses.

This MI quantity was computed at every electrode and every time point, producing 4D MI matrix (pixels × pixels × electrodes × time points) per participant. To reveal which local information mostly influences brain responses, we computed the maximum MI(PIX,(ERP, ERPg]) across electrodes and time points separately for the left and right hemispheres. We refer to these MI maps as classification images.

Eye mask analyses

Behavioural and ERP modulations strongly co-vary with eye pixel intensity which had been found in previous studies (Rousselet et al., 2014; Jaworska et al., in prep) and chapter 2. Thus to simplify results presentation, we reduce the dimensionality of the Bubble masks per trial to track the corresponding responses. In detail, first, a left eye mask was created by drawing a circle of 16 pixel radius centred at the maximum value of the group-averaged *MI(PIX, RT)* for the original faces in the current study. Then we horizontally flipped this mask to create the right eye mask. We used these left and right eye masks to sum the pixel intensities within each eye region, leading to one scalar value representing the visibility of each eye on each trial. Last, we computed MI between scalar visibility of each eye and behaviour responses, providing new quantities: *MI(EYE, RT), MI(EYE, CORRECT).*

For brain responses, we computed MI between scalar visibility of each eye and the corresponding ERP bivariate responses, providing *MI(EYE, [ERP, ERP_g])*. We repeated the calculation for each time point and electrode to get a MI matrix (electrodes vs. time points) for each eye mask. To avoid missing any effect, instead of identifying one electrode per hemisphere we obtained maximum MI(EYE, [ERP, ERP_g]) across contralateral posterior lateral electrodes of interest for each eye mask, hereafter MI curves. To reveal which electrodes are involved in eye information processing, we computed maximum MI(EYE, [ERP, ERP_g]) across time points for each eye mask to obtain topographic maps.

MI latency measures

The latency measure that depends on one time point is problematic because of a lack of robustness with respect to the time selected (Ince et al., 2016). Figure 2.5B (left) shows curves with low variability, the latency of which can be appropriately quantified by a simple peak-to-peak measure. However, if the peak-to-peak measure is applied to examples in the middle and right, the difference in latency is too small (middle) and in the

wrong direction (right). These differences do not reflect the real relationship between two curves. Thus instead of a simple peak-to-peak measure, we adopted 'integral latency' approach from Ince et al. (2016a) that considers the latency over a range of MI values. For curves with multiple peaks, integral latency approach more sensibly reflects the actual relationship. First, we normalised MI curves in the range of [0-1] in the time window 100 – 300 ms post-stimulus. We split the range of normalised MI values where both curves were significant into 100 values. We then averaged the latency differences between two MI curves over these 100 MI values. The corresponding latency is the fitted value calculated by using piecewise linear interpolation (fit function in MATLAB).

Electrode selection

The N170 was quantified at two electrodes of interest, LE & RE, one per hemisphere on which we restricted to 19 posterior-lateral electrodes (same as chapter 2). For upright faces, the electrode selection was based on *UPRabove*, for inverted faces on *INVbelow*, which both correspond to stimuli in chapter 2. LE & RE were identified independently for each face orientation as the electrodes with maximum MI(EYE, [ERP, ERP_g]) across electrodes and time points.

Results

Throughout the chapter, unless stated otherwise, (1) median is the Harrell-Davis estimates of the 0.5 quantile (Harrell & Davis, 1982); (2) 95% confidence intervals (CI) were computed using the percentile bootstrap technique, with 1000 samples. (3) three contrasts of interest compared upright and inverted faces when the eyes of these faces were presented in the same position, in which the eyes appeared *Above*, *Below* or at the *Centre* of the screen. (3) red is used for the upright condition, blue for the inverted condition.

Task related information: the eye area

In practice trials, regardless of orientation and position, faces were detected in high accuracy (upright, *Above*: mean correct = 100% [98.21%, 100%], *Centre*: 100% [99.11%, 100%], *Below*: 100% [99.12%, 100%]; inverted, *Above*: 100% [99.34%, 100%], Centre: 100% [98.43%, 100%], *Below*: 100% [99.12%, 100%]) and short reaction times (upright, *Above*: median RT = 281.32 [254.27, 335.36] ms, *Centre*: 272.97 [248.01, 343.78] ms, *Below*: 279.18 [253.6, 341.57] ms; inverted, *Above*: 303.52 [280.12, 333.31] ms, *Centre*: 286.55 [265.75, 321.34] ms, *Below*: 289.76 [268.21, 314.55] ms). When the eyes of upright and inverted faces were presented in the same position, no significant differences between upright and inverted faces can be found in terms of accuracy ($differences_{upright-inverted}$, *Above*: 0% [1.11%, 0%], *Centre*: 0% [-1.24%, 2.17%], *Below*: 0% [-1.12%, 1.49%]) and RT ($differences_{upright-inverted}$, *Above*: -13.15 [-52.3, 23.47] ms, *Centre*: -13.43 [-46.8, 29.58] ms, *Below*: -0.38 [-39, 39] ms).

For Bubble trials, we quantified the relationship between behavioural modulations and each pixel's intensities from Bubble masks. We found that RT modulations were strongly associated with pixels representing the eye region in the images of face, particularly the left eye for each condition (Figure 3.2). We then compared across participants the maximum MI value between upright and inverted faces for each position. There was larger left eye sensitivity in inverted faces compared to upright when the eyes of these faces appeared at *Above* ($differences_{upright-inverted}$, -0.02 [-0.03, 0) bits). No such effect can be seen at *Centre* (0 [-0.02, 0.01] bits) and *Below* (0.01 [0, 0.04] bits). For CORRECT or not, besides eye sensitivity, weaker sensitivities to nose, the forehead and parts of cheeks can also be seen. Face inversion did not affect eye sensitivity at each position ($differences_{upright-inverted}$, *Above*: -0.01 [-0.03, 0.01] bits, *Centre*: 0[-0.02, 0] bits, *Below*: 0 [-0.02, 0.02] bits).

For texture trials MI value was low. Therefore, we only considered the face trials in the ensuing analyses. For all pairwise comparison results, see Figure S3.1.

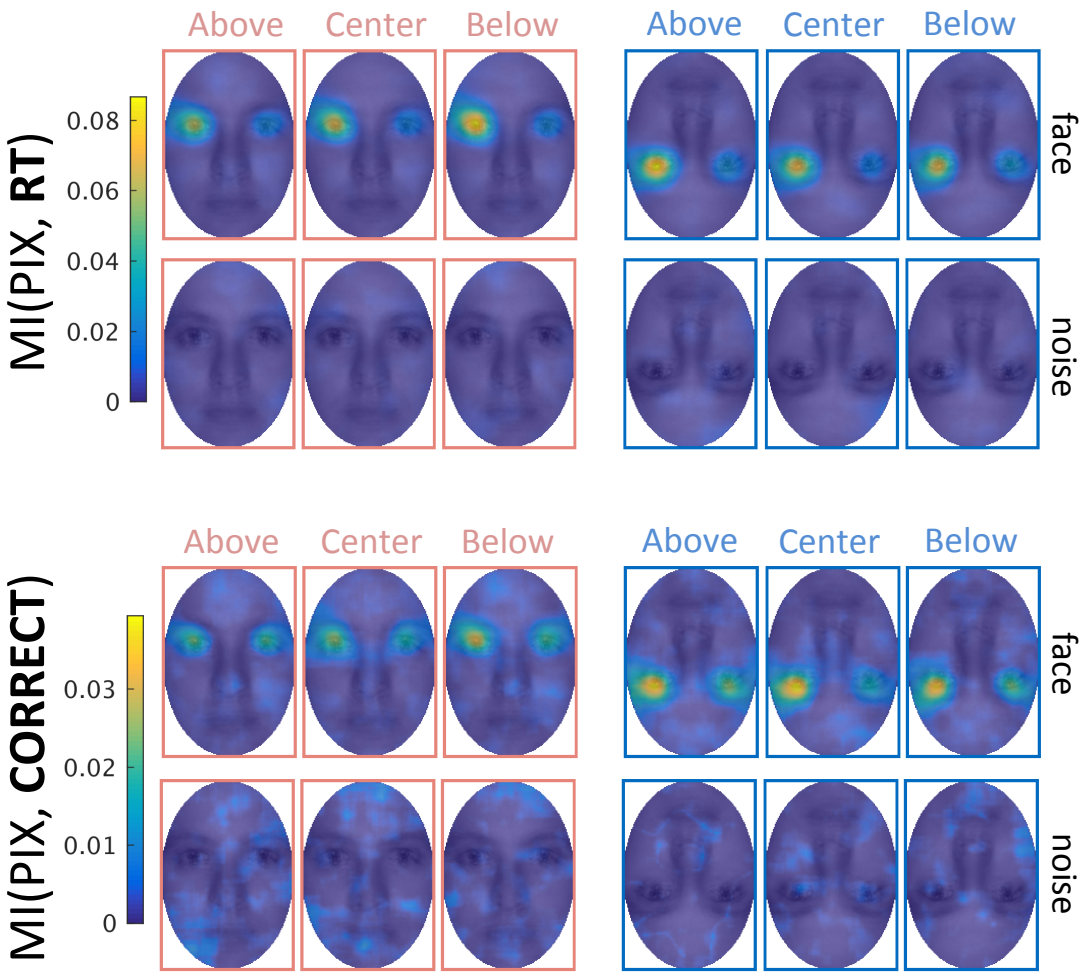

Figure 3.2 Group-averaged MI classification images for RT and correct

In addition to eye sensitivity, there was weaker sensitivity to the nose, the forehead and parts of the cheeks in accuracy results.

To determine how the visibility of the left eye modulates behaviour, we next applied reverse analyses. We group the face trials into 10 equi-populated bins according to left eye visibility, and then computed mean accuracy and median RT of the trials in each bin. The differences between bin 1 and bin 10 revealed that regardless of face orientation and position 8 out of 8 participants responded quicker and more accuracy to images of faces with increased left eye visibility (Figure 3.3). For upright and inverted faces the visibility of the left eye modulated RT to the same extent regardless of position. The eye sensitivity was stronger for upright faces compared to inverted when the eyes were presented at *Above*. There was no difference in eye sensitivity between upright and inverted faces at *Centre* and *Below*. For all pairwise comparison results, see Figure S3.2.

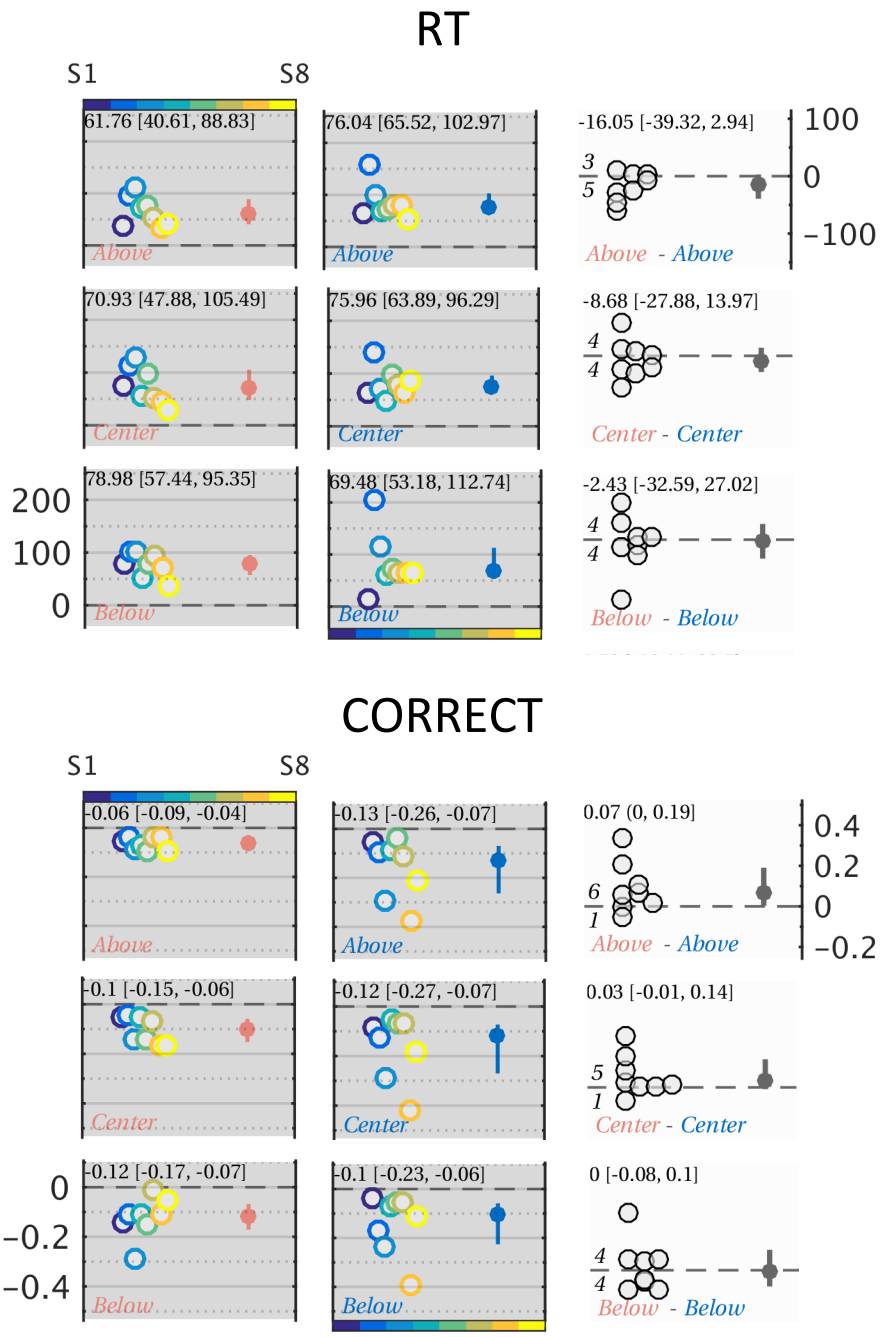

Figure 3.3 Behavioural modulations

Upper panels are for RT, lower for correct. In the first (upright faces) and second (inverted faces) column, scatterplots show the behavioural performance differences (bin1 - bin10) for participants (colour-coded circles) and group medians with 95% CI (disks and horizontal bar), separately for each face condition. In the third column, the black scatterplot shows the distribution of differences of modulations (bin 1 - bin 10) between upright and inverted faces per condition. The group results are also detailed on the top. Italic numbers above or below the x-axis show the number of circles above or below the x-axis.

Face inversion related changes in the N170 when the eyes appeared in the same position

Using information-theoretic analyses coupled with reverse analyses, we found that left eye information influences face detection behaviours more in inverted faces compared to upright when the eyes appeared at *Above*. We next investigated the face inversion related differences in the N170 waveform when the eyes were presented in the same position (Figure 3.4). We averaged CSD ERPs across practice trials (without Bubbles) for each participant at two selected electrodes (LE & RE), independently for each face condition. These electrodes that recorded the maximum MI(PIX, [ERP, ERP_g]) across left and right posterior-lateral sensors of interest were selected based on *UPRabove* and *INVbelow*. One participant was singled out in the N170 measure because of poor signal in the practise block.

At LE the N170 amplitude was similar for upright and inverted faces for each position. The latency of the N170 was delayed by face inversion, which can be observed in 6/7 participants when faces were presented at *Above* and *Centre* position, 7/7 for *Below*. At RE the amplitude of the N170 was larger for inverted than upright faces independently of position. This effect was observed in 6/7 participants for *Above*, 7/7 for *Centre* and *Below*. The N170 latency was also delayed by inversion at *Above* and *Centre*, which was observed in 7/7 and 6/7 participants. At *Below*, the inversion effect was not significant with 4/7 participants showing delayed N170.

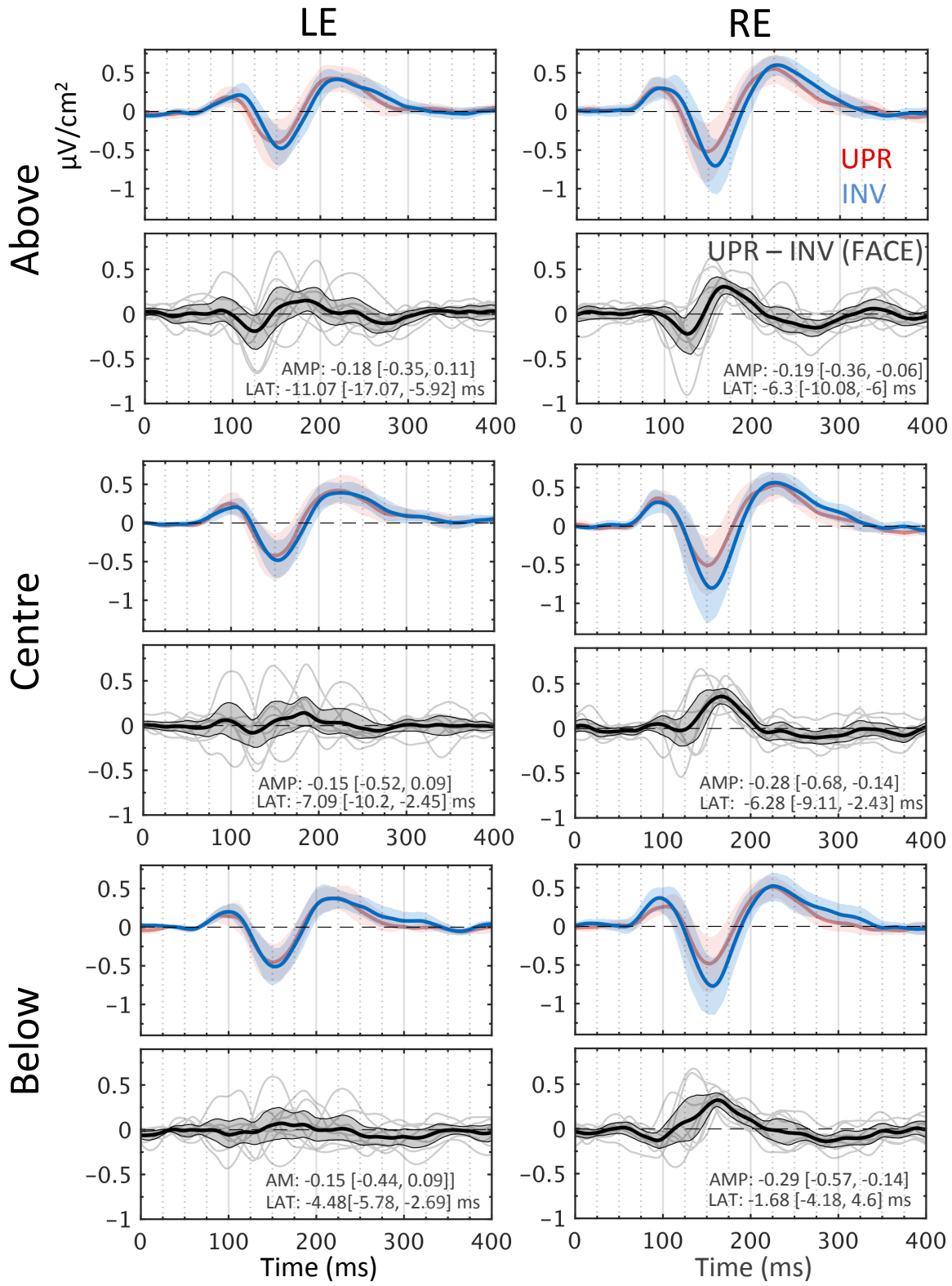

Figure 3.4 Group-averaged ERPs for face trials without bubbles

Left and right columns show results from LE and RE. First row shows the mean N170 across 7 participants and 95% CI for upright and inverted intact faces at *Above*. The thick black line in the second row shows the mean across participants of the differences between upright and inverted faces. The shaded areas show the 95% CI. Thin grey lines show individual results. The third and fourth row are for *Centre*, the last two rows are for *Below*. For amplitude, we report the median of

the inversion index, whereas for latency we report the median of the differences in ms.

Eye sensitivity contralateral to posterior-lateral electrodes

We next replicated the previous studies reporting strong EEG sensitivity to the contralateral eye. We computed maximum MI(PIX, (ERP, ERP_g]) across two regions of interest, left and right posterior-lateral sensors and time points, to obtain classification images for each participant. Figure 3.5A showed strong dependence between pixels representing eye regions and ERP bivariate responses recorded at contralateral posterior lateral electrodes for each face condition. Topographic maps showed that this association is larger in the right hemisphere (Figure 3.5B) for 7 out of 8 participants (Figure S3.3-3.10), which in line with right hemisphere dominance for face processing (Sergent, Ohta, & MacDonald, 1992). However, one participant showed larger contralateral eye sensitivity in the left hemisphere versus right for each face condition (Figure S3.6). Additionally, we are not interested in the differences between the left and right hemisphere. Thus, we focused on EEG sensitivity recorded from the dominant hemisphere to reduce the dimensionality of data in the following analyses. For textures there were no clear MI clusters.

Face inversion weakened the contralateral eye sensitivity in the N170 time window when the eyes appeared in the same position

To determine how this contralateral eye sensitivity evolved over time, we obtained maximum MI(EYE, (ERP, ERP_g]) across contralateral posterior lateral electrodes of interest, refer to as MI curve. Figure 3.5B showed group averaged MI curve was strong in a time window 100 – 300 ms and peaked ~ 150 – 200 ms for each face condition.

We next determined how MI curves affected by face inversion for each position. In chapter 2, we found that face inversion weakened contralateral eye sensitivity in the transition between the P1 and the N170 (Figure 2.5). Therefore, we focus on same time window: 100 – 200 ms. When the eyes were presented at *Above*, there was no difference between upright and inverted faces in the time window of interested (Figure 3.5C). For *Centre* and *Below*, larger contralateral eye sensitivity can be found ~ 140 – 160 ms and ~ 130 – 170 ms for upright versus inverted faces.

We also provide single participant results to determine if the majority of participants showed results consistent with these group results. We applied a permutation test combined with method of maximum statistics to determine statistical significance and

control for multiple comparisons (Holmes et al., 1996). For each of 1000 permutations, we randomly shuffled summed pixel intensities within each eye mask (details in *region of interest analysis*) across trials. We then repeated the MI(EYE, (ERP, ERP_g]) calculation for contralateral posterior-lateral electrode of interest and time points for each permutation, producing an MI matrix (electrodes × time points × permutation). We then took the maximum value of MI across electrodes and time points as a permutation distribution and compared the real MI(EYE, (ERP, ERP_g]) against the 95^{th} percentile of the permutation distribution as the statistical threshold separately for the left and right hemisphere. Figures S3.3-3.10 detail, for every participant, how contralateral eye sensitivity unfolded over time, and when it reached significance.

Then we obtained the absolute differences of maximum MI between upright and inverted faces across electrodes of interest, leading to a vector or each permutation and each hemisphere. We computed maximum of the resulting MI vector for each permutation. For each participant we compared differences of original MI(EYE, (ERP, ERP_g]) between upright and inverted faces against the statistical threshold.

To give complementary information to group analyses, we focus on the same time windows: ~ 140 – 160 ms for *Centre* and ~ 130 - 170 ms for *Below* as illustrated in group analyses. At *Centre,* 5/8 showed a weaker effect in inverted compared with upright faces, 1/8 showed no effect and 2/8 showed stronger one. At *Below*, 6/8 showed a weaker effect in inverted compared with upright faces, 1/8 showed no effect and 1/8 showed stronger one (Figure 3.5C). Noted that in ~ 140 – 170 ms, At *Above*, 5/8 participants showed weaker contralateral eye sensitivity in inverted versus upright faces, 1/8 showed no effect and 2/8 showed stronger effect.

Because the non-causal high-pass filter might distort onsets of ERPs (Acunzo, MacKenzieb, & van Rossum, 2012; Rousselet, 2012), we also applied permutation analysis to the causal dataset. Figure S3.12 reports that no difference between upright and inverted faces ~ 100 ms in each position, in which the eyes appear.

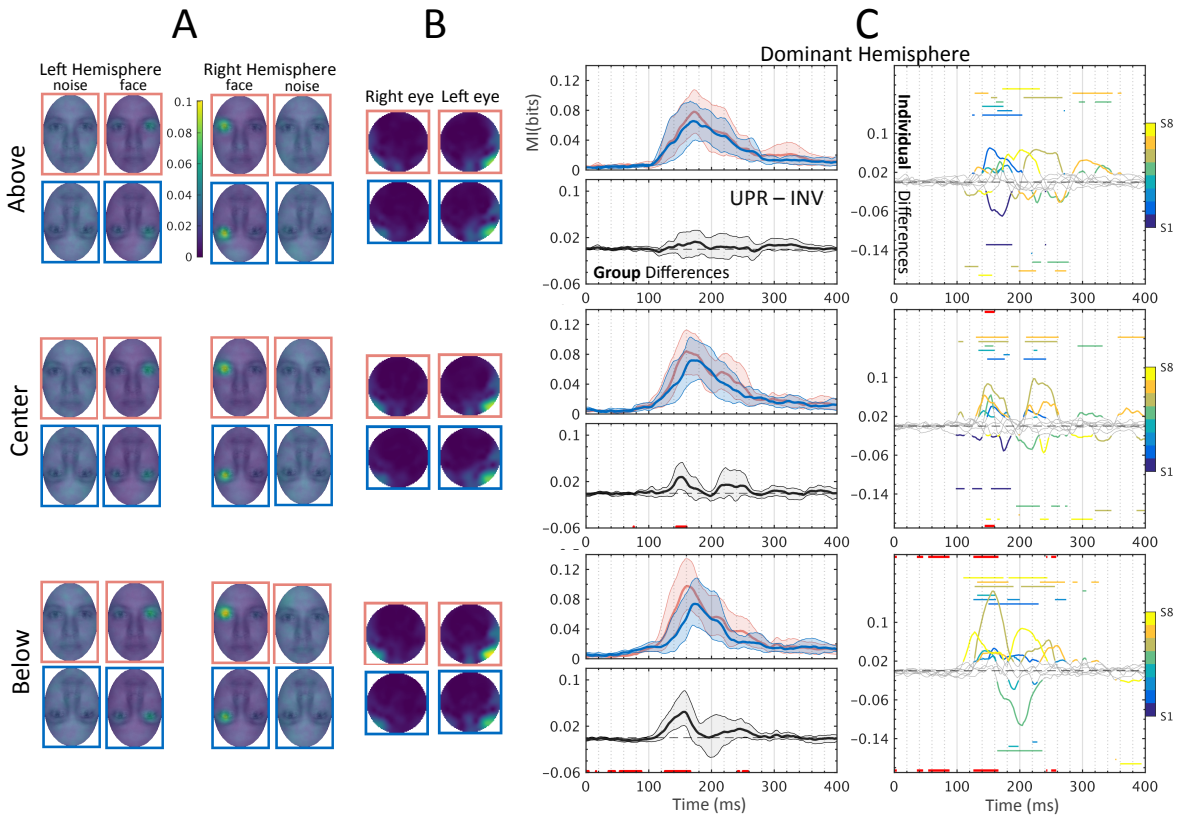

Figure 3.5 MI EEG results (in bits)

(A) Group averaged MI classification images show contralateral eye hotspots only for face trials. No clear MI cluster in noise trials. **(B)** Group-averaged topographic maps indicate MI congregate at posterior-lateral electrodes, primarily right hemisphere electrodes. **(C)** Group MI curves are placed in the left. In the first, third and fifth row, the panels illustrate the time course of group averaged MI for each face condition. Curves with shades show mean maximum MI across 8 participants with 95% CI. In the second, fourth and last row, panels show mean across participants of the MI differences between upright and inverted with 95% CI. The red horizontal bar indicates time points of significant differences. The right panels show individual differences. Colour parts of waves indicate statistically significant differences per participant. Colour-coded horizontal lines above the x-axis show stronger effects in upright versus inverted, and opposite effects are placed below. All pairwise comparison results are shown in Figure S3.11.

Face inversion delayed processing of the contralateral eye when the eyes appeared in the same position

We next quantify the relative time between upright and inverted faces in processing of the contralateral eye information in the dominant hemisphere per position. Instead of peak-to-peak measures, we applied 'Integral Latency' approach that adopted from Ince, et al. (2016). This approach can measure latency difference between two curves over values at a range of y-axis value. In detail, we first normalised the MI curves to the range of [0-1] and

then calculated the average delay between two MI curves over the *y*-axis region where both were significant (Figure 3.6A). There was no latency difference between upright and inverted faces at *Above*. At *Centre* and *Below* face inversion prolonged integral latency of contralateral eye sensitivity. However, whatever the position of the eyes, the majority of participants showed delayed contralateral eye sensitivity by face inversion for each position (*Above*: 6/8 participants, *Centre*: 7/8, *Below*: 7/8).

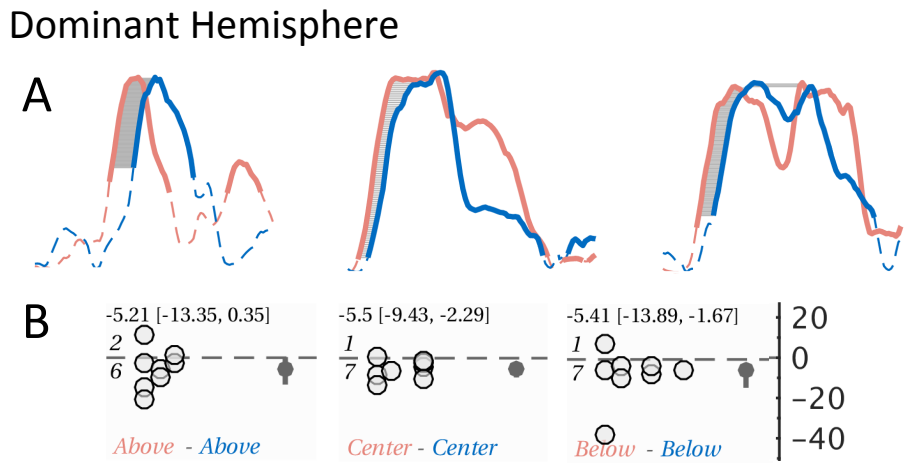

Figure 3.6 Integral latency

(A) Integral latency calculation visualization. Red and blue lines respectively refer to the normalised MI curves of upright and inverted faces. Thicker sections of the MI curves represent statistical significance. Shaded region refers to the delays between two curves over the y-axis region where both were significant. **(B)** Integral latency differences (in ms) between upright and inverted faces per position. Each scatterplot shows the distribution of individual differences between upright and inverted faces (black circles) and group medians with 95% CI (black disk and horizontal bar). The pair to compare and the direction of differences are illustrated on the bottom. The group results are also detailed on the top. Italic numbers above or below the x-axis show the number of circles above or below the x-axis. All pairwise comparisons results are shown in Figure S3.13.

Contralateral eye visibility modulated ERPs

We next applied the reverse approach as used previously for behaviour to determine how the presence of the eyes modulates single-trial ERP distributions recorded at contralateral electrodes. We grouped the face trials into 10 equi-populated bins according to the visibility of the contralateral eye, and then computed the mean ERPs for each bin. Figure 3.7 visualize how the contralateral eye visibility covaried with the N170 waveform. We then quantified the N170 peak modulations. We found that increasing left eye visibility

resulted in a larger and earlier N170 for each face condition for most of participants. The differences in the amplitude and latency modulation of the N170 peak by the presence of the left eye between upright and inverted faces were not significant for each position. This suggests the N170 reflects eye coding mechanisms in all face conditions.

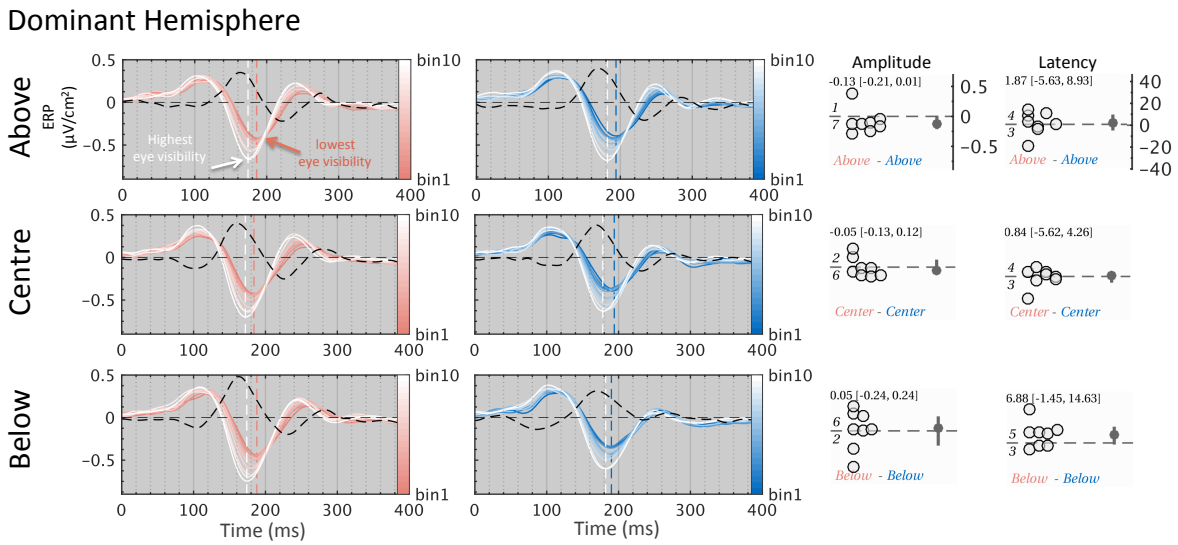

Figure 3.7 ERPs modulations due to left eye visibility

Averaged ERPs are colour-coded at each level of contralateral eye visibility. The red and white vertical dash lines mark the N170 peak of bin1 (lowest eye visibility) and bin10 (highest eye visibility). Differences (bin1 - bin10) are shown in the black dashed curve. Differences of ERP peak (bin1 - bin10) show the N170 for upright faces is enlarged (*Above*: 0.2 [0.1, 0.36] μV/cm^2, *Centre*: 0.29 [0.14, 0.46] μV/cm^2, *Below*: 0.32 [0.15, 0.49] μV/cm^2) and peaks earlier (*Above*: 16.2 [10.8, 19.74] ms, *Centre*: 14.11 [8.94, 19.92] ms, *Below*: 16.34 [13.03, 19] ms) as contralateral eye visibility increased. Similarly, for inverted faces, a significant enlarged (*Above*: 0.3 [0.19, 0.43] μV/cm^2, *Centre*: 0.3 [0.24, 0.39] μV/cm^2, *Below*: 0.27 [0.16, 0.46] μV/cm^2) and earlier N170 (*Above*: 15.3 [6.13, 20.98] ms, *Centre*: 16.08 [9.59, 21.05] ms, *Below*: 8.06 [0.44, 18.59] ms) can be observed. The scatterplots show that the N170 amplitude and latency modulations are similar between upright and inverted faces (upright - inverted) for each position. The group results are also detailed on the top. Italic numbers above or below the x-axis show the number of circles above or below the x-axis. All pairwise comparisons results are shown in Figure S3.14.

In addition, to replicate results in chapter 2, we are interested in the differences between two face conditions, upright faces with the eyes appeared at *Above* (abbr. *UPRabove*), and inverted faces with the eyes were presented at *Below* (abbr. *INVbelow*). These two face conditions are the same stimulus used in chapter 2. We here replicated previous findings in chapter 2.

First, at LE, the N170 amplitude was similar between *UPRabove* and *INVbelow*; but face inversion delayed the latency of it (differences$_{\text{upright-inverted}}$, -0.26 [-0.45, 0.08] μV/cm^2; -7.69 [-12.12, -4.55] ms); at RE the N170 peak was enlarged and delayed by face inversion (-0.25 [-0.4, -0.12] μV/cm^2, -4.89 [-7.29, 3.35] ms). Second, we found that the visibility of left eye region influenced face detection behaviour for *UPRabove* and *INVbelow* to the same extent (Figure S3.1, Figure S3.2). Third, in terms of bivariate brain sensitivity to eye regions, we found the processing of contralateral eye underlying the N170 was weakened in the transition between the P1 and the N170 for *INVbelow* versus *UPRabove* in the right hemisphere (Figure S3.11). There were no group-level differences in integral latency of contralateral eye sensitivity between *UPRabove* and *INVbelow*, (Figure S3.13). Fourth, reverse analyses revealed that the N170 modulation due to the left eye visibility in *UPRabove* is comparable with that in *INVbelow* at RE (Figure S3.14). Further, these results were consistent with single-participant analysis.

Discussion

In the previous chapter, we have found that the N170 waveform was modulated by the presence of the contralateral eye in the image whatever the orientation of faces, but the early processing of contralateral eye was weakened in the transition between the P1 and the N170 and delayed by face inversion. However, for the image of faces used in chapter 2, the eye position and face orientation were confounded. In the current study, we manipulated three vertical locations of images in which the eyes are presented in upper, centre and lower visual field relative to fixation cross (the centre of the screen).

First, we here replicated findings in chapter 2 by comparing upright and inverted faces, in which the eyes appeared upper and lower visual field correspondingly. Second, regardless of face orientation and position, earlier and larger N170 peaks were associated with higher visibility of the contralateral eye, suggesting eye coding mechanisms underlying the N170 in all face conditions. Third, face inversion delayed the eye coding and weakened it in the N170 time window, when the eyes of faces were presented in the same position, *Above*, *Below* or at the *Centre* of the screen. The results suggest that face inversion related changes in processing of the contralateral eye cannot be simply considered as the results of differences of eye position.

Eye regions are diagnostic for face detection

Figure 3.2&3.3 showed that regardless of face orientation and position the presence of the eyes was associated with face detection behaviours. Participants responded quicker and more accuracy to images of faces with increased eye visibility (Figure 3.3). These results are in line with previous studies (Rousselet et al., 2014; Jaworska et al., in preparation) and chapter 2, suggesting that eye information was used to detect faces accurately and quickly. We next investigated how face inversion affected behaviour modulations when the eyes were presented in the same position. Figure 3.3 found that left eye information influences face detection behaviours more in inverted faces compared to upright when the eyes appeared at *Above*. One possible explanation for the stronger dependence on the eyes is that less feature information, besides the eyes, of inverted faces can be collected from foveal vision compared to upright faces when the eyes were presented above the fixation cross.

Face inversion weakened contralateral eye coding in the early N170 and delayed this pattern when the eyes appeared at the same position

In terms of brain activity, consistent with previous findings (Rousselet et al., 2014; Jaworska et al., in preparation, Yi et al., in preparation), we found EEG sensitivity to the eyes contralateral to the posterior-lateral electrodes, which peaked in the time window 100 – 200 ms post-stimulus for each condition in face trials (Figure 3.5).

Importantly, for most of our participants, face inversion delayed the coding of the contralateral eye and weakened it in the N170 time window, when the eyes of faces were presented in the same position, *Above*, *Below* or at the *Centre* of the screen (Figure 3.5&3.6). The results are in line with one previous monkey study (Taubert et al., 2015). They found that the face inversion reduced neuronal response in the middle and anterior lateral face patches, when the eyes appeared in the same position. Our results suggest that face inversion related changes in processing of the contralateral eye cannot be simply considered as the results of differences of eye position.

Using fMRI, de Haas et al., (2016) showed that the location influences the processing of isolated face parts. They found that right inferior occipital gyrus responded more when the eye appeared in the upper visual field than in the lower visual field. They also reported the recognition cost of reversed locations of individual features was equal to 60% of that for whole face inversion. Thus, the FIE cannot be fully explained by atypical positions of isolated features (i.e., the eyes appearing in the lower visual field). It is important to note that 7 out 8 participants showed right hemisphere dominance for face processing (Sergent, Ohta, & MacDonald, 1992), one showed left hemisphere dominance. In our case, for pairwise comparisons in contralateral eye sensitivity between face conditions we focused on the recordings from the dominant hemisphere. Thus, our results cannot be directly compared to that of de Haas et al. (2016).

Conclusion

In summary, face inversion still delayed the eye coding and weakened it in the N170 time window, when the eyes of faces were presented in the same position, *Above*, *Below* or at the *Centre* of the screen. The results suggest that face inversion related changes in processing of the contralateral eye cannot be simply considered as the results of differences of eye position.

Chapter 4: Low Eye Saliency and Contrast Polarity Reversal Impair Contralateral Eye Coding In A Face Detection Task

Introduction

Face detection is an easy and essential daily task. Humans can detect faces with extremely limited information, i.e., images consisting of only a few pixels (Bentin et al., 2002) and faces masked through noise (Jiang et al., 2011; Rousselet et al., 2008). Thus, the whole of the face is not necessarily involved in face detection (Ullman et al., 2002).

A key question is what specific image properties enable us to perceive faces so efficiently. Recent research reported that filtering out or randomizing horizontal phase information of images hampers face detection and identification behaviour, suggesting that diagnostic information is in a horizontal band (Balas et al., 2015; Dakin and Watt, 2009; Goffaux, 2010; Pachai et al., 2013). However, it is still unclear what face features have a privileged role in driving face detection performance, as horizontal information is spread across the entire face including the eyes, the mouth and the bottom of the nose. Pachai (2015) reported that the horizontal structure from the eyes is preferentially extracted during face identification tasks. This result is consistent with previous evidence that information sampling is biased to the eye region in face categorisation task (Gosselin and Schyns, 2001; Peterson and Eckstein, 2012; Sekuler et al., 2004). Thus, information in the eye regions might be the major contributor to face categorisation performance.

Behavioural measures represent the output of a sequence of processing, while electrophysiological recording allows continuous track the time course of processing of eye information. The face preferential event-related potentials (ERP) component has been found to peak ~ 170 ms after stimulus onset in human scalp recordings. The N170 is larger in amplitude for face compared to non-face stimuli (Rossion and Jacques, 2008; Bentin et al., 1996; Rossion and Jacques, 2011). Previous Bubble studies have illustrated that the eyes are primarily processed in the N170 time window across tasks (Rousselet et al., 2014; Schyns et al., 2003, 2007, 2007, 2011, Smith et al., 2004, 2007, 2009). Similarly, a monkey study revealed independent processing of local feature occurred in the early responses (60 – 100 ms following image onset), suggesting bottom-up face processing is feature-based.

With bottom-up processing, visual attention is directed to salient areas that based on the basic information of an input image such as intensity (Itti et al., 1998, p. 1; Itti and Koch, 2000; Parkhurst et al., 2002). In human faces, eyes are inherently more salient compared to other parts of the face, on the basis of the physical properties of faces, such as local contrast and luminance (Zerouali et al., 2013). For accurate face identification, information is extracted within the first one or two fixations (Hsiao, n.d.) that are biased to the centre of the face, just below the eyes (Peterson and Eckstein, 2012). This evidence leads us to a question of whether the coding function to encode the eyes is due to the significance in the eye regions.

To address the question, we introduced two altered version of original faces: normalised and reversed contrast faces in a face detection task. For normalised contrast faces, we equalised the local contrast across a face so that the eyes were not standing out. The face maintained the structure, such as the lines and edges of facial features as a function of their higher-order statistics. Reversed contrast faces were generated by reversing the contrast polarity of faces, i.e., turning dark regions light and vice versa. Amplitude spectrum and contrast variance are controlled, so that reversed polarity faces are not darker than their positive counterpart. We then used the Bubble technique, similar to Rousselet et al. (2014), to sample the input image space through randomly selected Gaussian apertures. We then computed mutual information to map, independently per participant, the relationship between pixel intensities of the image, and behaviour and brain activity (Ince et al., 2016b). Because uncontrolled amplitude spectrum differences across stimuli might affect brain measurements (Bieniek et al., 2012; Clarke et al., 2012), the power spectrum was normalised across face and noise conditions by introducing a phase-scrambled background.

Based on previous studies (Rousselet et al, 2014; Schyns et al., 2011; Smith et al, 2007), we first predicted that the eye region is the major contributor to ERP and behavioural response modulations to original face images. If contralateral eye sensitivity is purely due to eye feature processing, for normalised contrast faces we should observe that brain activity is sensitive to the pixels of the eyes and the pattern of the activity remained unchanged. Furthermore, for reversed contrast face, since reversed contrast of a face influences the feature per se, we should observe lower contralateral eye sensitivity compared to original and normalised faces. If higher local contrast within the eye region is the only contributor to contralateral eye sensitivity, for normalised contrast faces we expect to observe the association between eye pixels and brain activity is weaker than for other two face conditions because of less eye saliency compared to other face conditions. In

addition, for reversed contrast faces that maintain the eye saliency, the eye sensitivity should be similar between original and reversed contrast faces. If these two factors in combination affect processing of the eyes, we should observe that an impaired processing of the eyes in normalised and reversed contrast faces compared to original faces.

Method

Participants

Twenty-four participants (16 females, median age=26; age range 21-31) took part in the study. Prior to the experiment, all participants signed an informed consent form and filled in a general health questionnaire. Participants' visual acuity and contrast sensitivity were assessed using a Colenbrander Mixed Contrast Card Set and a Mars Letter Contrast Sensitivity Test. All participants had normal or corrected to normal visual acuity and contrast sensitivity. Participants did not report history of mental or physical illness including neurological conditions, head injury, or taking psychotropic medications at the time of testing or prior. The study was approved by the local ethics committee at the College of Science and Engineering, University of Glasgow (approval no. CSE01361), and conducted in line with the British Psychological Society ethics guidelines. Participants were compensated £6/h. Participants received £6 per hour.

Stimuli

All stimuli were 9.3° x 9.3° of visual angle (256 x 256 pixels), had 0.02 contrast variance, and the same amplitude spectrum, set to the mean across faces. The face oval was 4.9° x 7.0° of visual angle. Figure 4.1 shows examples of stimuli. The original face stimuli were gray-scale pictures of 10 individuals (Gold et al., 1999). Normalised contrast faces were generated by first whitening the power spectrum of the original faces, followed by contrast normalization using a 16-pixel Gaussian neighborhood (Simoncelli and Olshausen, 2001). Reversed contrast faces were generated by reversed the contrast polarity of faces i.e., turning dark regions light and vice versa. Textures were created by using the Portilla-Simoncelli algorithm with parameters set to four scales, four orientations, a 9×9 spatial neighborhood, and 50 iterations (Portilla and Simoncelli, 2000). Synthesized textures had the same second and higher-order statistics as the original faces, without their global shapes. Unlike unnatural artificial textures such as white noise, random dots or repeat shapes, our textures contain disorganized local elements like edges and 'blobs' that are similar to corresponding original faces from the real world.

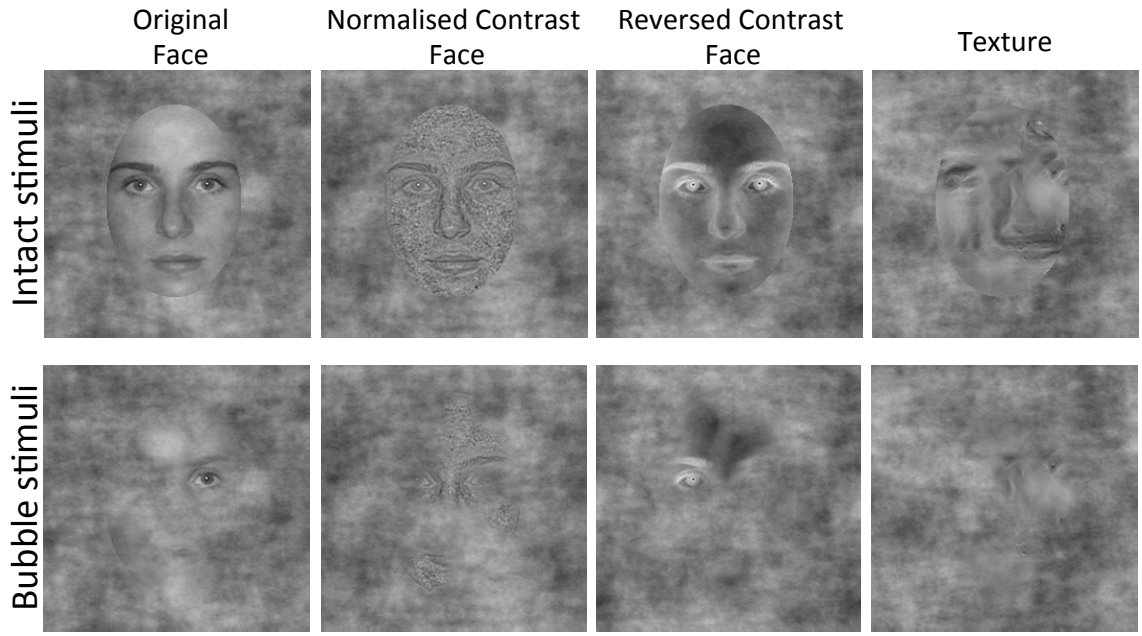

Figure 4.1 Examples of stimuli

The first row shows examples of intact stimuli presented in the practice block. The second row shows examples of stimuli masked by ten Bubbles.

In the bubble blocks, all images were masked with 10 two-dimensional Gaussian apertures (σ = ~ 0.55°), hereafter referred to as Bubbles with the constraint that the centre of each Bubble was randomly located in the face oval (Figure 4.2). To avoid global image contrast differences due to the sampling of different face features in Bubble trials, the Bubbles were embedded in a background of phase-scrambled noise that had the same power spectrum as the original faces.

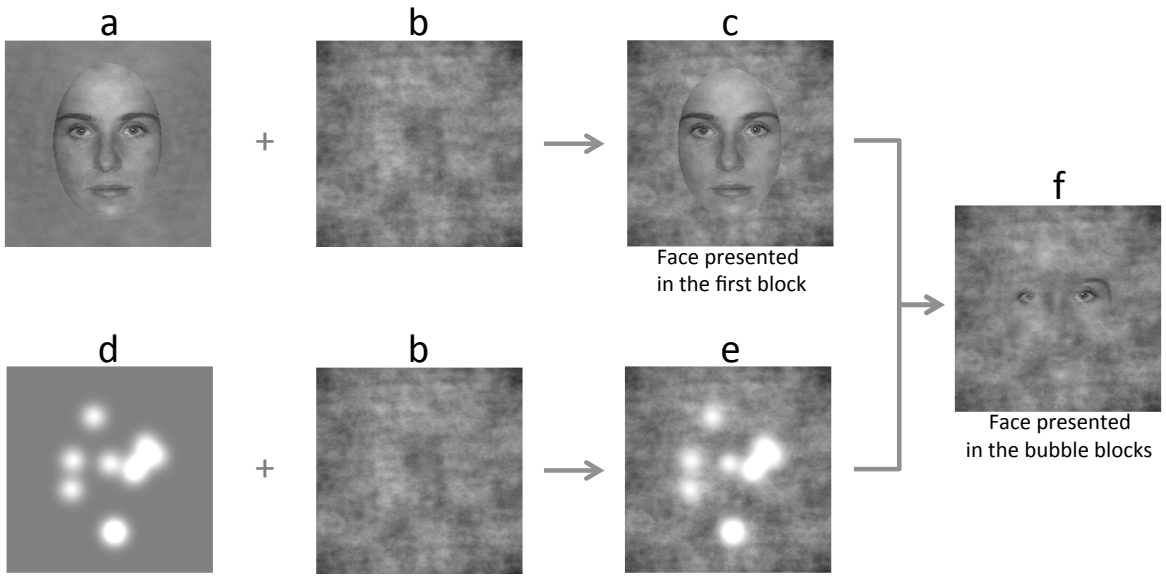

Figure 4.2 Stimulus generation

(a) An example of front view, oval-cropped original face. (b) Phase-scrambled noise with the same power spectrum as the face stimuli. (c) Face combined with the phase-scrambled background for practice block. (d) Ten randomly sampled Gaussian apertures. (e) Ten Bubbles embedded in the phase-scrambled noise. (f) Bubble stimulus presented in the Bubble blocks.

Stimuli were displayed on a 23.6-inch VIEWPixx LCD monitor with 1920 x 1080 pixel resolution and 120 Hz refresh rate. The screen was ~ 33° x 20° of visual angle. We wrote the experimental scripts in MATLAB 2013b using the Psychophysics Toolbox extensions (Brainard, 1997; Pelli, 1997; Kleiner et al., 2007).

Procedure

Participants were tested in two sessions on two separate days in a dim and soundproof booth and viewed a series of randomly interleaved original faces (abbr. ORI), normalised contrast faces (abbr. NOR), reversed contrast faces (abbr. REV) and textures. All stimuli were presented at fixation. Viewing distance was 56 cm with a chinrest. Each trial began with a small black central fixation cross (0.4° x 0.4° visual angle) for a random time interval of ~ 500-1000 ms, followed by a stimulus presented for ~ 82 ms. A blank grey screen followed stimulus presentation.

Participants were asked to respond as quickly and accurately as possible by pressing button '1' with index finger for a face, and button '2' with middle finger for a texture on the numeric keypad of a keyboard. Feedback was given after every block on their overall performance and after block two on their performance in the previous block: median reaction time and percent correct remained on the screen until participants press a key to move on to the next block. The fixation cross, the stimulus and the blank response screen were all displayed on a uniform grey background with mean luminance 33 cd/m^2. In addition, participants were asked to try not to blink during stimulus presentation and to minimize movement during a block.

Prior to the actual experiment, we asked participants to view un-masked images in a practice block. During the actual experiment, participants responded to 12 blocks of images with Bubble masks. Each block consisted of 117 trials (10 face identities, repeated randomly), including 26 × 3 face conditions and 39 unique textures. Each session lasted up to 100 minutes.

EEG recording and pre-processing

EEG data were acquired with a 128-channel Active Electrode Amplifier System from BIOSEMI. Two additional electrodes were placed at the outer canthi of the eyes and two below the eyes.

EEG data were pre-processed using Matlab 2015b and the open-source EEGLAB toolbox (Delorme et al., 2004; Delorme et al., 2011). Data were re-referenced off-line to an average reference. The signal was then applied a 0.5-30 Hz band-pass non-causal 4^{th}-order Butterworth filter to create the non-causal dataset (zero-phase digital filtering, Acunzo et al., 2012; Rousselet, 2012; Widmann and Schröger, 2012). To check for timing distortions by the non-causal high-pass filter, we created a second dataset by applying a 2 Hz high-pass causal and a 30 Hz low-pass non-causal 4^{th}-order Butterworth filter (hereafter, causal dataset). Both datasets were epoched between -300 to 1000 ms around stimulus onset. To increase Independent Component Analysis (ICA) reliability for the non-causal dataset, channel mean was removed from each channel (Groppe et al., 2009). Channel baseline (-300 ms to stimulus onset) means were removed in the causal dataset. Noisy electrodes and epochs were detected by visual inspection of the non-causal dataset and rejected from both datasets on a participant-by-participant basis. The median number of electrodes rejected was 13 (min=5, max=28) out of 128. Infomax ICA from EEGLAB was applied to extract horizontal eye movements and blinks (Delorme et al., 2004; Delorme et al., 2007), separately on each dataset. After rejection of artifactual components (non-causal dataset: median=6; min=1; max=29; causal dataset: median=4; min=1; max=25), baseline correction was performed. Artifactual data epochs were then removed based on an absolute threshold value larger than 100 μV and an absolute linear trend slope larger than 75 μV per epoch and R^2 larger than 0.3. The median number of trials accepted for analyses was 1449 [min: 1339, max: 1517] out of 1521 per session. Last, single-trial spherical spline current source density waveforms were computed by using the CSD toolbox (Kayser et al., 2009; Tenke et al., 2012), with parameters: 10 cm head radius; 50 iterations; $\lambda = 10^{-5}$; m = 4. The ERP units in all figures are thus $\mu V/cm^2$.

Electrode selection for N170 measurements

For each participant, we report one pair of electrodes (LE & RE) selected from the left and right posterior-lateral electrodes of interest (same as chapter 2)., at which the N170 to original faces was maximal within a 200 ms time window following stimulus onset. Corresponding electrodes of interest are marked in the electrode map (Figure 4.4).

Mutual Information

Mutual Information (MI) is a non-parametric measurement of all (linear and non-linear) dependence between two random variables (Ince et al., 2009, 2016a; Magri et al., 2009;). In this study, MI was calculated using a bin-less rank-based approach based on Gaussian copulas, which has the advantage of being robust to outliers: a tutorial with Matlab and Python code is available in Ince et al. (2016a).

Whole stimulus sampling analyses

To quantify the dependence between pixel intensity in the Bubble masks and behavioural and neuronal responses, we calculated several MI quantities in every participant, independently at each pixel: *MI(PIX, RT)* and *MI(PIX, CORRECT)* to establish the relationship between each pixel's intensity distribution across trials and distributions of behavioural reaction times (RT) and CORRECT or not responses. For neuronal responses, we combined single-trial distributions of EEG responses together with their temporal gradient into a bivariate response for each trial. This helps assess how pixel sampling affects both the instantaneous EEG amplitude and the local signal shape (Ince et al. 2016a). We then calculate *MI(PIX, [ERP, ERP_g])* to establish the relationship between each pixel's intensity distribution and the bivariate responses. This quantity was computed at every electrode and every time point, resulting in one 4D MI matrix (pixels × pixels × electrodes × time points) per participant. To reveal which local information mostly influences brain responses, we computed the maximum MI(PIX,(ERP, ERP_g]) across electrodes and time points separately for the left and right hemispheres. We refer to these MI maps as classification images.

Eye mask analyses

Previous work from the lab identified that behavioural and ERP modulations strongly co-vary with eye pixel intensity (Rousselet et al., 2014; Jaworska et al., in preparation; Yi et al., in preparation). To quantify the sensitivity of behaviour and ERP to the visibility of the eyes, we performed eye regions of interest analyses. First, a left eye mask was created by drawing a circle of 16 pixel radius centred at the maximum value of the group-averaged *MI(PIX, RT)* for the original faces in the current study. Then we horizontally flipped this mask to create the right eye mask. We used these left and right eye masks to sum the pixel intensities within each eye region, leading to one scalar value representing the visibility of each eye on each trial. Last, we computed MI between scalar visibility of each eye and

behaviour responses, providing new quantities: *MI(EYE, RT), MI(EYE, CORRECT)*. For brain responses, we computed MI between scalar visibility of each eye and the corresponding ERP bivariate responses, providing *MI(EYE, [ERP, ERP_g])*. We repeated the calculation for each time point and electrode to get a 2D MI matrix (electrodes vs. time points) for each eye mask. To avoid missing any effect, instead of identifying one electrode per hemisphere we obtained maximum MI(EYE, [ERP, ERP_g]) across contralateral posterior lateral electrodes for each eye mask, hereafter MI curves. To reveal which electrodes are involved in eye information processing, we computed maximum MI(EYE, [ERP, ERP_g]) across time points to obtain topographic maps.

To compare MI between conditions, we computed the ratio: $(MI_{conditionX} - MI_{conditionY}) / (MI_{conditionX} + MI_{condtionY})$, whereas for the latency we report the median of the differences in ms.

MI Integral latency measures

We confirmed this by measuring the time it takes to integrate 50% of the contralateral eye sensitivity in different conditions. Instead of peak measurement, this method probed potential changes in the entire waveform of the MI curves. To do so, we first normalised maximum MI(EYE, [ERP, ERP_g]) across electrodes of interests per hemisphere between 0 and 1. We then measured the time at which a single participant reached 50% of normalised data by using a linear interpolation, referred to as 50IT (in ms), within 0-500ms (Bieniek et al., 2013; Rousselet, 2010).

Results

Throughout the paper, unless stated otherwise, (1) median is the Harrell-Davis estimates of the 0.5 quantile (Harrell and Davis, 1982); (2) 95% confidence intervals (CI) are computed using the percentile bootstrap technique, with 1000 samples.

Behavioural diagnostic information: the eye area

In all face conditions, pixels around the eyes, in particular, the left eye, were associated with participants' behaviour (Figure 4.3A), in line with previous studies (Rousselet et al., 2014, Jaworska et al., in preparation, Yi et al., in preparation). No such effects were observed in texture trials, despite the presence of local edges.

To quantify the contrast-related differences in this association, we compared across participants the maximum MI values between pairs of face conditions (Figure 4.3B & Figure S4.1). MI was similar between ORI and NOR (original and normalised-contrast faces) and was largest in REV (contrast-reversal faces), for the majority of participants (details in Figure S4.1). We also calculated MI values using a left eye region of interest and the results were similar to those computed by whole stimulus sampling analyses (Figure 4.3C & Figure S4.1). It suggests that participants relied on eye information to detect faces to an equal extent in ORI and NOR, and this eye sensitivity is larger in REV compared to ORI and NOR.

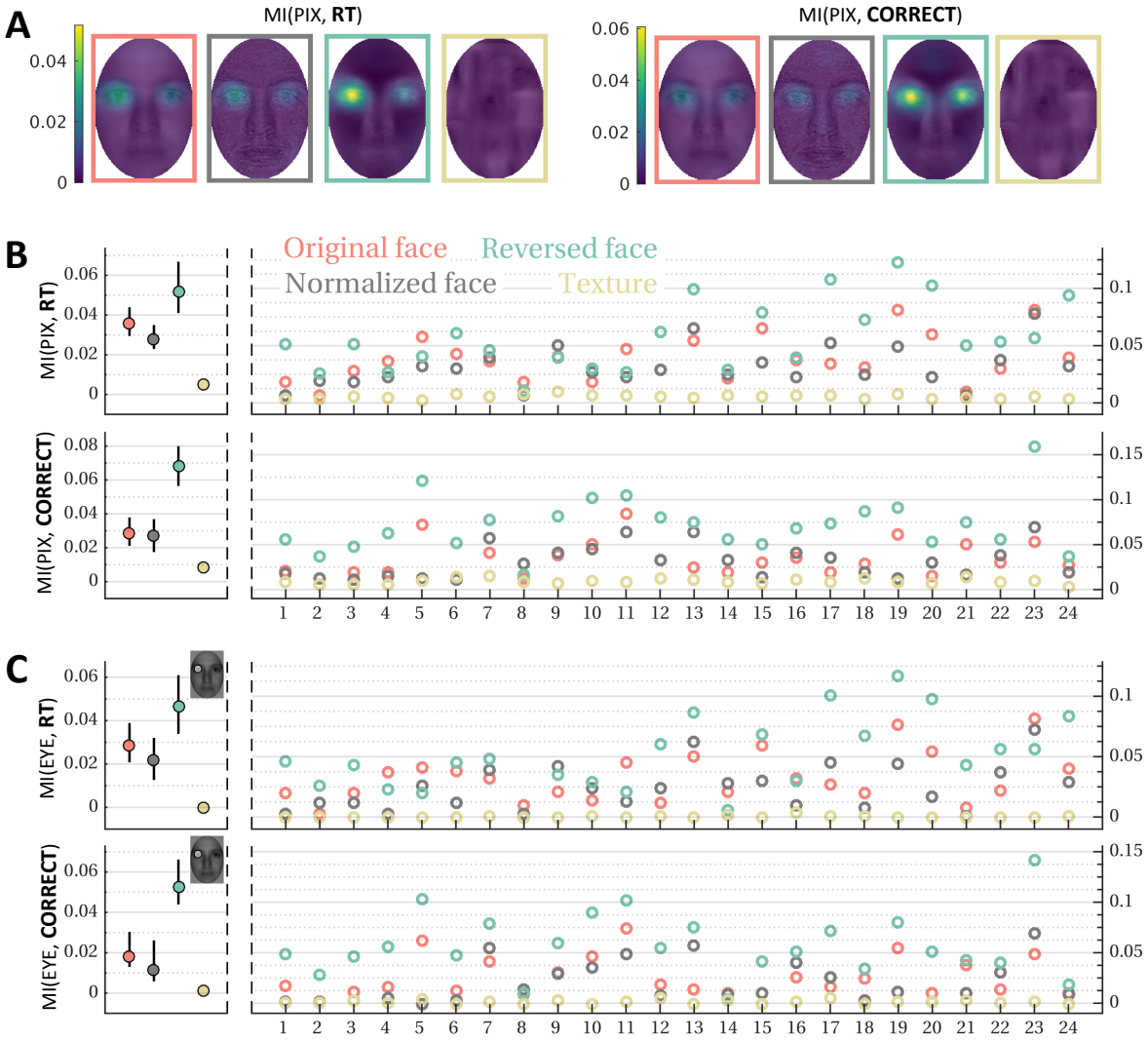

Figure 4.3 MI behavioural results (in bits)

(A) Mean MI(PIX, RT) and MI(PIX, CORRECT) across 24 participants show MI clustered around eye regions in each face condition for RT (left) and CORRECT or not (right). There was no clear MI cluster in the texture condition. **(B)** Whole stimulus sampling results. On the left the coloured disks show the group medians of the maximum MI computed across pixels. The vertical black bars indicate the 95% CI in RT (ORI: 0.04 [0.03, 0.05], NOR: 0.03 [0.02, 0.03], REV: 0.05 [0.04, 0.07], texture: 0.01 (0, 0.01]) and CORRECT or not (ORI: 0.03 [0.02, 0.04], NOR: 0.03 [0.02, 0.04], REV: 0.07 [0.06, 0.08], texture: 0.01 [0.01, 0.01]). On the right the coloured circles show individual results, with participants numbered from 1 to 24. **(C)** Eye mask results are similar to the results by using whole stimulus sampling analysis in RT (ORI: 0.03 [0.02, 0.04], NOR: 0.02 [0.01, 0.03], REV: 0.05 [0.03, 0.06], texture: 0 [0, 0]) and CORRECT or not (ORI: 0.02 [0.01, 0.03], NOR: 0.01 [0.01, 0.03], REV: 0.05 [0.04, 0.07], texture: 0 [0, 0]). Pairwise comparison results are shown in Figure S4.1.

Face contrast normalization and inversion delayed the N170

Before looking at the Bubble results, we considered the ERPs to intact images (without Bubbles). One previous study has found that the latency and amplitude of the face-sensitive N170 are both increased by reversing the contrast polarity of a face (Fisher et al., 2016; Gandhi et al., 2012; Itier and Taylor, 2002). However, our data that the N170 latency was delayed by REV at RE was not in line with their data. This mismatch can be due to uncontrolled low-level properties. Not like our current study, all stimuli had the same contrast variance and amplitude spectrum, in these previous studies amplitude spectrum and contrast variance are not controlled, so that reversed polarity faces are darker than their positive counterpart.

We first averaged ERPs across practice trials (without Bubbles) for each participant and condition. We then picked a pair of electrodes (LE & RE) that recorded the maximum N170 to original faces within 200 ms post-stimulus from the left and right posterior-lateral electrodes of interest (Figure 4.4). We compared the N170 latency and amplitude of each face condition at LE and RE (table 1). At LE, the N170 amplitude and latency were equal in NOR and REV compared to ORI. At RE, NOR and REV both prolonged the N170 latency compared to ORI, while no amplitude difference can be found. At both LE and RE, there were no significant amplitude and latency differences between NOR and REV. Relative to any face condition, the N170 was delayed and shrank for textures at LE and RE.

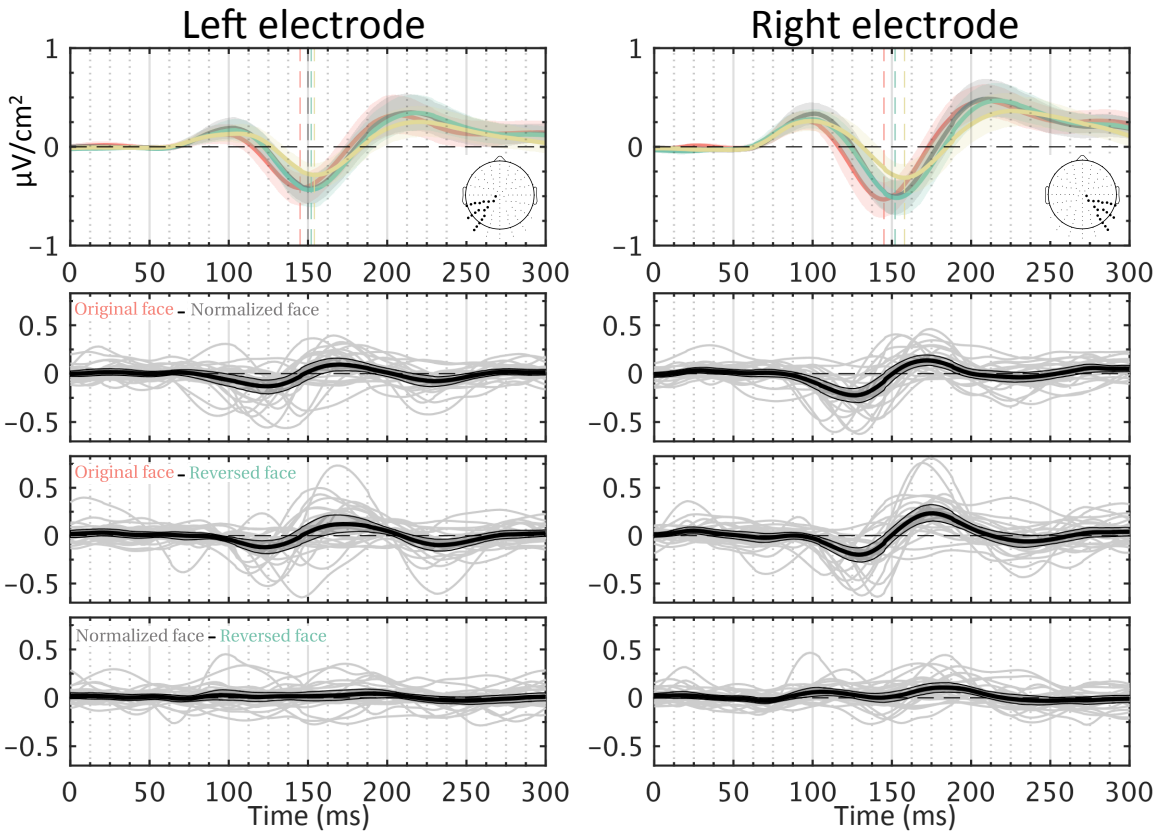

Figure 4.4 Mean group ERPs across trials without Bubbles

LE and RE are selected from the electrodes of interest in the left and right hemisphere. Corresponding electrodes were marked in the BIOSEMI electrode maps in the top. The first row shows the mean ERPs across participants with 95% CI in each condition at LE and RE. Rows 2 to 4 show the time-courses of the pairwise differences between face conditions. Thin grey lines show individual results. Thick black lines and shaded areas illustrate the group means with their 95% CI.

Table 1. N170 *group differences for practice trials (without Bubbles).*

	Left electrode	
	Amplitude ($\mu V/cm^2$)	Latency (ms)
ORI - NOR	0 [-0.05, 0.05]	-5.04 [-7, 3.3]
ORI - REV	-0.01 [-0.06, 0.06]	-5.56 [-8.47, 3.04]
NOR - REV	0.02 [-0.02, 0.06]	-0.2 [-1.6, 0.35]
ORI - TEX	-0.14 [-0.21, -0.08]	-8.68 [-13.41, -3.47]
NOR - TEX	-0.15 [-0.21, -0.07]	-2.4 [-5.68, -0.24]
REV - TEX	-0.18 [-0.23, -0.09]	-2.54 [-4.61, -1.31]
	Right electrode	
	Amplitude ($\mu V/cm^2$)	Latency (ms)
ORI - NOR	-0.03 [-0.1, 0.04]	-6.09 [-7.43, -5]
ORI - REV	0.06 [-0.01, 0.11]	-6.66 [-8.61, -4.49]
NOR - REV	0.04 [-0.02, 0.09]	-0.32 [-1.9, 1.29]
ORI - TEX	-0.12 [-0.26, -0.05]	-12.23 [-15.15, -8.87]
NOR - TEX	-0.15 [-0.23, -0.06]	-4.78 [-8.21, -3.47]
REV - TEX	-0.21 [-0.28, -0.13]	-5.24 [-7.1, -3.81]

Contralateral eye sensitivity at posterior-lateral electrodes

We have found that the N170 latency was delayed by NOR and REV at RE. To go beyond this mean analysis, we next applied MI analyses to specify which image pixels are associated with modulations of ERP responses. We observed that the eye region information was associated with modulations of contralateral ERPs in each face condition (Figure 4.5A). For each participant we calculated the maximum MI using the whole stimulus sampling analysis across electrodes and time points, separately for two regions of interest: left and right posterior-lateral. We referred this maximum MI to as classification images. For each face condition, the group averaged classification image in Figure 4.5A

shows MI values clustered around the contralateral eye regions. Specifically, the single-trial bivariate ERPs recorded at right posterior lateral electrodes were strongly modulated by the intensities of pixels in the left eye region, and right eye region was associated with ERP responses in the left hemisphere. However, there was no strong association between any region of the texture images and brain responses. This lack of effect suggests that contralateral eye sensitivity is not due to an attention bias.

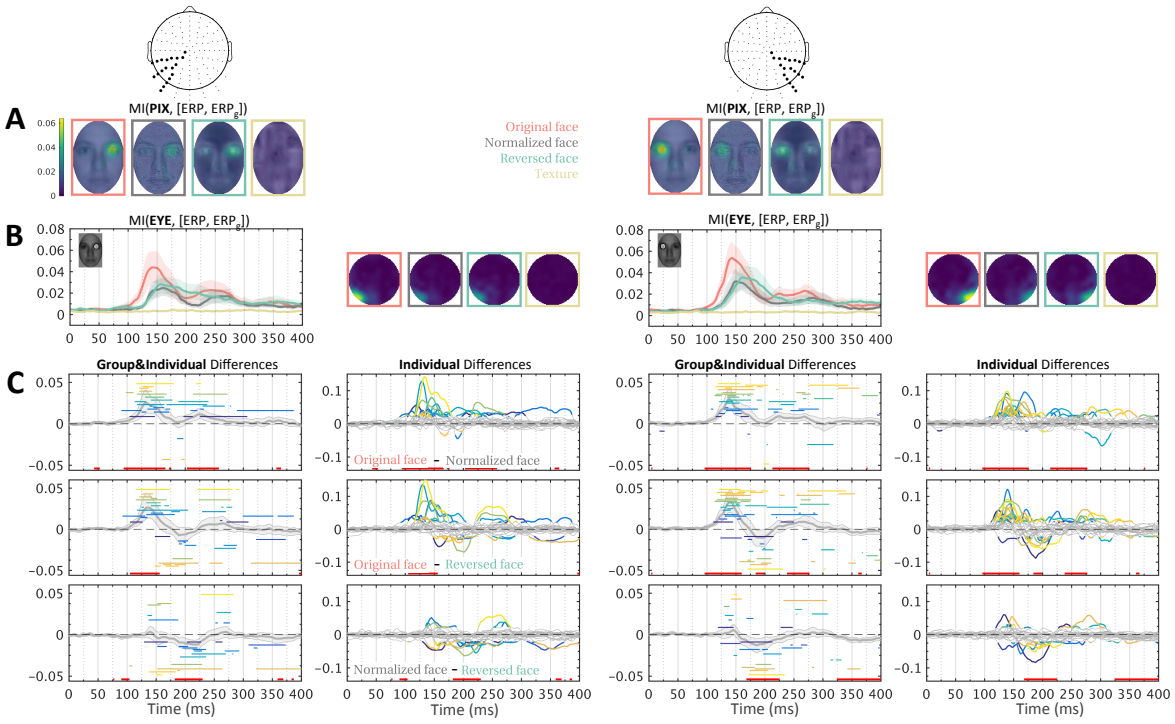

Figure 4.5 MI EEG results (in bits)

Results are presented for left electrodes in the left two columns, and right electrodes in the right two columns. **(A)** The group mean classification images revealed a predominant sensitivity to pixels around the eye contralateral to the recording electrode in each face condition. Textures don't show this pattern. **(B)** The MI(EYE, [ERP, ERP$_g$]) time-courses are plotted in coloured curves with 95% CI per condition. Insets are eye masks used in MI calculation (details in *eye mask analyses*). The group averaged topographic map of maximum MI across time points indicates that recordings from posterior-lateral electrodes are mainly sensitive to the contralateral eye in each face condition. **(C)** Paired comparisons of face conditions. In first and third columns, the light grey curves with shaded area show the mean of differences between pairs of face conditions (ORI vs. NOR, ORI vs. REV, NOR vs. REV) with 95% CI. The red horizontal bar right above the x-axis indicates periods of statistically significant group differences. Individual significant differences computed using permutation analyses are indicated in horizontal colour-coded bars. These bars above the x-axis show stronger effects in ORI versus NOR or ORI versus REV or NOR versus REV, and bars below the x-axis show opposite effects. Individual differences are also shown in the second and fourth column. Coloured sections represent statistically significant differences.

Face contrast normalization and inversion changed contralateral eye coding over time

Contralateral eye sensitivity was found in each of face conditions. To avoid missing any effect throughout the entire time course, we next sought to compare contralateral eye sensitivity between pairs of face conditions over time. Both group and individual-level results showed that ~ 100 – 160 ms NOR and REV both weakened contralateral eye sensitivity compared to ORI in both hemispheres. In ~ 170 – 200 ms time window, there was a stronger MI in REV compared to ORI and NOR at right electrodes, but which was observed in a few participants.

During ~ 220 – 270 ms we also found contrast-related differences in contralateral eye sensitivity, but it can be observed in a few participants. Also, since we are interested in brain activity to the contralateral eye in the N170 time window, we focus on the effects of ~ 100 – 200 ms time window.

Group analyses

We first obtained the time course of *MI(EYE, [ERP, ERP$_g$])* by saving its maxima across contralateral electrodes of interest. The maximum MI peaked around in the ~ 120 – 170 ms time window for each face condition. No such effect can be found in texture trials (Figure 4.5B). The pairwise comparison analyses between face conditions showed differences in 100 – 200 ms.

In ~ 100 – 160 ms, compared to ORI, the contralateral eye sensitivity was lower in NOR and REV for both hemispheres. In ~ 170 – 200 ms, we found weakened right eye sensitivity in NOR compared to REV at left electrodes; Also, in comparison with REV, the MI was weaker in both ORI and NOR at right electrodes.

Single-participant analyses

To validate that those effects detected in the group analyses were representative of the majority of participants, we conducted single-participant analyses by using a permutation test combined with a method of maximum statistics to determine statistical significance and control for multiple comparisons (Holmes et al., 1996), independently for each condition and each hemisphere. Because of similar MI results between whole stimulus and eye mask analyses (Figure S4.3), we focus on MI computed using eye masks to reduce the

dimensionality of data.

We first repeated the MI(EYE, (ERP, ERP_g]) calculation 1000 times, each time randomly permuting the sum of stimulus intensities (luminance) within each eye mask across trials. We calculated MI at every electrode of interest on the contralateral scalp and every time point, producing an MI matrix (electrodes × time points × permutation), independently for each participant. We then took the maximum value of MI across electrodes and time points as a permutation distribution and compared the real MI(EYE, (ERP, ERP_g]) against the 95^{th} percentile of this distribution.

Figure S4.4 details, for every participant, how contralateral eye sensitivity unfolded over time, and when it reached significance. In 20/24, 14/24 and 15/24 participants there were significant effects between left electrodes and right eye pixels for ORI, NOR and REV. In most of participants there were the significant associations between right electrodes and left eye region for ORI (21/24), NOR (15/24) and REV (17/24). No significant effect can be found in textures throughout the entire time window on either hemisphere.

For comparison of face conditions, we took the absolute differences of maximum value over electrodes between pairs of face conditions, separately for each hemisphere, leading to a new MI matrix (time point × permutation). We then took the maximum of MI over time points for each permutation and used the 95^{th} percentile of these maximum values as the statistical threshold for significance. For each participant we compared absolute differences of real MI(EYE, (ERP, ERP_g]) between pairs of face conditions against the threshold. To give complementary information to group analyses, we focus on the similar time windows as described in group analyses:

It is important to note that in 320 - 400 ms even though there was a significant group effect at right electrodes, only 2/24 participants showed larger left eye sensitivity in REV versus NOR (Figure 4.5C, Figure S4.7). Group analyses pulled out effects that are not significant across participants. This mismatch emphasized that group statistics can be misleading.

In the ~ 100 – 160 ms time window: at left electrodes, compared to NOR, 15/24 showed a stronger right eye sensitivity and 1/24 showed a stronger effect then a weaker later in ORI (Figure 4.5C, Figure S4.5); at right electrodes 17/24 participants showed a statistically significant larger effect and 1/24 showed a weaker effect in ORI versus NOR. Relative to REV, in ORI at left electrodes, 13/24 showed stronger effect, 1/24 showed a stronger effect then a weaker later then a weaker later (~ 170 - 200 ms) and 1/24 showed weaker one; at right electrodes, 16/24 showed stronger effect, 2/24 showed a stronger effect then a weaker

later then a weaker later and 1/24 showed weaker one (Figure 4.5C, Figure S4.6).

In the ~ 170 - 200 ms time window, in ORI versus REV 11/24 showed a weaker effect at right electrodes (Figure 4.5C, Figure S4.6); in NOR versus REV, 11/24 and 8/24 participants showed a weaker effect at the left and right electrodes (Figure 4.5C, Figure S4.7).

Contrast effect on peaks, onsets and 50% integration times of contralateral eye coding

In the group and individual-level results, we found that ~ 100 – 160 ms NOR and REV both weakened contralateral eye sensitivity compared to ORI in both hemispheres. In the ~ 170 – 200 time window, there was a stronger MI in REV compared to ORI and NOR at right electrodes, but which was observed in a few participants. We first speculated that lower MI ~ 100 – 160 ms for NOR and REV compared to ORI might be related to weakened peak and delayed onsets of MI. We then speculated that stronger MI in REV ~ 170 – 200 ms, compared to ORI and NOR, which might be related to slower coding speed of the eyes in REV.

We thus detail the differences in term of peak, onset and integration times of contralateral eye information processing. And the results were matched with our predictions. We observed that compared to ORI, the onset of this eye coding was delayed in NOR (left electrodes: ~ 20 ms, right: ~14 ms) and REV (left: 18 ms, right: 16 ms). Compared to ORI and NOR, REV slowed the coding speed of left eye regions by ~ 25 ms and ~23 ms at the right electrodes. These results can be observed in the majority of our participants.

The amplitude of MI peak

We looked at how the maxima of contralateral eye sensitivity varied by face contrast manipulations. Because of no ERP sensitivity to any area of texture noises, we focused on the effects of face contrast manipulations on brain activity sensitivity to the contralateral eye. Figure 4.6A and Figure S4.2 report lower contralateral eye sensitivity in NOR and REV compared to ORI at both right and left electrodes. No group-level differences can be found between NOR and REV in either hemisphere. We also analyzed MI computed using eye masks (more details in eye mask analyses) in bivariate ERPs recorded from the electrodes of interest on contralateral hemisphere, showing a similar effect compared to whole stimulus sampling analysis (Figure 4.6B & Figure S4.2).

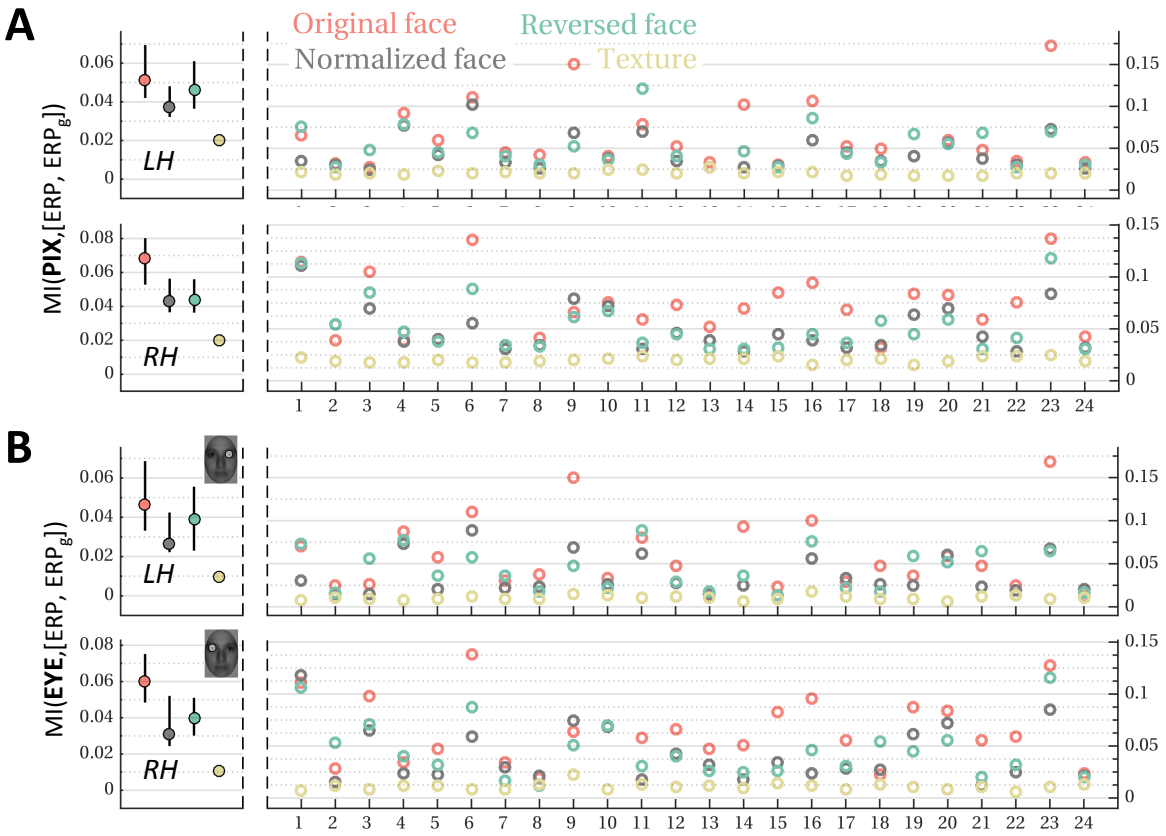

Figure 4.6 Peak analyses of MI curves (in bits)

(A) Whole stimulus sampling. Upper panel for the left hemisphere (LH), lower for right (RH). The coloured diskes with lines show group medians of maximum MI(PIX, [ERP, ERP_g]) across pixels, electrodes of interest and time points, with their 95% CI (LH: ORI, 0.05 [0.04, 0.07], NOR, 0.04 [0.03, 0.05], REV, 0.05 [0.04, 0.06], texture, 0.02 [0.02, 0.02]); RH: ORI, 0.07 [0.05, 0.08], NOR, 0.04 [0.04, 0.06], REV, 0.04 [0.04, 0.06], text, 0.02 [0.02, 0.02]). Coloured circles on the right panel represent individual MI peak values. **(B)** Eye mask analysis show similar results with whole stimulus sampling analysis (LH: ORI, 0.05 [0.03, 0.07], NOR, 0.03 [0.02, 0.04], REV, 0.04 [0.02, 0.06], texture, 0.01 [0.01, 0.01]; RH: ORI, 0.06 [0.05, 0.08], NOR, 0.03 [0.02, 0.05], REV, 0.04 [0.03, 0.05], texture, 0.01 [0.01, 0.01]). Pairwise comparison of MI peak between face conditions are shown in Figure S4.2.

Onset

The non-causal high-pass filter might distort onsets of ERPs (Acunzo et al., 2012; Rousselet, 2012). We thus applied cluster statistics (Maris and Oostenveld, 2007; Pernet et al., 2011) to the permutation test results for the causal dataset per participant to determine the onset of contralateral eye coding. Since for a few participants contralateral eye sensitivity did not reach significance over time (LH, ORI: 4/24, NOR: 7/24, REV: 6/24,

RH, ORI: 2/24, NOR: 4/24, REV: 3/24), these participants were not involved in onset measurement (Figure S4.8). Our explicit assessment of onsets confirmed that a delayed onset of eye processing in NOR and REV compared to ORI in both hemispheres. Figure 4.7 showed that the onset of contralateral eye sensitivity was delayed by ~ 20 ms in NOR and ~ 18 ms REV compared to ORI at left electrodes, ~14 ms and ~16 ms at right electrodes. The majority of participants showed delayed onset in REV (LH: 16/16, RH: 18/20) and NOR (LH: 16/18, RH: 19/19). There was no significant difference between NOR and REV in either hemisphere.

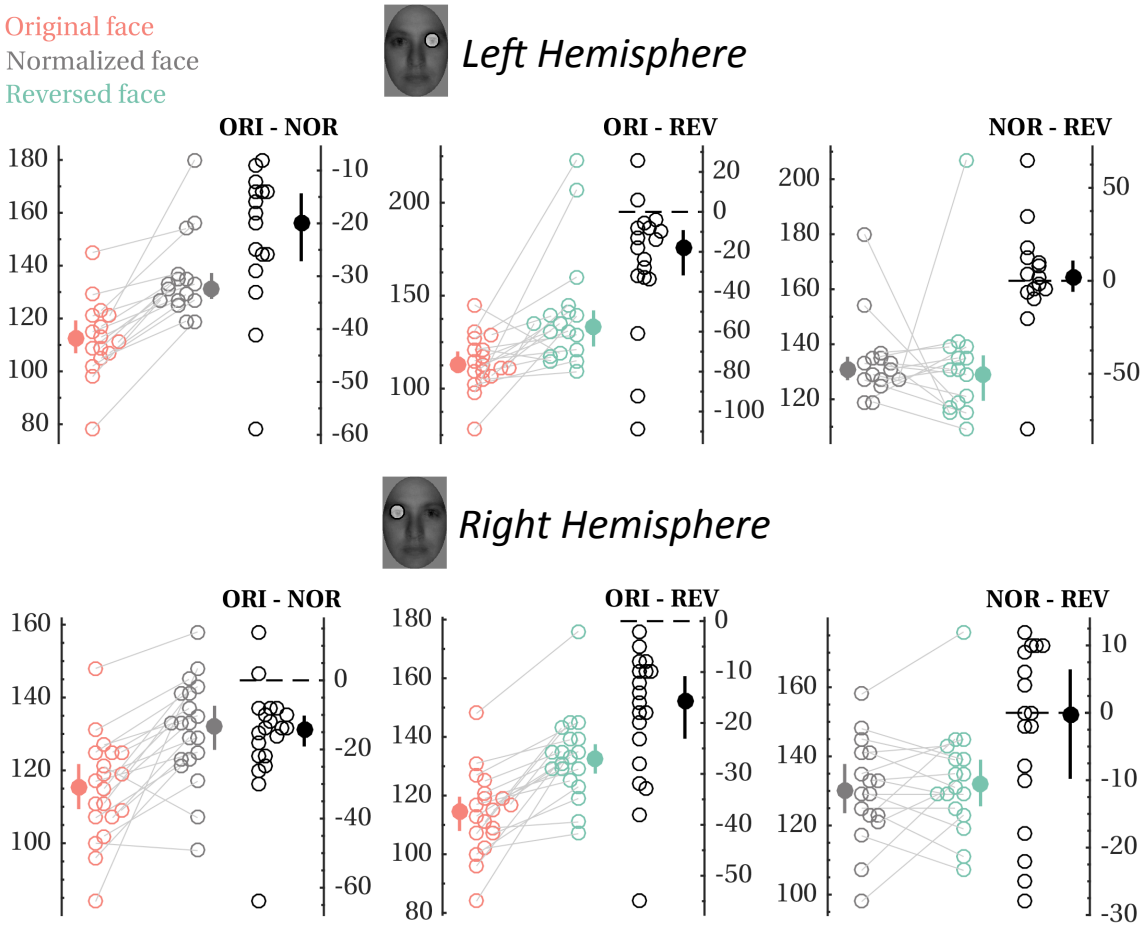

Figure 4.7 Face contrast manipulations delay eye sensitivity onsets (in ms)

Coloured circles show the distribution of individual onsets for each face condition. The coloured diskes show the group medians and 95% CI (LH, ORI: 112.38 [107.18, 119.26], NOR: 131.45 [127.36, 138.08], REV: 132.45 [122.64, 140.92]; RH, ORI: 115.41 [109.36, 121.73], NOR: 131.95 [125.62, 137.73], REV: 132.65 [127.49, 137.51]). Each black scatterplot shows the distribution of individual differences between pairs of face conditions and group results. NOR and REV delayed the onset of contralateral eye sensitivity at LH (*ORI – NOR:* -19.81 [-26.65, -14.41], *ORI – REV:* -17.92 [-31.12, -9.2]) and RH (*ORI – NOR*: -14.25 [-19.15, -10.21], *ORI – REV*: -15.72 [-23.1, -10.8]). There was no difference between NOR and REV in both hemispheres (LH: *NOR – REV:* 1.82 [-5.18, 11.22], RH: *NOR – REV*: -0.33 [-9.8, 6.45]).

50% integration time

We determined the MI latency by measuring the time it takes to integrate 50% of the contralateral eye sensitivity in different conditions. Instead of peak measurement, this method probed potential changes in the entire waveform of the MI curves. Figure 4.8 & Figure S4.9 report pairwise comparison results between face conditions. On the left hemisphere, there was no difference for processing speed of the contralateral eye between any pair of face conditions. In the right hemisphere, there were no differences of 50IT between ORI and NOR. However, REV slowed down the coding of the contralateral eye by ~ 25 ms and ~ 23 ms compared with ORI and NOR, with more than 67% of participants showing the effect.

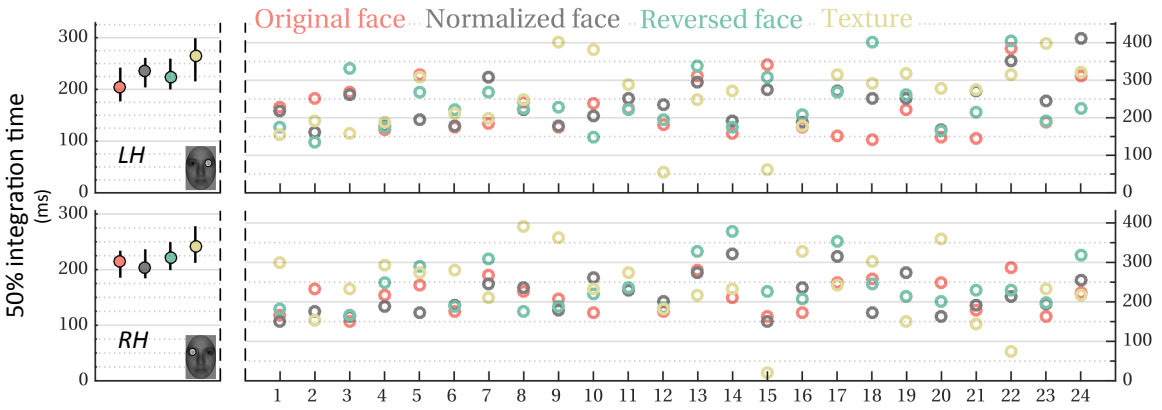

Figure 4.8 Integration time of contralateral eye sensitivity (in ms)

Left scatterplots show group medians (coloured disks) of 50IT with 95% CI at LH (ORI: 205.11 [177.04, 245.74], NOR: 235.11 [202.77, 259.54]; REV: 224.83 [201.91,258.06], texture: 264.84 [213.42, 299.76]) and RH (ORI: 213.96 [183.29, 233.17], NOR: 204.02 [182.72, 235.76]; REV: 221.24 [199.77, 253.55], texture: 241.23 [211.32, 278.9]). Individual 50IT (coloured circle) per condition is shown in the right side. Pairwise comparison results are shown in Figure S4.9.

Discussion

To further understand the eye coding mechanisms underlying the N170 recorded at posterior-lateral electrodes (Rousselet et al., 2014; Jaworska et al., in preparation; Yi et al., in preparation), this study focused on the question of whether the eye sensitivity is due to eye feature processing or higher local contrast around the eye regions or their combination. To address the question, we introduced two contrast-manipulated faces: normalised and reversed contrast faces. We then used the Bubble technique coupled with information theoretic analyses try to understand the processing of a succession of image features that were associated with the behavioural and brain responses in a face detection task.

We reported four main results that are consistent across the majority of observers. First, the association between the eyes and behavioural performance is similar between original and normalised contrast faces, and is enhanced in contrast reversal faces (Figure 4.3 & Figure S4.1). Second, we found ERP sensitivity to the contralateral eye in all face conditions. Third, we observed weakened MI peaks and delayed onsets of this contralateral eye sensitivity for normalised and reversed compared to original faces (Figure 4.6&4.7, Figure S4.8), might leading to lower MI in the ~ 100 – 160 ms time window for two contrast-manipulated faces (Figure 4.5&Figure S4.5-4.6). Fourth, removing the saliency of eye regions slowed the processing speed of the left eye region at right electrodes compared to original and normalised contrast faces (Figure 4.8 & Figure S4.9).

Diagnostic information of behavioural responses

In original faces, we found that the most diagnostic information is within the eye regions. This is consistent with previous human behavioural studies, in which eye sensitivity has been replicated consistently across a variety of tasks using reverse correlation (Schyns et al., 2002; Sekuler et al., 2004) and eye tracking (Peterson and Eckstein, 2012). Since the scan-paths traced by human eye movements are similar to the low-level computation saliency maps produced by contrast based computer vision algorithms (Itti et al., 1998), the bias towards the eyes might be simply due to their increased saliency and prominent compared to other areas of the face. This conclusion is challenged by analysis of behaviour in normalised-contrast faces in which we equalised the local contrast across a face so that the eyes were not standing out. We observed that the presence of the eyes equally influenced the behavioural responses to both original and normalised-contrast faces. In addition, compared to original faces, observers relied more on the eyes to detect reversed-

contrast faces that maintain the eye saliency. The heavy dependence on the eye region in reversed-contrast faces in our case is inconsistent with a previous study showing a less effective use of available physical information in these faces (C. M. Gaspar et al., 2008). The diagnostic use of face features is variant across tasks at hand (Schyns, 1998; Schyns et al., 2003). Thus, their results cannot be directly compared with ours because of different task requirements (face discrimination vs. face detection). Additionally, our experiment presenting stimuli embedded in phase-scrambled noise background with Bubbles cannot be compared directly to Gaspar et al., (2008) using stimuli in white Gaussian noise. Thus, the eye is the key for face detection behaviours, which is not because of higher local contrast in the eye.

Face contrast normalization and inversion weakened contralateral eye coding in ~ 100 – 160 ms

We found that ERP responses were predominantly sensitive to contralateral eye information over time whatever the contrast of faces, which is comparable to a series of electrophysiological studies (Rousselet et al., 2014; Schyns et al., 2003; Marie L. Smith et al., 2007; van Rijsbergen and Schyns, 2009; Jaworska et al., in preparation; Yi et al., in preparation). Importantly, in the current study, we try to answer a question of whether low-level information, local contrast, influences the eye sensitivity in the N170 time window. We found that face contrast normalization and inversion weakened contralateral eye sensitivity in ~ 100 – 160 ms time window, which might be related to weaker peaks and later onsets of MI for the two contrast-manipulated faces compared to original faces. Also, in the same time window, contralateral eye sensitivity was comparable between normalised and reversed contrast faces. These results suggest that eye sensitivity might be due to two factors, local contrast and feature specificity, in combination in ~ 100 – 160 ms.

We observed that removing the saliency of the eyes decreased the association between the contralateral eye region and brain activity ~ 100 – 160 ms post-stimulus. It seems eye saliency is the explanation for this contralateral eye sensitivity. If higher local contrast in eye region is the only explanation, we should obverse higher contralateral eye sensitivity in reversed compared to normalised contrast faces ~ 100 – 160 ms since reversed contrast faces still keep the eye saliency. In contrast, we found that contralateral eye sensitivity was comparable between normalised and reversed contrast faces. Thus, besides eye saliency, feature-specificity might also be crucial for contralateral eye sensitivity. It was further evidenced by the result that compared to original faces there was impaired eye sensitivity ~

100 – 160 ms for reversed contrast faces in which eye feature per se was influenced. Thus, contralateral eye sensitivity might be attributed to the low-level properties, local contrast in our case, and high-level visual feature in combination in ~ 100 – 160 ms.

The contrast-related changes in ~ 100 – 160 ms are consistent with a macaque study (Issa and DiCarlo, 2012). They showed reduced responses of face-selective neurons in posterior face patch (PL) by contrast equalization across a face and reversed contrast polarity of faces. In humans, Sweep visual evoked potential (VEP) studies investigated how much phase information of face images was used to detect faces and how face contrast reversal changes information extraction (J. Liu-Shuang et al., 2015; Joan Liu-Shuang et al., 2015). They found that for upright faces, ~ 35% phase coherence of a face was enough for saturated responses and face inversion increased the threshold by ~ 30% - 60% coherence. Also, for negative polarity faces, they found lower responses compared to positive ones. Their results are in consistent with our results that impaired eye information processing by face contrast inversion. However, these sweep VEP studies, in which periodic signal was decomposed into a sum of sinusoids by Discrete Fourier Transform, block the way of understanding the time information content of signals and shape of these signals. Moreover, in these studies, the contribution of face features to face detection was hidden. In our case, taking advantage of Bubble technique that can tease out the information content that associated responses, we further reported what face information modulated neural activity that recorded on the scalp, when and how was it affected by face contrast inversion.

Face contrast inversion slowed processing speed of the contralateral eye

We found slowest processing speed of the eyes in reversed contrast faces compared to other faces. It might lead to a stronger contralateral eye sensitivity for reversed in the right hemisphere in ~ 170 – 200 ms compared to the other two face conditions, but note that 11 out of 24 participants contributed to this group effect for original versus reversed contrast faces, and 8/24 for normalised versus reversed contrast faces. No such differences can be found between original and normalised contrast faces. Thus, these results suggest that processing speed of the eye might be affected by feature specificity, but not eye saliency. The feature could be contrast polarity relationship between an eye and adjacent regions.

Studies that manipulated contrast polarity of local features in facial stimuli revealed ordinal relationship around the eyes is a determinant role in facial recognisability (Fisher et al., 2015, 2016; Gandhi et al., 2012; Gilad et al., 2009). Local contrast polarity

relationships between the eye regions and neighbourhoods have also been reported to provide a computational means for face detection (Sinha, 2002). In addition, a single-unit recording monkey study that motivated by Sinha's computer vision algorithm stepped further by systematically manipulating contrast across face parts (Ohayon et al., 2012). They found that cells in middle face patches (ML/MF) were sensitive to illumination-invariant contrast features, predominantly contrast pair of left eye and nose (Ohayon et al., 2012). Sadagopan et al. (2017) provided a causal evidence for the role of ML in face detection by reporting that inactivation of ML caused face detection deficits. While the homologies between monkey and human face processing systems are unclear, following the 3/5 rule (Kelly et al., 2013), the timings of activities in ML might be comparable to the later part of the N170 in humans. In ML/MF, activity began at 88 ms and peaked at 126 ms (Freiwald and Tsao, 2010). Thus, the slower processing speed of the eyes for reversed contrast faces might be attributed to the distorted contrast polarity relationship between eye and adjacent regions by face contrast reversal.

Conclusion

In summary, removing eye saliency and reversing face contrast polarity delayed the onset of the earliest eye information extraction and the contrast-related impairments appeared in ~ 100 – 160 ms, suggesting the processing of contralateral eye is due partially to low-level factors. However, whatever the face contrast manipulations, the same information the contralateral eye was associated with brain activity in the N170 time window, thus suggesting that whatever the contrast of faces, face processing is feature-based in the early N170 in a simple face detection task.

Chapter 5: General conclusions and future directions

Face detection is an easy and essential daily task. Humans can detect faces with extremely limited information (Bentin et al., 2002; Jiang et al., 2011; Rousselet et al., 2008). Thus, the whole of the face is not necessarily involved in face detection (Ullman et al., 2002). The key question is to answer with what information the human brain analyses faces, when and how the information is processed. Previous Bubble studies reported that early brain activity to faces is strongly modulated by the presence of the contralateral eye across tasks (Schyns et al., 2011, 2007, Smith et al., 2009, 2007, 2004; van Rijsbergen and Schyns, 2009; Ince et al., 2016; Rousselet et al., 2014). In this thesis, we use Bubble technique to investigate the robustness of eye coding mechanisms in a face detection task.

Presenting a face upside down causes impairments in face recognition performance (Hochberg & Galper, 1967). This effect is stronger for faces than for other objects, which is called the face inversion effect (FIE; Yin, 1969).

This property has been taken as evidence that face perception relies on specific mechanism that not shared by other objects. Since compared to non-face objects faces share the same basic structure, upright faces perception might involve a template-matching process. Inverted faces that disrupt common basic configuration do not fit the holistic template, so they might be analyzed by the general object recognition system (i.e., feature-based mechanism) (Tsao and Livingstone, 2008). Thus, a classical view claimed that FIE is due to the disruption of simultaneous integration of facial features as a whole, leading to qualitative differences in upright and inverted face processing (i.e., holistic vs. feature based) (Rossion, 2013; Tanaka and Farah, 1993).

In contrast, psychophysical evidences support an alternative view that considers quantitative processing differences as an explanation for FIE (Gold et al., 2012). For example, Sekuler et al. (2004) reported that pixels near the eyes and eyebrows were used to discriminate faces regardless of their orientation. In spatial frequency (SF) domain, so far studies found that the lower performance for inverted faces is due to less efficient processing of the same SF compared to upright faces (C. Gaspar et al., 2008; Goffaux, 2010; Willenbockel et al., 2010). These behavioural studies converge to explain the FIE as a result of less efficient extraction of the same information in inverted compared to upright faces.

The FIE is robust and has been observed not only in tasks for processing familiar and unfamiliar faces, recognition task or matching task (for a review see Rossion and Gauthier, 2002), but also in face detection task from behavioural (Taubert et al., 2011) and single cell (Issa and DiCarlo, 2012), ERPs (Latinus and Taylor, 2005) and fMRI (Kanwisher et al., 1998) studies. Tsao and Livingstone, (2008) suggested that face detection precedes face discrimination. Psychophysical evidence suggests that objects are identified at the category level (e.g., face versus fruit) before they are identified at the individual level (Rosch, et al., 1976). Monkey studies reported that global information, categorizing stimuli as face versus non-face objects, is conveyed earlier (~ 50 ms) than fine information about identity (Sugase et al., 1999; Sugase-Miyamoto et al., 2014; Tsao, 2006). These findings indicate that after sufficient information is available for the face processing system to perform accurate face detection or to discriminate between individual faces.

Therefore, in chapter 2 we focused on face detection, the most fundamental component of face processing (Sinha, 2002; Tsao and Livingstone, 2008; Gilad et al., 2009) to understand the neural mechanisms underlying the FIE.

Using information theoretic analyses coupled with reverse analyses, we replicated the previous findings for upright faces that the eyes were coded contralateral to posterior-lateral electrodes in the N170 time window (Rousselet et al., 2014, Ince, et al., 2016b, Jaworska et al., in prep). Importantly, we further derived impaired eye information processing mechanisms to inverted faces in the early stage of the N170. We found that the eye coding function in the early N170 time window was weakened and delayed by ~ 15 – 19 ms in both hemispheres by face inversion. In line with our data, previous monkey studies have also shown that face-selective neurons decreased (PL, Issa and DiCarlo, 2012; ML and MF, Freiwald et al., 2009; ML, Jessica Taubert et al., 2015; J. Taubert et al., 2015; Taubert et al., 2016) and delayed (MF; Perrett et al., 1985) responses for inverted compared with upright faces in temporal cortex. Freiwald et al. (2009) reported that neural responses in ML to eyebrows were lost entirely under face inversion. Also, ML neurons were profoundly sensitive to eye orientation in upright but not in inverted faces (J. Taubert et al., 2015). These monkey data might suggest that face inversion disrupt the processing of fine structure details around the eye region. Thus, the impaired eye coding function in the early N170 time window by face inversion might be due to less neural responses to the details of the eye region in inverted compared to upright faces. Also, the N170 FIE during face detection might be due to the difference between upright and inverted faces in the coding of the contralateral eye in the early N170.

In chapter 2, for images of faces, eye position and face orientation were confounded, i.e., the upper visual field usually contains eyes in upright faces; in upside-down faces lower visual field contains eyes. Thus, the impaired processing of the contralateral eye by inversion might be simply attributed to that face inversion removes the eyes away from upper visual field. In chapter 3, we manipulated three vertical locations of images in which eyes are presented in upper, centre and lower visual field relative to fixation cross (the centre of the screen) so that in upright and inverted faces the eyes can shift from the upper to the lower visual field.

We first replicated findings in chapter 2 by comparing upright and inverted faces, in which the eyes appeared upper and lower visual field correspondingly. Second, regardless of face orientation and position, earlier and larger N170 peaks were associated with higher visibility of the contralateral eye, suggesting eye coding mechanisms underlying the N170 in all face conditions. Third, face inversion delayed the eye coding and weakened it in the N170 time window, when the eyes of faces were presented in the same position, *Above*, *Below* or at the *Centre* of the screen. The results suggest that face inversion related changes in processing of the contralateral eye cannot be simply considered as the results of differences of eye position.

The scan-paths traced by human eye movements are similar to the low-level computation saliency maps produced by contrast based computer vision algorithms (Itti et al., 1998). This evidence leads us to a question of whether the coding function to encode the eyes is due to the significance in the eye regions. To answer the question, we introduced two altered version of original faces: normalised and reversed contrast faces in a face detection task - removing eye saliency (Simoncelli and Olshausen, 2001) and reversing face contrast polarity (Gilad et al., 2009) in a simple face detection task. In each face condition, we observed ERPs, that recorded at contralateral posterior lateral electrodes, were sensitive to eye regions.

We observed that removing the saliency of the eyes decreased the association between the contralateral eye region and brain activity ~ 100 – 160 ms post-stimulus. It seems eye saliency is the explanation for this contralateral eye sensitivity. If higher local contrast in eye region is the only explanation, we should obverse higher contralateral eye sensitivity in reversed compared to normalised contrast faces ~ 100 – 160 ms since reversed contrast faces still keep the eye saliency. In contrast, we found that contralateral eye sensitivity was comparable between normalised and reversed contrast faces. Thus, besides eye saliency, feature-specificity might also be crucial for contralateral eye sensitivity. It was further

evidenced by the result that compared to original faces there was impaired eye sensitivity ~ 100 – 160 ms for reversed contrast faces in which eye feature per se was influenced. These results were observed in the majority of participants. Thus, contralateral eye sensitivity might be attributed to the low-level properties, local contrast in our case, and high-level visual feature in combination in the early N170.

In chapter 2, we determined the latency differences in MI curves by using peak-to-peak measures, because the waveform has the relative canonical shape. However, for a curve with high variability, the latency measure that depends on one time point is problematic because of a lack of robustness with respect to the time selected (Ince et al., 2016). Thus, in chapter 3, we went beyond simple peak measures and determined the latency of MI by measuring the time it takes to integrate 50% of the contralateral eye sensitivity in different conditions. This method probed potential changes in the entire waveform of the MI curves. In chapter 4, we adopted 'integral latency' approach from Ince et al. (2016) that considers the latency over a range of MI values. For curves with multiple peaks, integral latency approach more sensibly reflects the actual relationship.

In this thesis, we provide detailed graphical representations that showing group and single participant results for two reasons. First, it can help to increase openness, transparency and reproducibility of neuroscience research. Second, there can be a mismatch between the outcome of statistical tests, their interpretations, and the information available in the data distributions (Rousselet et al., 2016). Rich results of single participant can help us to avoid misunderstanding group results, particularly for a small size study (Rousselet, 2011; Rousselet and Pernet, 2011; Rousselet et al., 2016). In our case, for example, Figure 2.5 showed that in ~ 50 – 80 ms there are group effects at right electrodes, but statistical analyses of single participants revealed null effects in every participant. Thus, Group analyses should be shown in conjunction with detailed single participant results, i.e., the number of participants showing an effect in the same direction as the group or opposite direction or no effect, or how large are these individual effects.

Moving forward from this work, there is still much research to be done to fully understand the coding of contralateral eye underlying the early neuronal responses. First, detecting a face from the background and telling this face apart from other faces have opposing demands: detection requires extracting first-order relational properties, i.e. the T-shaped configuration. The identification of individuals requires a fine-grained analysis to extract second-order properties, the information in which faces differ from each other, i.e. distance between face features. It would be interesting to determine whether the effects we found in

this thesis are robust across task. Second, in this thesis, we are interested in one single feature, the contralateral eye; it would also be interesting to track face information integration and determine how it affected by face manipulations, i.e. face inversion, removing eye saliency and reversing face contrast polarity. To do so, Bubble technique combined with combine sweep VEP provide objective signatures of integration of specific features (Boremanse et al., 2013). Third, with a very high temporal resolution, non-invasively scalp EEG can precisely track the time course of task-related neural activity: event-related potentials (ERPs). However, with low spatial resolution, EEG studies cannot answer the questions of (1) which brain areas contributed to the effects we found in this thesis; (2) whether the sources (or processes) for the effects are same when participants were tested on separate days. In the future work, a single-trial fMRI-EEG or MEG experiment using Bubble technique would help solve this problem, or more directly, an intracranial study.

References

Acunzo, D.J., MacKenzie, G., van Rossum, M.C.W., 2012. Systematic biases in early ERP and ERF components as a result of high-pass filtering. J. Neurosci. Methods 209, 212–218. https://doi.org/10.1016/j.jneumeth.2012.06.011

Arcurio, L.R., Gold, J.M., James, T.W., 2012. The response of face-selective cortex with single face parts and part combinations. Neuropsychologia 50, 2454–2459. https://doi.org/10.1016/j.neuropsychologia.2012.06.016

Ahlfors, S.P., Han, J., Belliveau, J.W. and Hämäläinen, M.S., 2010. Sensitivity of MEG and EEG to source orientation. Brain topography, 23(3), pp.227-232.

Arizpe, J., Kravitz, D.J., Yovel, G., Baker, C.I., 2012. Start Position Strongly Influences Fixation Patterns during Face Processing: Difficulties with Eye Movements as a Measure of Information Use. PLoS ONE 7, e31106. https://doi.org/10.1371/journal.pone.0031106

Balas, B.J., Schmidt, J., Saville, A., 2015. A face detection bias for horizontal orientations develops in middle childhood. Front. Psychol. 06. https://doi.org/10.3389/fpsyg.2015.00772

Baseler, H.A., Harris, R.J., Young, A.W., Andrews, T.J., 2014. Neural Responses to Expression and Gaze in the Posterior Superior Temporal Sulcus Interact with Facial Identity. Cereb. Cortex 24, 737–744. https://doi.org/10.1093/cercor/bhs360

Batki, A., Baron-Cohen, S., Wheelwright, S., Connellan, J., Ahluwalia, J., 2000. Is there an innate gaze module? Evidence from human neonates. Infant Behav. Dev. 23, 223–229.

Bell, A.H., Hadj-Bouziane, F., Frihauf, J.B., Tootell, R.B.H., Ungerleider, L.G., 2008. Object Representations in the Temporal Cortex of Monkeys and Humans as Revealed by Functional Magnetic Resonance Imaging. J. Neurophysiol. 101, 688–700. https://doi.org/10.1152/jn.90657.2008

Bell, A. H., Hadj-Bouziane, F., Frihauf, J. B., Tootell, R. B., & Ungerleider, L. G. (2009). Object representations in the temporal cortex of monkeys and humans as revealed by functional magnetic resonance imaging. Journal of neurophysiology, 101(2), 688-700.

Bentin, S., Allison, T., Puce, A., Perez, E., McCarthy, G., 1996. Electrophysiological Studies of Face Perception in Humans. J. Cogn. Neurosci. 8, 551–565. https://doi.org/10.1162/jocn.1996.8.6.551

Bentin, S., Sagiv, N., Mecklinger, A., Friederici, A., von Cramon, Y.D., 2002. Priming visual face-processing mechanisms: Electrophysiological evidence. Psychol. Sci. 13, 190–193.

Bernstein, M., Yovel, G., 2015. Two neural pathways of face processing: A critical evaluation of current models. Neurosci. Biobehav. Rev. 55, 536–546. https://doi.org/10.1016/j.neubiorev.2015.06.010

Bieniek, M.M., Frei, L.S., Rousselet, G.A., 2013. Early ERPs to faces: aging, luminance, and individual differences. Front. Psychol. 4. https://doi.org/10.3389/fpsyg.2013.00268

Bieniek, M.M., Pernet, C.R., Rousselet, G.A., 2012. Early ERPs to faces and objects are driven by phase, not amplitude spectrum information: Evidence from parametric, test-retest, single-subject analyses. J. Vis. 12, 12–12. https://doi.org/10.1167/12.13.12

Boremanse, A., Norcia, A.M., Rossion, B., 2013. An objective signature for visual binding of face parts in the human brain. J. Vis. 13, 6–6. https://doi.org/10.1167/13.11.6

Brainard, D. H., & Vision, S. (1997). The psychophysics toolbox. Spatial vision, 10, 433-436.

Brown, J.M., Koch, C., 2000. Influences of occlusion, color, and luminance on the perception of fragmented pictures. Percept. Mot. Skills 90, 1033–1044.

Bukach, C.M., Grand, R., Kaiser, M.D., Bub, D.N., Tanaka, J.W., 2008. Preservation of mouth region processing in two cases of prosopagnosia. J. Neuropsychol. 2, 227–244. https://doi.org/10.1348/174866407X231010

Caharel S., Fiori N., Bernard C., Lalonde R., Rebaï M. (2006). The effects of inversion and eye displacements of familiar and unknown faces on early and late-stage ERPs. Int. J. Psychophysiol. 62, 141–151. 10.1016/j.ijpsycho.2006.03.002

Caldara, R., Schyns, P., Mayer, E., Smith, M.L., Gosselin, F., Rossion, B., 2005. Does Prosopagnosia Take the Eyes Out of Face Representations? Evidence for a Defect in Representing Diagnostic Facial Information following Brain Damage. J. Cogn. Neurosci. 17, 1652–1666. https://doi.org/10.1162/089892905774597254

Clarke, A.D.F., Green, P.R., Chantler, M.J., 2012. The effects of display time and eccentricity on the detection of amplitude and phase degradations in textured stimuli. J. Vis. 12, 7–7. https://doi.org/10.1167/12.3.7

Cohen, M.X., 2014. Analyzing neural time series data: theory and practice, Issues in clinical and cognitive neuropsychology. The MIT Press, Cambridge, Massachusetts.

Colombatto, C., & McCarthy, G. (2017). The effects of face inversion and face race on the P100 ERP. Journal of cognitive neuroscience.

Gosselin, F., Schyns, P.G., 2004. No troubles with bubbles: a reply to Murray and Gold. Vision Res. 44, 471–477. https://doi.org/10.1016/j.visres.2003.10.007

Cover, T.M., Thomas, J.A., 1991. Elements of information theory, Wiley series in telecommunications. Wiley, New York.

Crouzet, S., 2011. Low-level cues and ultra-fast face detection. Front. Psychol. 2. https://doi.org/10.3389/fpsyg.2011.00342

Dakin, S.C., Watt, R.J., 2009. Biological “bar codes” in human faces. J. Vis. 9, 2–2. https://doi.org/10.1167/9.4.2

Dalrymple, K.A., Oruç, I., Duchaine, B., Pancaroglu, R., Fox, C.J., Iaria, G., Handy, T.C., Barton, J.J.S., 2011. The anatomic basis of the right face-selective N170 IN acquired prosopagnosia: A combined ERP/fMRI study. Neuropsychologia 49, 2553–2563. https://doi.org/10.1016/j.neuropsychologia.2011.05.003

Da Silva, F.L., 2009. EEG: origin and measurement. In EEg-fMRI (pp. 19-38). Springer, Berlin, Heidelberg.

de Haas, B., Schwarzkopf, D.S., Alvarez, I., Lawson, R.P., Henriksson, L., Kriegeskorte, N., Rees, G., 2016. Perception and Processing of Faces in the Human Brain Is Tuned to Typical Feature Locations. J. Neurosci. 36, 9289–9302. https://doi.org/10.1523/JNEUROSCI.4131-14.2016

Delorme, A., Mullen, T., Kothe, C., Acar, Z. A., Bigdely-Shamlo, N., Vankov, A., & Makeig, S. (2011). EEGLAB, SIFT, NFT, BCILAB, and ERICA: new tools for advanced EEG processing. Computational intelligence and neuroscience, 2011, 10.

Delorme, A., Rousselet, G.A., Macé, M.J.-M., Fabre-Thorpe, M., 2004. Interaction of top-down and bottom-up processing in the fast visual analysis of natural scenes. Cogn. Brain Res. 19, 103–113. https://doi.org/10.1016/j.cogbrainres.2003.11.010

Delorme, A., Sejnowski, T., Makeig, S., 2007. Enhanced detection of artifacts in EEG data using higher-order statistics and independent component analysis. NeuroImage 34, 1443–1449. https://doi.org/10.1016/j.neuroimage.2006.11.004

Delvenne, J.-F., Seron, X., Coyette, F., Rossion, B., 2004. Evidence for perceptual deficits in associative visual (prosop)agnosia: a single-case study. Neuropsychologia 42, 597–612. https://doi.org/10.1016/j.neuropsychologia.2003.10.008

DiCarlo, J.J., Cox, D.D., 2007. Untangling invariant object recognition. Trends Cogn. Sci. 11, 333–341. https://doi.org/10.1016/j.tics.2007.06.010

Dricot, L., Sorger, B., Schiltz, C., Goebel, R., Rossion, B., 2008. The roles of "face" and "non-face" areas during individual face perception: Evidence by fMRI adaptation in a brain-damaged prosopagnosic patient. NeuroImage 40, 318–332. https://doi.org/10.1016/j.neuroimage.2007.11.012

Duchaine, B., Yovel, G., 2015. A Revised Neural Framework for Face Processing. Annu. Rev. Vis. Sci. 1, 393–416. https://doi.org/10.1146/annurev-vision-082114-035518

Eimer, M., 2000. Effects of face inversion on the structural encoding and recognition of faces: Evidence from event-related brain potentials. Cogn. Brain Res. 10, 145–158.

Engell, A.D., Haxby, J.V., 2007. Facial expression and gaze-direction in human superior temporal sulcus. Neuropsychologia 45, 3234–3241. https://doi.org/10.1016/j.neuropsychologia.2007.06.022

Farroni, T., Csibra, G., Simion, F., Johnson, M.H., 2002. Eye contact detection in humans from birth. Proc. Natl. Acad. Sci. 99, 9602–9605.

Fisher, K., Towler, J., Eimer, M., 2016. Reduced sensitivity to contrast signals from the eye region in developmental prosopagnosia. Cortex 81, 64–78. https://doi.org/10.1016/j.cortex.2016.04.005

Fisher, K., Towler, J., Eimer, M., 2015. Effects of contrast inversion on face perception depend on gaze location: Evidence from the N170 component. Cogn. Neurosci. 1–10. https://doi.org/10.1080/17588928.2015.1053441

Freiwald, W., Duchaine, B., Yovel, G., 2016. Face Processing Systems: From Neurons to Real-World Social Perception. Annu. Rev. Neurosci. 39, 325–346. https://doi.org/10.1146/annurev-neuro-070815-013934

Freiwald, W.A., Tsao, D.Y., 2010. Functional Compartmentalization and Viewpoint Generalization Within the Macaque Face-Processing System. Science 330, 845–851. https://doi.org/10.1126/science.1194908

Freiwald, W.A., Tsao, D.Y., Livingstone, M.S., 2009. A face feature space in the macaque temporal lobe. Nat. Neurosci. 12, 1187–1196. https://doi.org/10.1038/nn.2363

Gandhi, T., Suresh, N., Sinha, P., 2012. EEG responses to facial contrast-chimeras. J. Integr. Neurosci. 11, 201–211. https://doi.org/10.1142/S021963521250015X

Garrido, L., Duchaine, B., Nakayama, K., 2008. Face detection in normal and prosopagnosic individuals. J. Neuropsychol. 2, 119–140. https://doi.org/10.1348/174866407X246843

Gaspar, C., Sekuler, A.B., Bennett, P.J., 2008. Spatial frequency tuning of upright and inverted face identification. Vision Res. 48, 2817–2826. https://doi.org/10.1016/j.visres.2008.09.015

Gaspar, C.M., Bennett, P.J., Sekuler, A.B., 2008. The effects of face inversion and contrast-reversal on efficiency and internal noise. Vision Res. 48, 1084–1095. https://doi.org/10.1016/j.visres.2007.12.014

Gauthier, I., 2000. What constrains the organization of the ventral temporal cortex? Trends Cogn. Sci. 4, 1–2.

Gilad, S., Meng, M., Sinha, P., 2009. Role of ordinal contrast relationships in face encoding. Proc. Natl. Acad. Sci. 106, 5353–5358.

Goffaux, V., 2010. Horizontal information drives the behavioral signatures of face processing. Front. Psychol. 1. https://doi.org/10.3389/fpsyg.2010.00143

Gold, J., Bennett, P.J., Sekuler, A.B., 1999. Identification of band-pass filtered letters and faces by human and ideal observers. Vision Res. 39, 3537–3560.

Gold, J.M., Mundy, P.J., Tjan, B.S., 2012. The Perception of a Face Is No More Than the Sum of Its Parts. Psychol. Sci. 23, 427–434. https://doi.org/10.1177/0956797611427407

Gosselin, F., Schyns, P.G., 2001. Bubbles: a technique to reveal the use of information in recognition tasks. Vision Res. 41, 2261–2271.

Grill-Spector, K., Knouf, N., Kanwisher, N., 2004. The fusiform face area subserves face perception, not generic within-category identification. Nat. Neurosci. 7, 555–562. https://doi.org/10.1038/nn1224

Groppe, D.M., Makeig, S., Kutas, M., 2009. Identifying reliable independent components via split-half comparisons. NeuroImage 45, 1199–1211. https://doi.org/10.1016/j.neuroimage.2008.12.038

Gschwind, M., Pourtois, G., Schwartz, S., Van De Ville, D., Vuilleumier, P., 2012. White-Matter Connectivity between Face-Responsive Regions in the Human Brain. Cereb. Cortex 22, 1564–1576. https://doi.org/10.1093/cercor/bhr226

Haith, M. M., Bergman, T., & Moore, M. J. (1977). Eye contact and face scanning in early infancy. Science, 198(4319), 853-855.

Hanson, S.J., Schmidt, A., 2011. High-resolution imaging of the fusiform face area (FFA) using multivariate non-linear classifiers shows diagnosticity for non-face categories. NeuroImage 54, 1715–1734. https://doi.org/10.1016/j.neuroimage.2010.08.028

Harrell, F.E., Davis, C.E., 1982. A new distribution-free quantile estimator. Biometrika 69, 635–640.

Harris, A., Aguirre, G.K., 2010. Neural Tuning for Face Wholes and Parts in Human Fusiform Gyrus Revealed by fMRI Adaptation. J. Neurophysiol. 104, 336–345. https://doi.org/10.1152/jn.00626.2009

Harris, R.J., Young, A.W., Andrews, T.J., 2014. Brain regions involved in processing facial identity and expression are differentially selective for surface and edge information. NeuroImage 97, 217–223. https://doi.org/10.1016/j.neuroimage.2014.04.032

Harris, R.J., Young, A.W., Andrews, T.J., 2012. Morphing between expressions dissociates continuous from categorical representations of facial expression in the human brain. Proc. Natl. Acad. Sci. 109, 21164–21169. https://doi.org/10.1073/pnas.1212207110

Haxby, J.V., Gobbini, M.I., Furey, M.L., Ishai, A., Schouten, J.L., Pietrini, P., 2001. Distributed and overlapping representations of faces and objects in ventral temporal cortex. Science 293, 2425–2430.

Haxby, J.V., Hoffman, E.A., Gobbini, M.I., 2000. The distributed human neural system for face perception. Trends Cogn. Sci. 4, 223–233.

Hemond, C.C., Kanwisher, N.G., Op de Beeck, H.P., 2007. A Preference for Contralateral Stimuli in Human Object- and Face-Selective Cortex. PLoS ONE 2, e574. https://doi.org/10.1371/journal.pone.0000574

Henriksson, L., Mur, M., Kriegeskorte, N., 2015. Faciotopy—A face-feature map with face-like topology in the human occipital face area. Cortex 72, 156–167. https://doi.org/10.1016/j.cortex.2015.06.030

Hochberg, J. and Galper, R.E., 1967. Recognition of faces: I. An exploratory study. Psychonomic Science, 9(12), pp.619-620.

Horovitz, S.G., Rossion, B., Skudlarski, P., Gore, J.C., 2004. Parametric design and correlational analyses help integrating fMRI and electrophysiological data during face processing. NeuroImage 22, 1587–1595. https://doi.org/10.1016/j.neuroimage.2004.04.018

Hsiao, J.H., n.d. Two Fixations Suffice Janet Hui-wen Hsiao and Garrison Cottrell.

Ince, R.A., Mazzoni, A., Petersen, R.S., Panzeri, S., 2010. Open source tools for the information theoretic analysis of neural data. Front. Neurosci. 4.

Ince, R.A.A., Giordano, B.L., Kayser, C., Rousselet, G.A., Gross, J., Schyns, P.G., 2016a. A statistical framework for neuroimaging data analysis based on mutual information estimated via a Gaussian copula (No. biorxiv;043745v1).

Ince, R.A.A., Jaworska, K., Gross, J., Panzeri, S., van Rijsbergen, N.J., Rousselet, G.A., Schyns, P.G., 2016b. The Deceptively Simple N170 Reflects Network Information Processing Mechanisms Involving Visual Feature Coding and Transfer Across Hemispheres. Cereb. Cortex 26, 4123–4135. https://doi.org/10.1093/cercor/bhw196

Ince, R.A.A., Jaworska, K., Gross, J., Panzeri, S., van Rijsbergen, N.J., Rousselet, G.A., Schyns, P.G., 2016c. The Deceptively Simple N170 Reflects Network Information Processing Mechanisms Involving Visual Feature Coding and Transfer Across Hemispheres (No. biorxiv;044065v1).

Issa, E.B., DiCarlo, J.J., 2012. Precedence of the Eye Region in Neural Processing of Faces. J. Neurosci. 32, 16666–16682. https://doi.org/10.1523/JNEUROSCI.2391-12.2012

Itti, L., Koch, C., 2000. A saliency-based search mechanism for overt and covert shifts of visual attention. Vision Res. 40, 1489–1506.

Itti, L., Koch, C., Niebur, E., others, 1998. A model of saliency-based visual attention for rapid scene analysis. IEEE Trans. Pattern Anal. Mach. Intell. 20, 1254–1259.

Jackson, A.F., Bolger, D.J., 2014. The neurophysiological bases of EEG and EEG measurement: A review for the rest of us: Neurophysiological bases of EEG. Psychophysiology 51, 1061–1071. https://doi.org/10.1111/psyp.12283

Jacques, C., d'Arripe, O., Rossion, B., 2007. The time course of the inversion effect during individual face discrimination. J. Vis. 7, 3–3. https://doi.org/10.1167/7.8.3

Jiang, F., Dricot, L., Weber, J., Righi, G., Tarr, M.J., Goebel, R., Rossion, B., 2011. Face categorization in visual scenes may start in a higher order area of the right fusiform gyrus: evidence from dynamic visual stimulation in neuroimaging. J. Neurophysiol. 106, 2720–2736. https://doi.org/10.1152/jn.00672.2010

Johnson, J.S., Olshausen, B.A., 2005. The recognition of partially visible natural objects in the presence and absence of their occluders. Vision Res. 45, 3262–3276. https://doi.org/10.1016/j.visres.2005.06.007

Jonas, J., Descoins, M., Koessler, L., Colnat-Coulbois, S., Sauvée, M., Guye, M., Vignal, J.-P., Vespignani, H., Rossion, B., Maillard, L., 2012. Focal electrical intracerebral stimulation of a face-sensitive area causes transient prosopagnosia. Neuroscience 222, 281–288. https://doi.org/10.1016/j.neuroscience.2012.07.021

Jonas, J., Rossion, B., Krieg, J., Koessler, L., Colnat-Coulbois, S., Vespignani, H., Jacques, C., Vignal, J.-P., Brissart, H., Maillard, L., 2014. Intracerebral electrical stimulation of a face-selective area in the right inferior occipital cortex impairs individual face discrimination. NeuroImage 99, 487–497. https://doi.org/10.1016/j.neuroimage.2014.06.017

Jones, W., Carr, K., Klin, A., 2008. Absence of preferential looking to the eyes of approaching adults predicts level of social disability in 2-year-old toddlers with autism spectrum disorder. Arch. Gen. Psychiatry 65, 946–954.

Kanwisher, N., Tong, F., Nakayama, K., 1998. The effect of face inversion on the human fusiform face area. Cognition 68, B1–B11. https://doi.org/10.1016/S0010-0277(98)00035-3

Kanwisher, N., Yovel, G., 2006. The fusiform face area: a cortical region specialized for the perception of faces. Philos. Trans. R. Soc. B Biol. Sci. 361, 2109–2128. https://doi.org/10.1098/rstb.2006.1934

Kay, K. N., Weiner, K. S., & Grill-Spector, K. (2015). Attention reduces spatial uncertainty in human ventral temporal cortex. Current Biology, 25(5), 595-600.

Kayser, J. (2009). Current source density (CSD) interpolation using spherical splines - CSD Toolbox (Version 1.1) [http://psychophysiology.cpmc.columbia.edu/Software/CSDtoolbox]. New York State Psychiatric Institute: Division of Cognitive Neuroscienc

Kelly, S.P., Vanegas, M.I., Schroeder, C.E., Lalor, E.C., 2013. The cruciform model of striate generation of the early VEP, re-illustrated, not revoked: A reply to Ales et al. (2013). NeuroImage 82, 154–159. https://doi.org/10.1016/j.neuroimage.2013.05.112

Kleiner, M., Brainard, D., Pelli, D., Ingling, A., Murray, R., & Broussard, C. (2007). What's new in Psychtoolbox-3. Perception, 36(14), 1.

Kovács, G., Vogels, R., Orban, G.A., 1995. Selectivity of macaque inferior temporal neurons for partially occluded shapes. J. Neurosci. 15, 1984–1997.

Latinus, M., Taylor, M.J., 2005. Holistic Processing of Faces: Learning Effects with Mooney Faces. J. Cogn. Neurosci. 17, 1316–1327. https://doi.org/10.1162/0898929055002490

Liu, J., Harris, A., Kanwisher, N., 2010. Perception of Face Parts and Face Configurations: An fMRI Study. J. Cogn. Neurosci. 22, 203–211. https://doi.org/10.1162/jocn.2009.21203

Liu-Shuang, J., Ales, J., Rossion, B., Norcia, A.M., 2015. Separable effects of inversion and contrast-reversal on face detection thresholds and response functions: A sweep VEP study. J. Vis. 15, 11–11. https://doi.org/10.1167/15.2.11

Liu-Shuang, J., Ales, J.M., Rossion, B., Norcia, A.M., 2015. The effect of contrast polarity reversal on face detection: Evidence of perceptual asymmetry from sweep VEP. Vision Res. 108, 8–19. https://doi.org/10.1016/j.visres.2015.01.001

Macke, J.H., Wichmann, F.A., 2010. Estimating predictive stimulus features from psychophysical data: The decision image technique applied to human faces. J. Vis. 10, 22–22. https://doi.org/10.1167/10.5.22

Magri, C., Whittingstall, K., Singh, V., Logothetis, N.K., Panzeri, S., 2009. A toolbox for the fast information analysis of multiple-site LFP, EEG and spike train recordings. BMC Neurosci. 10, 81. https://doi.org/10.1186/1471-2202-10-81

Maris, E., Oostenveld, R., 2007. Nonparametric statistical testing of EEG- and MEG-data. J. Neurosci. Methods 164, 177–190. https://doi.org/10.1016/j.jneumeth.2007.03.024

Maurer, D., Le Grand, R., Mondloch, C.J., 2002. The many faces of configural processing. Trends Cogn. Sci. 6, 255–260.

Murray, R.F., Gold, J.M., 2004. Troubles with bubbles. Vision Res. 44, 461–470. https://doi.org/10.1016/j.visres.2003.10.006

Neath, K.N., Itier, R.J., 2013. Facial expression discrimination varies with presentation time but not with fixation on features: A backward masking study using eye-tracking. Cogn. Emot. 28, 115–131. https://doi.org/10.1080/02699931.2013.812557

Nguyen, V.T., Cunnington, R., 2014. The superior temporal sulcus and the N170 during face processing: Single trial analysis of concurrent EEG–fMRI. NeuroImage 86, 492–502. https://doi.org/10.1016/j.neuroimage.2013.10.047

Nielsen, K.J., 2006. Dissociation Between Local Field Potentials and Spiking Activity in Macaque Inferior Temporal Cortex Reveals Diagnosticity-Based Encoding of Complex Objects. J. Neurosci. 26, 9639–9645. https://doi.org/10.1523/JNEUROSCI.2273-06.2006

Oakes, L.M., Ellis, A.E., 2013. An Eye-Tracking Investigation of Developmental Changes in Infants' Exploration of Upright and Inverted Human Faces: INFANTS' EXPLORATION OF FACES. Infancy 18, 134–148. https://doi.org/10.1111/j.1532-7078.2011.00107.x

Ohayon, S., Freiwald, W.A., Tsao, D.Y., 2012. What Makes a Cell Face Selective? The Importance of Contrast. Neuron 74, 567–581. https://doi.org/10.1016/j.neuron.2012.03.024

Pachai, M., 2015. On the role of horizontal structure in human face identification.

Pachai, M.V., Sekuler, A.B., Bennett, P.J., 2013. Sensitivity to Information Conveyed by Horizontal Contours is Correlated with Face Identification Accuracy. Front. Psychol. 4. https://doi.org/10.3389/fpsyg.2013.00074

Parkhurst, D., Law, K., Niebur, E., 2002. Modeling the role of salience in the allocation of overt visual attention. Vision Res. 42, 107–123.

Parvizi, J., Jacques, C., Foster, B.L., Withoft, N., Rangarajan, V., Weiner, K.S., Grill-Spector, K., 2012. Electrical Stimulation of Human Fusiform Face-Selective Regions Distorts Face Perception. J. Neurosci. 32, 14915–14920. https://doi.org/10.1523/JNEUROSCI.2609-12.2012

Pelli, D. G. (1997). The VideoToolbox software for visual psychophysics: Transforming numbers into movies. Spatial vision, 10(4), 437-442.

Pernet, C.R., Chauveau, N., Gaspar, C., Rousselet, G.A., 2011. LIMO EEG: A Toolbox for Hierarchical LInear MOdeling of ElectroEncephaloGraphic Data. Comput. Intell. Neurosci. 2011, 1–11. https://doi.org/10.1155/2011/831409

Perrett, D.I., Smith, P.A.J., Potter, D.D., Mistlin, A.J., Head, A.S., Milner, A.D., Jeeves, M.A., 1985. Visual Cells in the Temporal Cortex Sensitive to Face View and Gaze Direction. Proc. R. Soc. B Biol. Sci. 223, 293–317. https://doi.org/10.1098/rspb.1985.0003

Peterson, M.F., Eckstein, M.P., 2012. Looking just below the eyes is optimal across face recognition tasks. Proc. Natl. Acad. Sci. 109, E3314–E3323. https://doi.org/10.1073/pnas.1214269109

Pitcher, D., Charles, L., Devlin, J.T., Walsh, V., Duchaine, B., 2009. Triple Dissociation of Faces, Bodies, and Objects in Extrastriate Cortex. Curr. Biol. 19, 319–324. https://doi.org/10.1016/j.cub.2009.01.007

Pitcher, D., Duchaine, B., Walsh, V., 2014. Combined TMS and fMRI Reveal Dissociable Cortical Pathways for Dynamic and Static Face Perception. Curr. Biol. 24, 2066–2070. https://doi.org/10.1016/j.cub.2014.07.060

Pitcher, D., Duchaine, B., Walsh, V., Yovel, G., Kanwisher, N., 2011a. The role of lateral occipital face and object areas in the face inversion effect. Neuropsychologia 49, 3448–3453. https://doi.org/10.1016/j.neuropsychologia.2011.08.020

Pitcher, D., Garrido, L., Walsh, V., Duchaine, B.C., 2008. Transcranial Magnetic Stimulation Disrupts the Perception and Embodiment of Facial Expressions. J. Neurosci. 28, 8929–8933. https://doi.org/10.1523/JNEUROSCI.1450-08.2008

Pitcher, D., Goldhaber, T., Duchaine, B., Walsh, V., Kanwisher, N., 2012. Two Critical and Functionally Distinct Stages of Face and Body Perception. J. Neurosci. 32, 15877–15885. https://doi.org/10.1523/JNEUROSCI.2624-12.2012

Pitcher, D., Walsh, V., Duchaine, B., 2011b. The role of the occipital face area in the cortical face perception network. Exp. Brain Res. 209, 481–493. https://doi.org/10.1007/s00221-011-2579-1

Pitcher, D., Walsh, V., Yovel, G., Duchaine, B., 2007. TMS Evidence for the Involvement of the Right Occipital Face Area in Early Face Processing. Curr. Biol. 17, 1568–1573. https://doi.org/10.1016/j.cub.2007.07.063

Portilla, J., Simoncelli, E.P., 2000. A parametric texture model based on joint statistics of complex wavelet coefficients. Int. J. Comput. Vis. 40, 49–70.

Prieto, E., 2011. Early (N170/M170) face-sensitivity despite right lateral occipital brain damage in acquired prosopagnosia. Front. Hum. Neurosci. 5. https://doi.org/10.3389/fnhum.2011.00138

Rajimehr, R., Young, J.C., Tootell, R.B., 2009. An anterior temporal face patch in human cortex, predicted by macaque maps. Proc. Natl. Acad. Sci. 106, 1995–2000.

Rosch, E., Mervis, C.B., Gray, W.D., Johnson, D.M. and Boyes-Braem, P., 1976. Basic objects in natural categories. Cognitive psychology, 8(3), pp.382-439.

Rossion, B., 2013. The composite face illusion: A whole window into our understanding of holistic face perception. Vis. Cogn. 21, 139–253. https://doi.org/10.1080/13506285.2013.772929

Rossion, B., 2009. Clarifying the functional neuro-anatomy of face perception by single case neuroimaging studies of acquired prosopagnosia. Cortical Mech. Vis. 171–207.

Rossion, B., 2013. The composite face illusion: A whole window into our understanding of holistic face perception. Vis. Cogn. 21, 139–253. https://doi.org/10.1080/13506285.2013.772929

Rossion, B., Gauthier, I., 2002. How Does the Brain Process Upright and Inverted Faces? Behav. Cogn. Neurosci. Rev. 1, 63–75. https://doi.org/10.1177/1534582302001001004

Rossion, B., Gauthier, I., Tarr, M.J., Despland, P., Bruyer, R., Linotte, S., Crommelinck, M., 2000. The N170 occipito-temporal component is delayed and enhanced to

inverted faces but not to inverted objects: an electrophysiological account of face-specific processes in the human brain. Neuroreport 11, 69–72.

Rossion, B., Hanseeuw, B., Dricot, L., 2012. Defining face perception areas in the human brain: A large-scale factorial fMRI face localizer analysis. Brain Cogn. 79, 138–157. https://doi.org/10.1016/j.bandc.2012.01.001

Rossion, B., Jacques, C., 2008. Does physical interstimulus variance account for early electrophysiological face sensitive responses in the human brain? Ten lessons on the N170. NeuroImage 39, 1959–1979. https://doi.org/10.1016/j.neuroimage.2007.10.011

Rossion, B., & Jacques, C. (2011). The N170: understanding the time-course of face perception in the human brain. The Oxford handbook of ERP components, 115-142.

Rossion, B., Kaiser, M.D., Bub, D., Tanaka, J.W., 2009. Is the loss of diagnosticity of the eye region of the face a common aspect of acquired prosopagnosia? J. Neuropsychol. 3, 69–78. https://doi.org/10.1348/174866408X289944

Rotshtein, P., Henson, R.N.A., Treves, A., Driver, J., Dolan, R.J., 2005. Morphing Marilyn into Maggie dissociates physical and identity face representations in the brain. Nat. Neurosci. 8, 107–113. https://doi.org/10.1038/nn1370

Rousselet, 2011. Modeling single-trial ERP reveals modulation of bottom-up face visual processing by top-down task constraints (in some subjects). Front. Psychol. https://doi.org/10.3389/fpsyg.2011.00137

Rousselet, 2010. Healthy aging delays scalp EEG sensitivity to noise in a face discrimination task. Front. Psychol. https://doi.org/10.3389/fpsyg.2010.00019

Rousselet, G.A., 2012. Does Filtering Preclude Us from Studying ERP Time-Courses? Front. Psychol. 3. https://doi.org/10.3389/fpsyg.2012.00131

Rousselet, G.A., Foxe, J.J., Bolam, J.P., 2016. A few simple steps to improve the description of group results in neuroscience. Eur. J. Neurosci. 44, 2647–2651. https://doi.org/10.1111/ejn.13400

Rousselet, G.A., Ince, R.A., van Rijsbergen, N.J., Schyns, P.G., 2014. Eye coding mechanisms in early human face event-related potentials. J. Vis. 14, 7–7.

Rousselet, G.A., Mace, M.J.-M., Fabre-Thorpe, M., 2004. Animal and human faces in natural scenes: How specific to human faces is the N170 ERP component? J. Vis. 4, 2–2. https://doi.org/10.1167/4.1.2

Rousselet, G.A., Macé, M.J.-M., Fabre-Thorpe, M., 2003. Is it an animal? Is it a human face? Fast processing in upright and inverted natural scenes. J. Vis. 3, 5.

Rousselet, G.A., Pernet, C.R., 2011. Quantifying the Time Course of Visual Object Processing Using ERPs: It's Time to Up the Game. Front. Psychol. 2. https://doi.org/10.3389/fpsyg.2011.00107

Rousselet, G.A., Pernet, C.R., Bennett, P.J., Sekuler, A.B., 2008. Parametric study of EEG sensitivity to phase noise during face processing. BMC Neurosci. 9, 98. https://doi.org/10.1186/1471-2202-9-98

Sadagopan, S., Zarco, W., Freiwald, W.A., 2017. A causal relationship between face-patch activity and face-detection behavior. eLife 6, e18558.

Sadeh, B., Podlipsky, I., Zhdanov, A., Yovel, G., 2010. Event-related potential and functional MRI measures of face-selectivity are highly correlated: A simultaneous ERP-fMRI investigation. Hum. Brain Mapp. 31, 1490–1501. https://doi.org/10.1002/hbm.20952

Schiltz, C., Rossion, B., 2006. Faces are represented holistically in the human occipito-temporal cortex. NeuroImage 32, 1385–1394. https://doi.org/10.1016/j.neuroimage.2006.05.037

Schneidman, E., Bialek, W., Berry II, M.J., 2003. Synergy, Redundancy, andIndependencein PopulationCodes.

Schwarzlose, R.F., Swisher, J.D., Dang, S., Kanwisher, N., 2008. The distribution of category and location information across object-selective regions in human visual cortex. Proc. Natl. Acad. Sci. 105, 4447–4452.

Schyns, P.G., 1998. Diagnostic recognition: task constraints, object information, and their interactions. Cognition 67, 147–179.

Schyns, P.G., Bonnar, L., Gosselin, F., 2002. Show me the features! Understanding recognition from the use of visual information. Psychol. Sci. 13, 402–409.

Schyns, P.G., Gosselin, F., Smith, M.L., 2009. Information processing algorithms in the brain. Trends Cogn. Sci. 13, 20–26. https://doi.org/10.1016/j.tics.2008.09.008

Schyns, P.G., Jentzsch, I., Johnson, M., Schweinberger, S.R., Gosselin, F., 2003. A principled method for determining the functionality of brain responses. Neuroreport 14, 1665–1669.

Schyns, P.G., Petro, L.S., Smith, M.L., 2007. Dynamics of Visual Information Integration in the Brain for Categorizing Facial Expressions. Curr. Biol. 17, 1580–1585. https://doi.org/10.1016/j.cub.2007.08.048

Schyns, P.G., Thut, G., Gross, J., 2011. Cracking the Code of Oscillatory Activity. PLoS Biol. 9, e1001064. https://doi.org/10.1371/journal.pbio.1001064

Schwarzlose, R. F., Swisher, J. D., Dang, S., & Kanwisher, N. (2008). The distribution of category and location information across object-selective regions in human visual cortex. Proceedings of the National Academy of Sciences, 105(11), 4447-4452.

Sekuler, A.B., Gaspar, C.M., Gold, J.M., Bennett, P.J., 2004. Inversion Leads to Quantitative, Not Qualitative, Changes in Face Processing. Curr. Biol. 14, 391–396. https://doi.org/10.1016/j.cub.2004.02.028

Sekuler, A.B., Gold, J.M., Murray, R.F. and Bennett, P.J., 2000. Visual completion of partly occluded objects: Insights from behavioral studies. Neuro-Ophtalmology, 23, pp.165-168.

Sergent, J., Ohta, S. & MacDonald, B. 1992 Functional neuroanatomy of face and object processing. A positron emission tomography study. Brain 115, 15–36. (doi:10. 1093/brain/115.1.15)

Simoncelli, E.P., Olshausen, B.A., 2001. Natural image statistics and neural representation. Annu. Rev. Neurosci. 24, 1193–1216.

Sinha, P., 2002. Qualitative representations for recognition, in: International Workshop on Biologically Motivated Computer Vision. Springer, pp. 249–262.

Smith, M.L., Fries, P., Gosselin, F., Goebel, R., Schyns, P.G., 2009. Inverse Mapping the Neuronal Substrates of Face Categorizations. Cereb. Cortex 19, 2428–2438. https://doi.org/10.1093/cercor/bhn257

Smith, M.L., Gosselin, F., Schyns, P.G., 2007. From a face to its category via a few information processing states in the brain. NeuroImage 37, 974–984. https://doi.org/10.1016/j.neuroimage.2007.05.030

Smith, M.L., Gosselin, F., Schyns, P.G., 2004. Receptive fields for flexible face categorizations. Psychol. Sci. 15, 753–761.

Sigala, N., & Logothetis, N. K. (2002). Visual categorization shapes feature selectivity in the primate temporal cortex. Nature, 415(6869), 318-320.

Sorger, B., Goebel, R., Schiltz, C., Rossion, B., 2007. Understanding the functional neuroanatomy of acquired prosopagnosia. NeuroImage 35, 836–852. https://doi.org/10.1016/j.neuroimage.2006.09.051

Steeves, J.K.E., Culham, J.C., Duchaine, B.C., Pratesi, C.C., Valyear, K.F., Schindler, I., Humphrey, G.K., Milner, A.D., Goodale, M.A., 2006. The fusiform face area is not sufficient for face recognition: Evidence from a patient with dense prosopagnosia and no occipital face area. Neuropsychologia 44, 594–609. https://doi.org/10.1016/j.neuropsychologia.2005.06.013

Sugase, Y., Yamane, S., Ueno, S., Kawano, K., 1999. Global and fine information coded by single neurons in the temporal visual cortex. Nature 400, 869–873. https://doi.org/10.1038/23703

Sugase-Miyamoto, Y., Matsumoto, N., Ohyama, K., Kawano, K., 2014. Face Inversion Decreased Information about Facial Identity and Expression in Face-Responsive Neurons in Macaque Area TE. J. Neurosci. 34, 12457–12469. https://doi.org/10.1523/JNEUROSCI.0485-14.2014

Tanaka, J.W., Farah, M.J., 1993. Parts and wholes in face recognition. Q. J. Exp. Psychol. 46, 225–245.

Tang, H., Buia, C., Madhavan, R., Crone, N.E., Madsen, J.R., Anderson, W.S., Kreiman, G., 2014. Spatiotemporal Dynamics Underlying Object Completion in Human Ventral Visual Cortex. Neuron 83, 736–748. https://doi.org/10.1016/j.neuron.2014.06.017

Tang, H., Lotter, B., Schrimpf, M., Paredes, A., Caro, J.O., Hardesty, W., Cox, D., Kreiman, G., 2017. Recurrent computations for visual pattern completion. ArXiv Prepr. ArXiv170602240.

Tanskanen, T., Näsänen, R., Montez, T., Päällysaho, J., Hari, R., 2005. Face Recognition and Cortical Responses Show Similar Sensitivity to Noise Spatial Frequency. Cereb. Cortex 15, 526–534. https://doi.org/10.1093/cercor/bhh152

Taubert, J., Apthorp, D., Aagten-Murphy, D., Alais, D., 2011. The role of holistic processing in face perception: Evidence from the face inversion effect. Vision Res. 51, 1273–1278. https://doi.org/10.1016/j.visres.2011.04.002

Taubert, J., Goffaux, V., Van Belle, G., Vanduffel, W., Vogels, R., 2016. The impact of orientation filtering on face-selective neurons in monkey inferior temporal cortex. Sci. Rep. 6, 21189. https://doi.org/10.1038/srep21189

Taubert, J., Van Belle, G., Vanduffel, W., Rossion, B., Vogels, R., 2015. The effect of face inversion for neurons inside and outside fMRI-defined face-selective cortical regions. J. Neurophysiol. 113, 1644–1655. https://doi.org/10.1152/jn.00700.2014

Taubert, J., Van Belle, G., Vanduffel, W., Rossion, B., Vogels, R., 2015. Neural Correlate of the Thatcher Face Illusion in a Monkey Face-Selective Patch. J. Neurosci. 35, 9872–9878. https://doi.org/10.1523/JNEUROSCI.0446-15.2015

Tenke, C.E., Kayser, J., 2012. Generator localization by current source density (CSD): Implications of volume conduction and field closure at intracranial and scalp resolutions. Clin. Neurophysiol. 123, 2328–2345. https://doi.org/10.1016/j.clinph.2012.06.005

Tong, F., Nakayama, K., Moscovitch, M., Weinrib, O., Kanwisher, N., 2000. Response properties of the human fusiform face area. Cogn. Neuropsychol. 17, 257–280.

Tsao, D.Y., 2006. A Cortical Region Consisting Entirely of Face-Selective Cells. Science 311, 670–674. https://doi.org/10.1126/science.1119983

Tsao, D.Y., Freiwald, W.A., Knutsen, T.A., Mandeville, J.B., Tootell, R.B.H., 2003. Faces and objects in macaque cerebral cortex. Nat. Neurosci. 6, 989–995. https://doi.org/10.1038/nn1111

Tsao, D.Y., Moeller, S., Freiwald, W.A., 2008. Comparing face patch systems in macaques and humans. Proc. Natl. Acad. Sci. 105, 19514–19519.

Turk-Browne, N.B., Norman-Haignere, S.V., McCarthy, G., 2010. Face-Specific Resting Functional Connectivity between the Fusiform Gyrus and Posterior Superior Temporal Sulcus. Front. Hum. Neurosci. 4. https://doi.org/10.3389/fnhum.2010.00176

Ullman, S., Vidal-Naquet, M., Sali, E., 2002. Visual features of intermediate complexity and their use in classification. Nat. Neurosci. https://doi.org/10.1038/nn870

van Rijsbergen, N.J., Schyns, P.G., 2009. Dynamics of Trimming the Content of Face Representations for Categorization in the Brain. PLoS Comput. Biol. 5, e1000561. https://doi.org/10.1371/journal.pcbi.1000561

Weiner, K.S., Jonas, J., Gomez, J., Maillard, L., Brissart, H., Hossu, G., Jacques, C., Loftus, D., Colnat-Coulbois, S., Stigliani, A., others, 2016. The Face-Processing Network Is Resilient to Focal Resection of Human Visual Cortex. J. Neurosci. 36, 8425–8440.

Widmann, A., Schröger, E., 2012. Filter Effects and Filter Artifacts in the Analysis of Electrophysiological Data. Front. Psychol. 3. https://doi.org/10.3389/fpsyg.2012.00233

Willenbockel, V., Fiset, D., Chauvin, A., Blais, C., Arguin, M., Tanaka, J.W., Bub, D.N., Gosselin, F., 2010. Does face inversion change spatial frequency tuning? J. Exp. Psychol. Hum. Percept. Perform. 36, 122–135. https://doi.org/10.1037/a0016465

Yang, H., Susilo, T., Duchaine, B., 2016. The Anterior Temporal Face Area Contains Invariant Representations of Face Identity That Can Persist Despite the Loss of Right FFA and OFA. Cereb. Cortex 26, 1096–1107. https://doi.org/10.1093/cercor/bhu289

Yin, R. K. (1969). Looking at upside-down faces. Journal of experimental psychology, 81(1), 141.

Yovel, G., Freiwald, W.A., 2013. Face recognition systems in monkey and human: are they the same thing. F1000Prime Rep 5, 10–12703.

Zerouali, Y., Lina, J.-M., Jemel, B., 2013. Optimal eye-gaze fixation position for face-related neural responses. PloS One 8, e60128.

Appendices

Appendix A

Supplementary material for Chapter 2

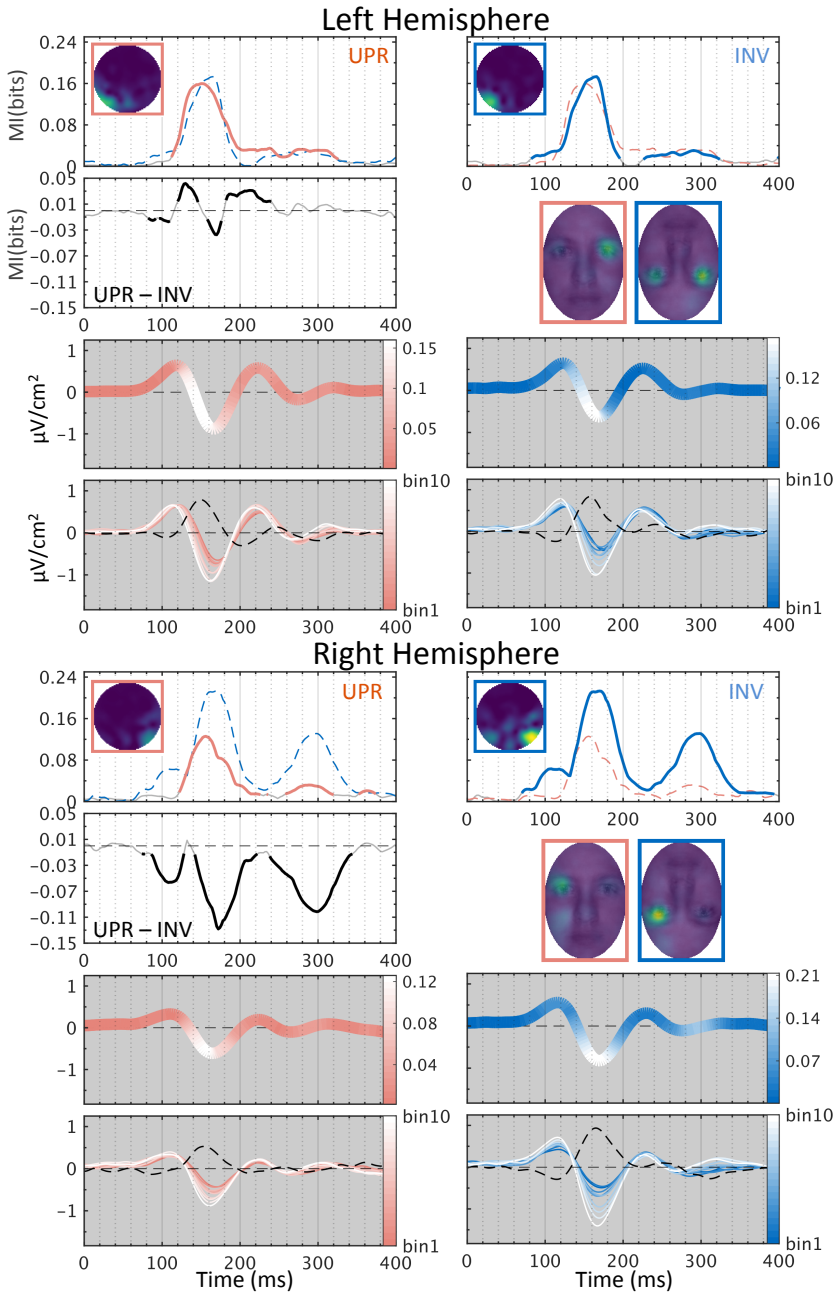

Figure S2.1. Coding of observer 1. First row: Topographic maps of MI(EYE, [ERP, ERP_g]) indicate the involvement of posterior-lateral sources in the coding of contralateral eyes. Time course of maximum MI(EYE, [ERP, ERP_g]) across electrodes of interest from left and right posterior-lateral regions separately are plotted in curves. Thicker parts of waves indicate statistically significant differences. **Second row:** MI differences are placed on first and third columns. Classification images on the second and fourth columns indicate that sensors mostly code contralateral eye regions. **Third row:** the maximum MI curves corresponding to the first

row unfold on the averaged ERPs in Bubble trials. **Fourth row:** averaged ERPs on Bubble trials are colour-coded at each level of eye visibility. The red and white waves indicate bin1 (lowest eye visibility) and bin10 (highest eye visibility). The black dashed curve represents the differences (bin1 - bin10).

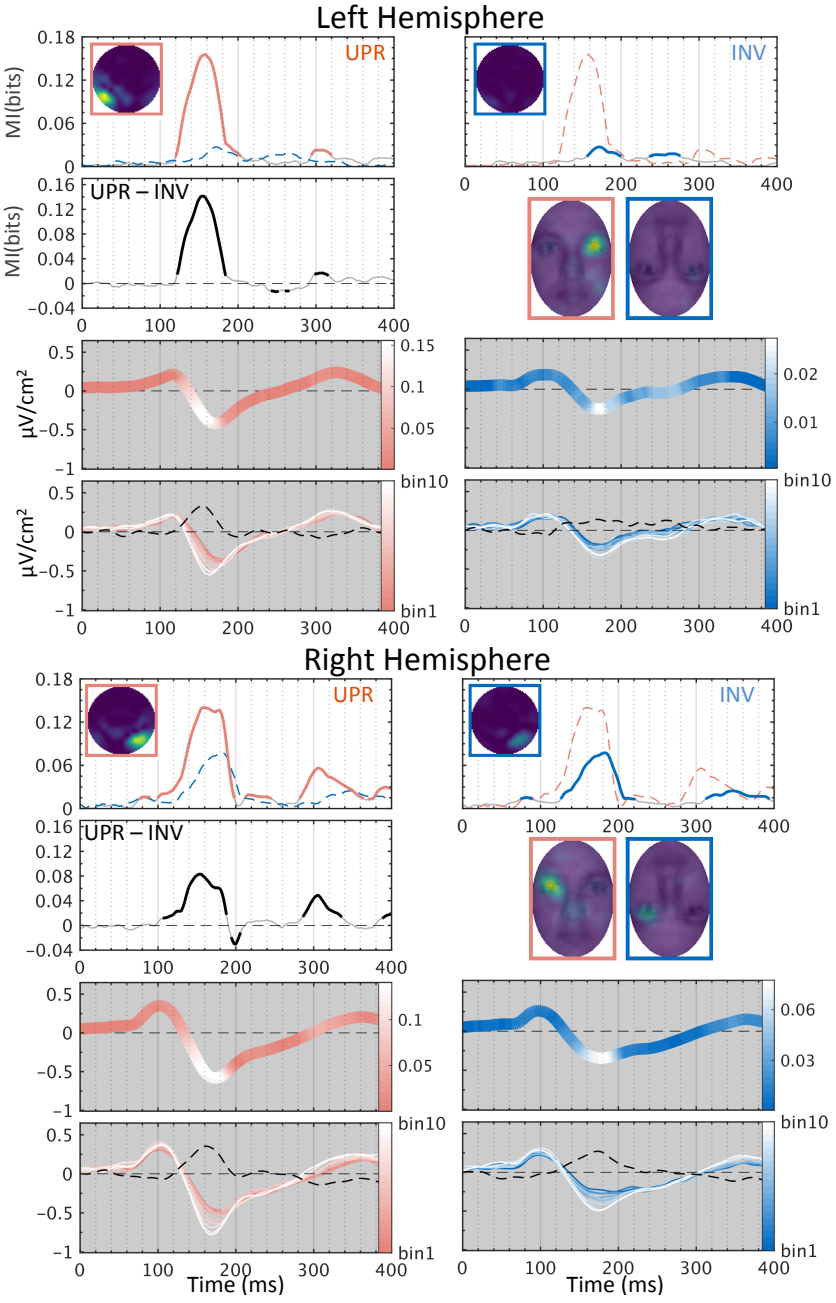

Figure S2.2. Coding of observer 2.

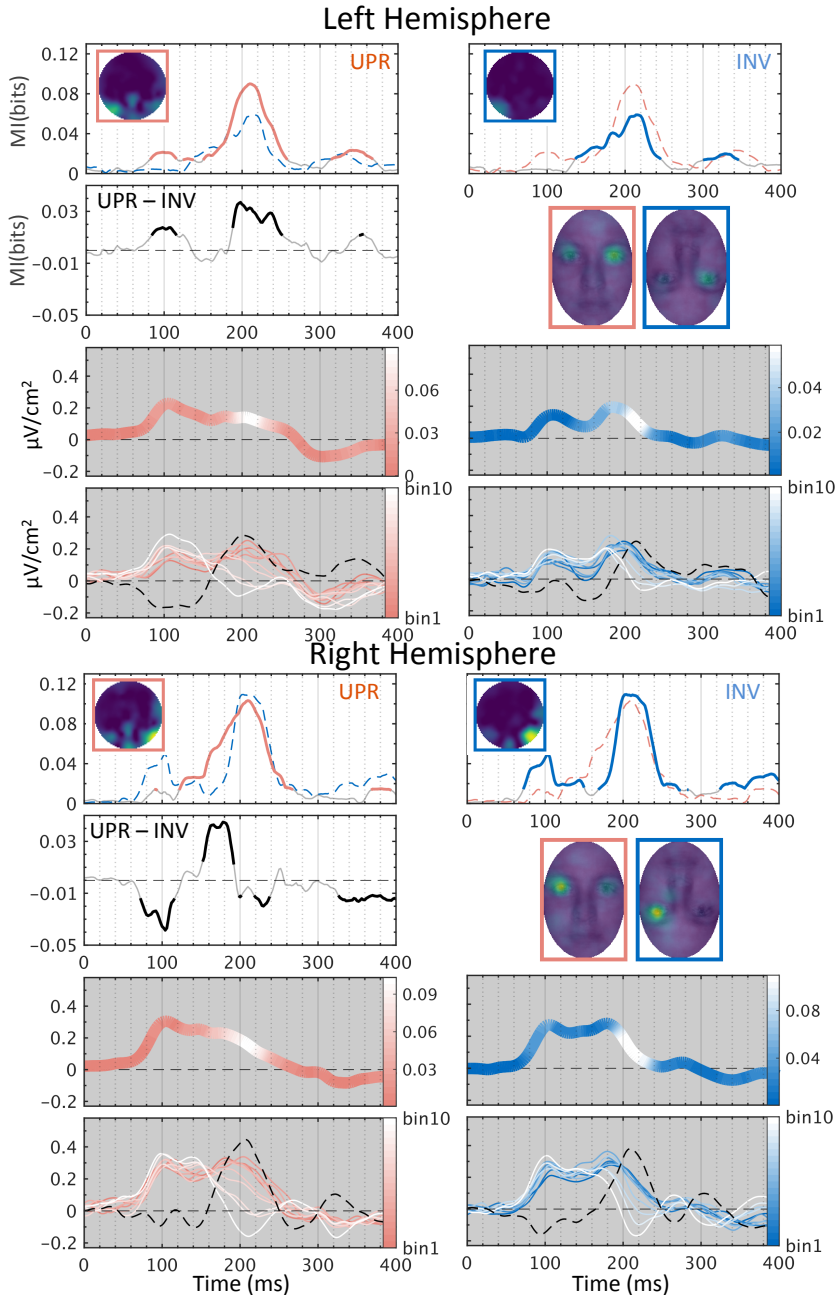

Figure S2.3. Coding of observer 3.

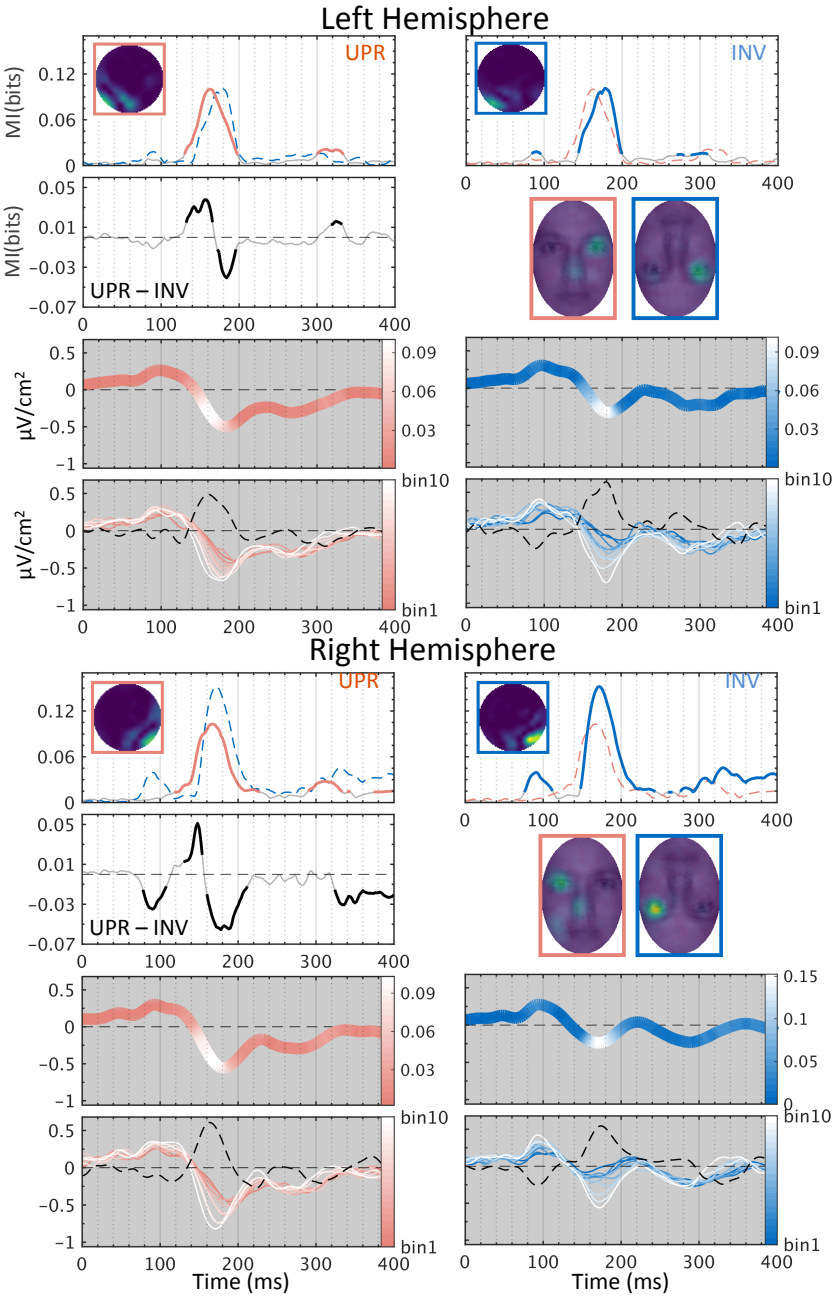

Figure S2.4. Coding of observer 4.

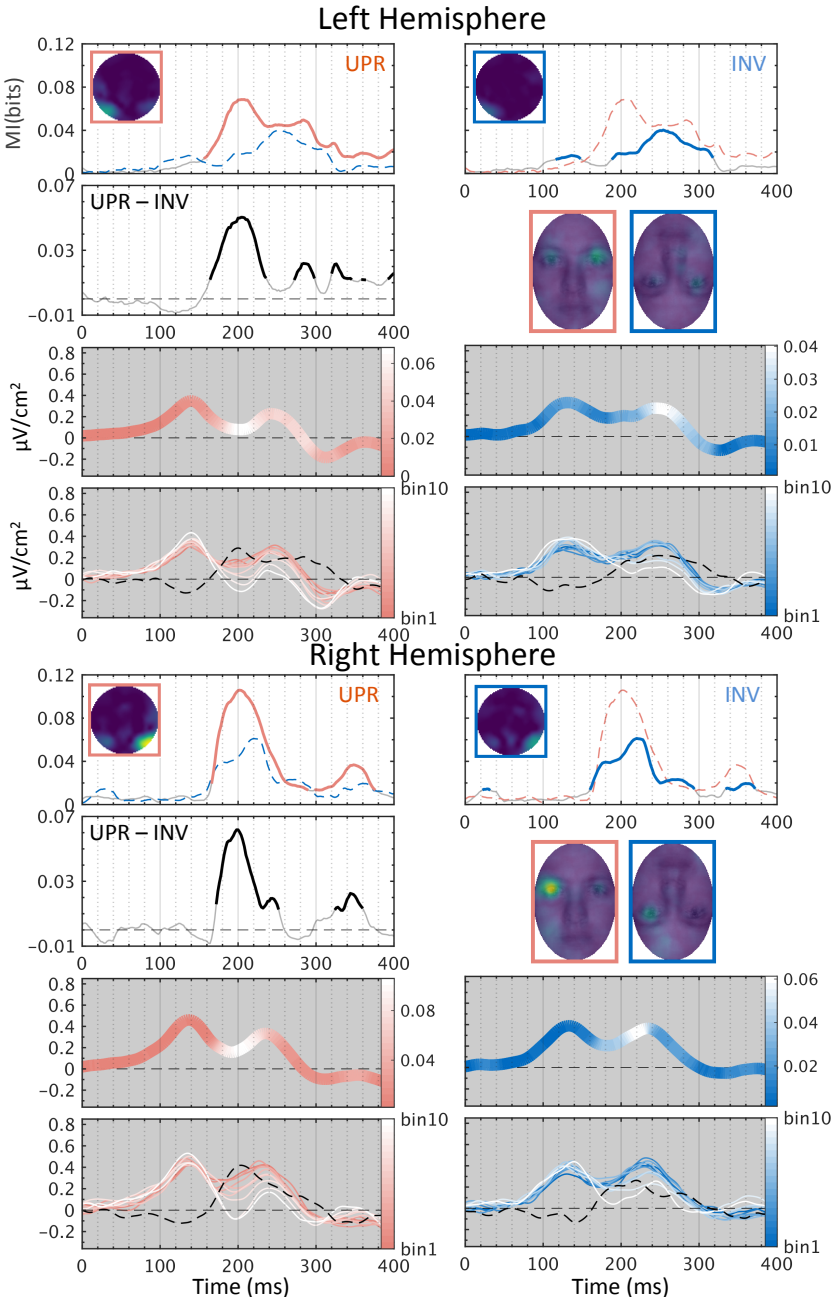

Figure S2.5. Coding of observer 5.

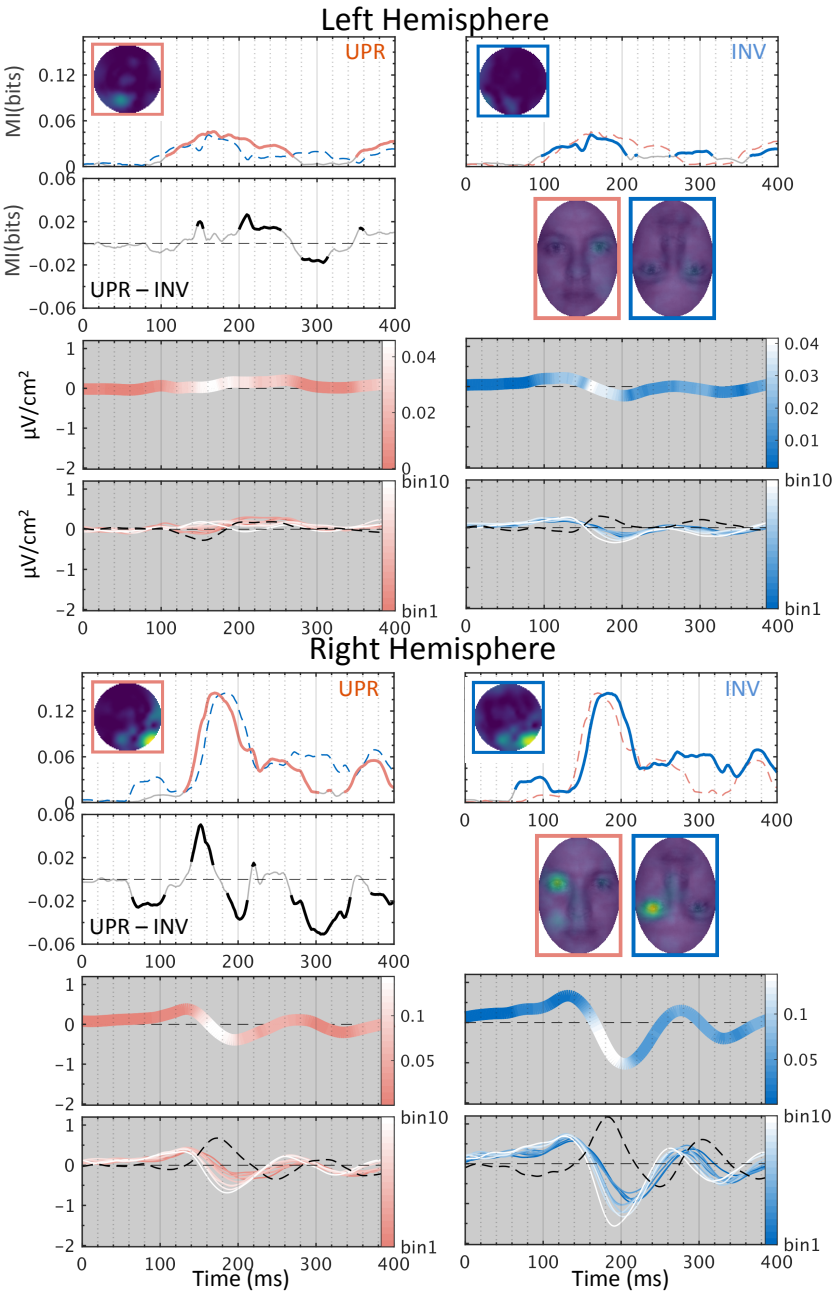

Figure S2.6. Coding of observer 6.

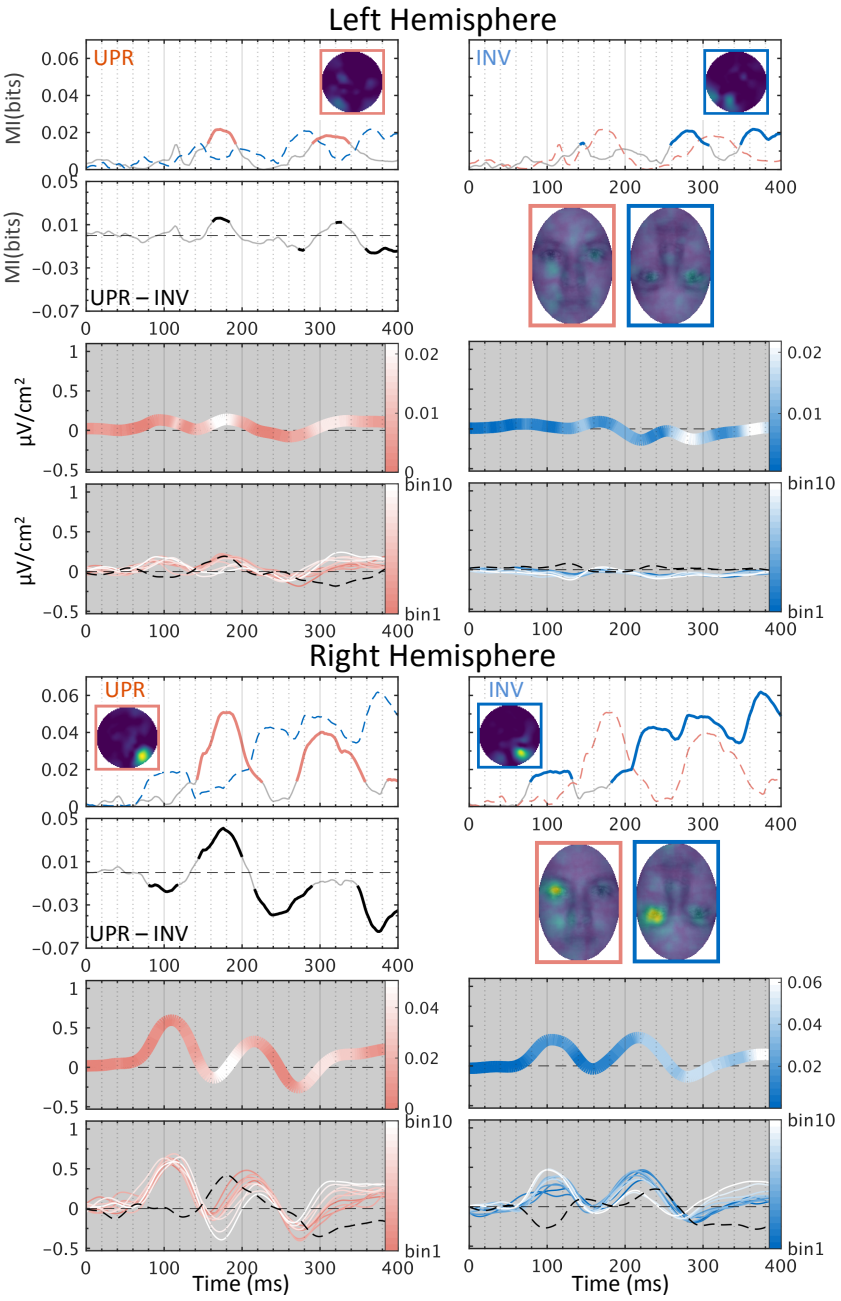

Figure S2.7. Coding of observer 7.

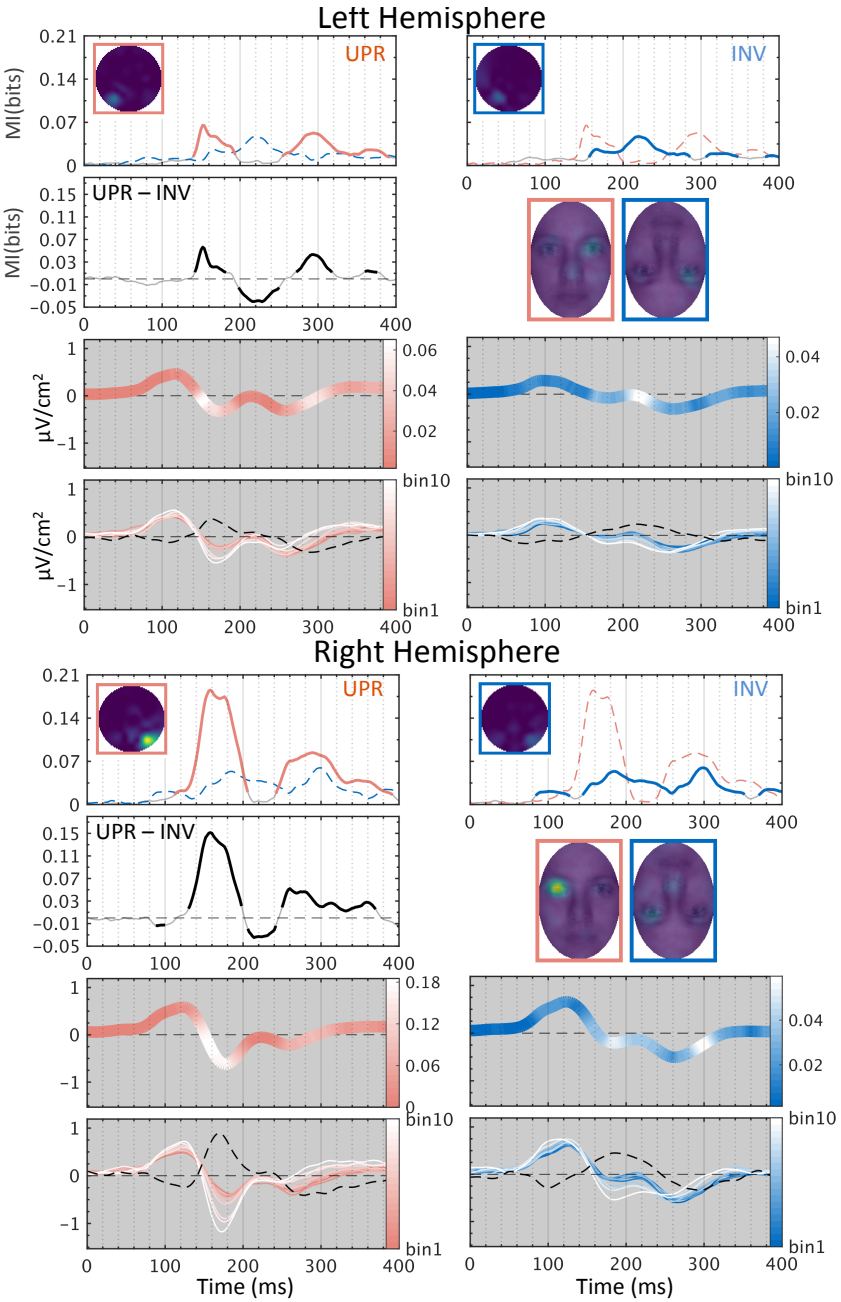

Figure S2.8. Coding of observer 8.

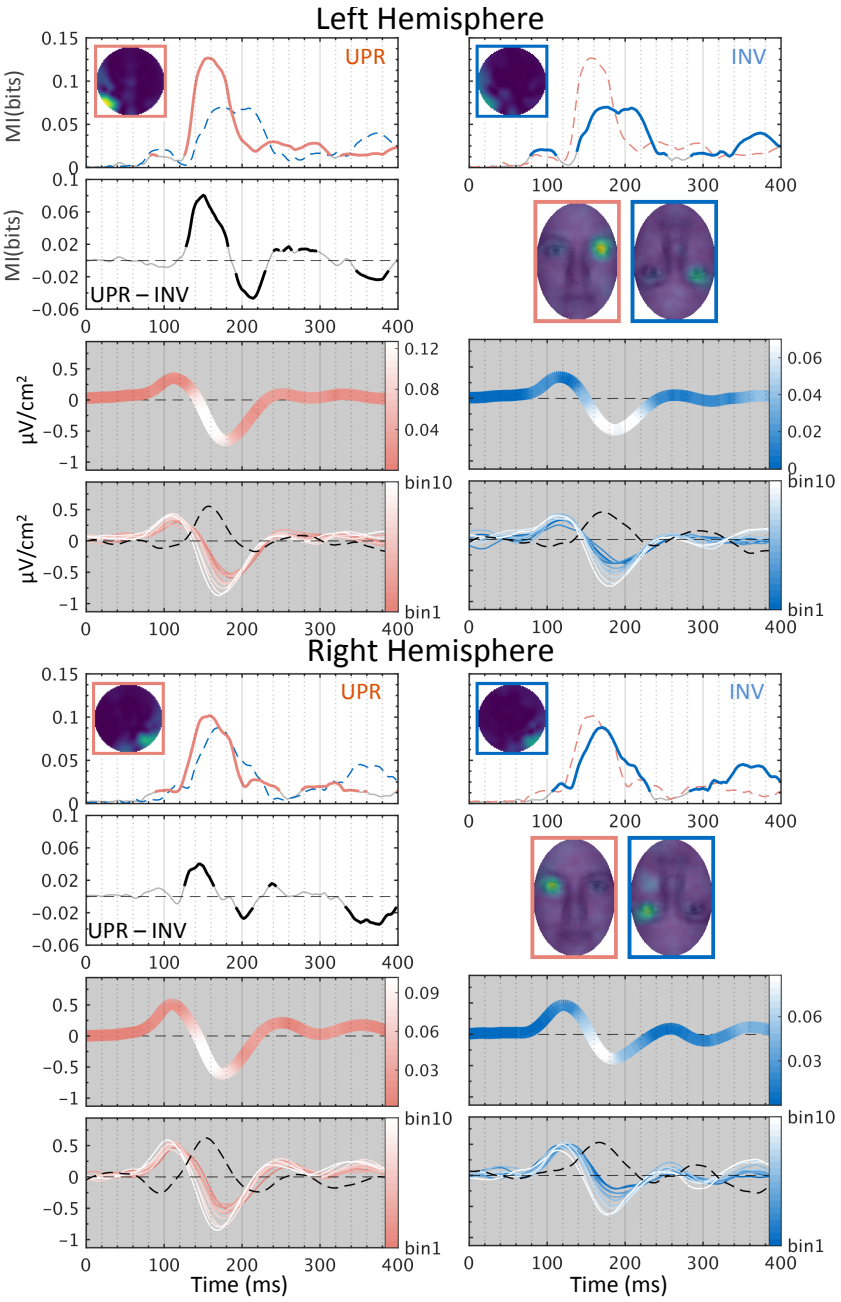

Figure S2.9. Coding of observer 9.

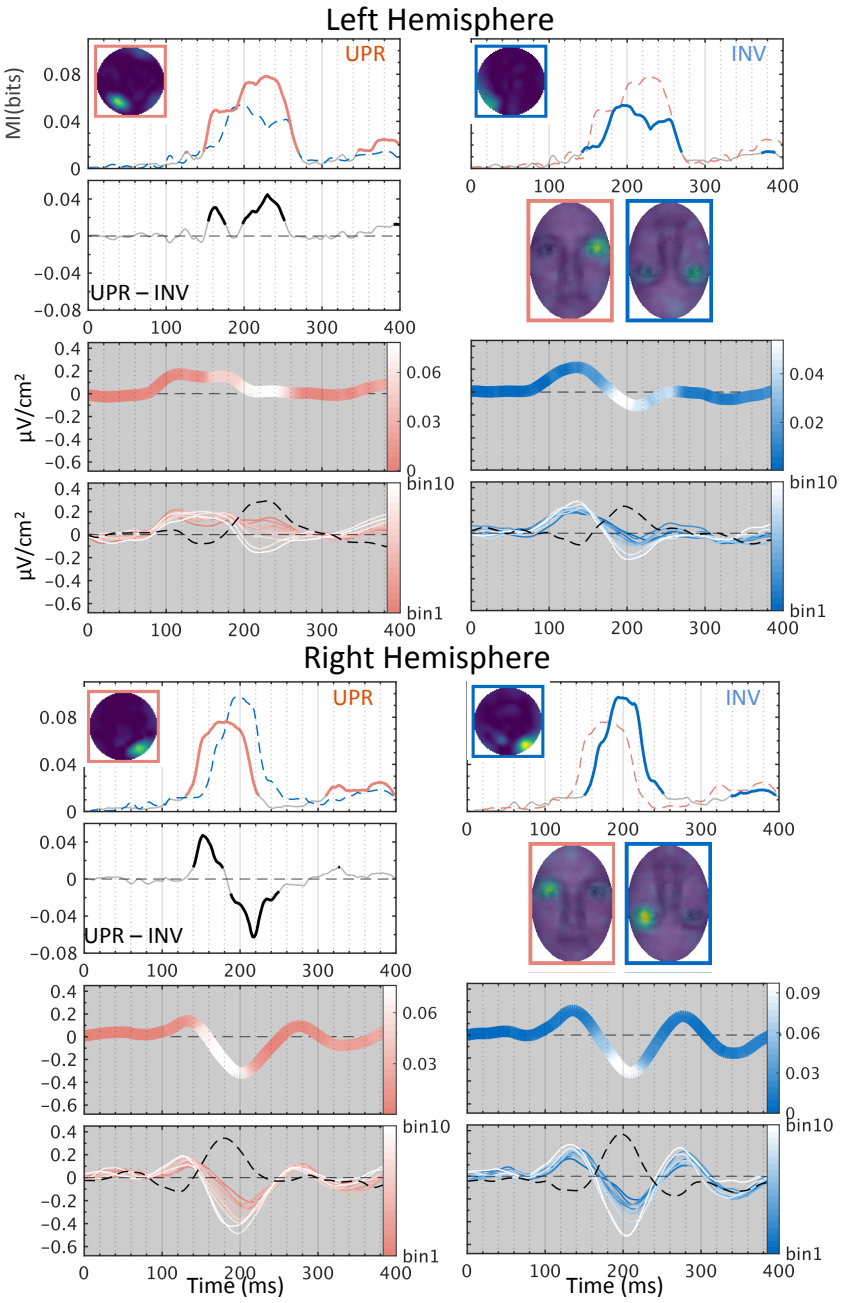

Figure S2.10. Coding of observer 10.

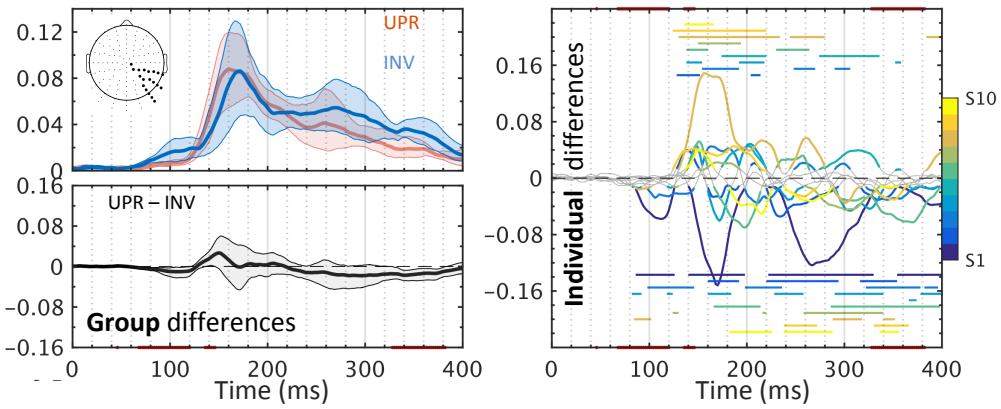

Figure S2.11. MI(EYE, [ERP, ERP$_g$]) results of the causal dataset using the left eye mask. Right electrodes of interest are highlighted in the electrode maps from the 10/10 system at the top. **Left:** First row shows how group averaged MI quantity across ten participants evolves over time separately for upright and inverted faces. The shade shows the 95% CI. The second row shows the mean MI across participants of the differences between upright and inverted faces and 95% CI. Red horizontal lines on the x-axis show the significant group effect. **Right:** Colour parts of waves indicate statistically significant Individual differences. Colour-coded horizontal lines above the x-axis show stronger effects in upright versus inverted, and opposite effects are placed below. Maximum MI across *19* posterior-lateral electrodes of interest that highlighted in the electrode map (inset).

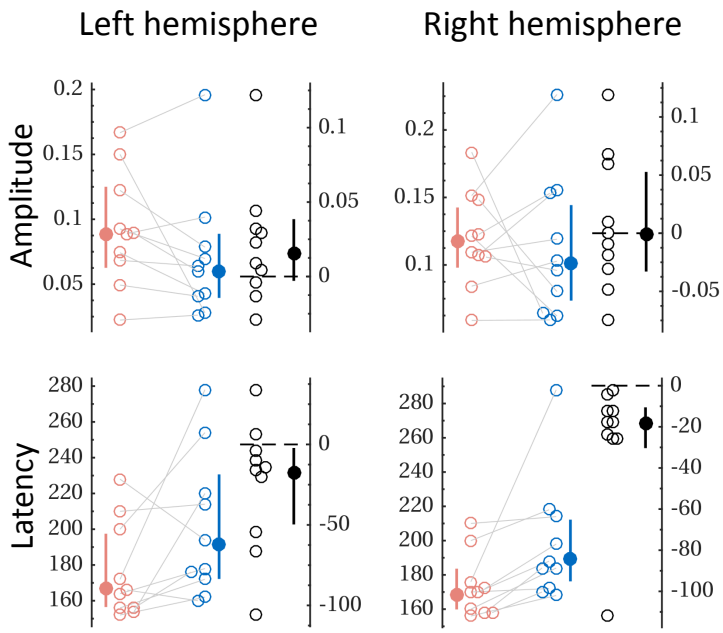

Figure S2.12. Peak analysis of MI(PIX, (ERP, ERP$_g$]). In both hemisphere the value of the MI peak is equivalent between upright and inverted faces (left: 0.02 [0, 0.04] bits; right: 0 [-0.03, 0.05] bits), but 7/10 show weaker MI to inverted versus upright faces on left sensors and 5/10 on right. On left posterior-lateral sensors 8 out of 10 participants show delayed peak to inverted faces, with group effects (-17.5 [-50.77, 2.61] ms). On right sensors there is a significant group latency difference (-18.10 [-30.93, -9.77] ms) and all participants show this effect.

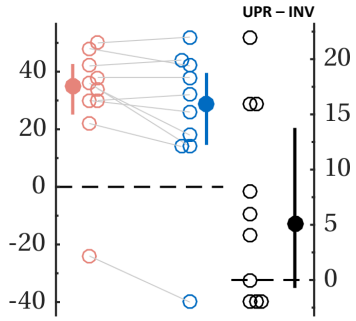

Figure S2.13. Occlusion related delays for face trials. The N170 latency to the masked faces is delayed with respect to intact faces by 34.79 [24.5, 42.47] ms in upright faces and 28.49 [12.6, 40.03] ms. No group-level differences between upright and inverted faces (5.02 [-0.66, 13.29] ms), but 6/10 participants have longer delays in upright faces, 3/10 showed opposite effect.

Appendix B

Supplementary material for Chapter 3.

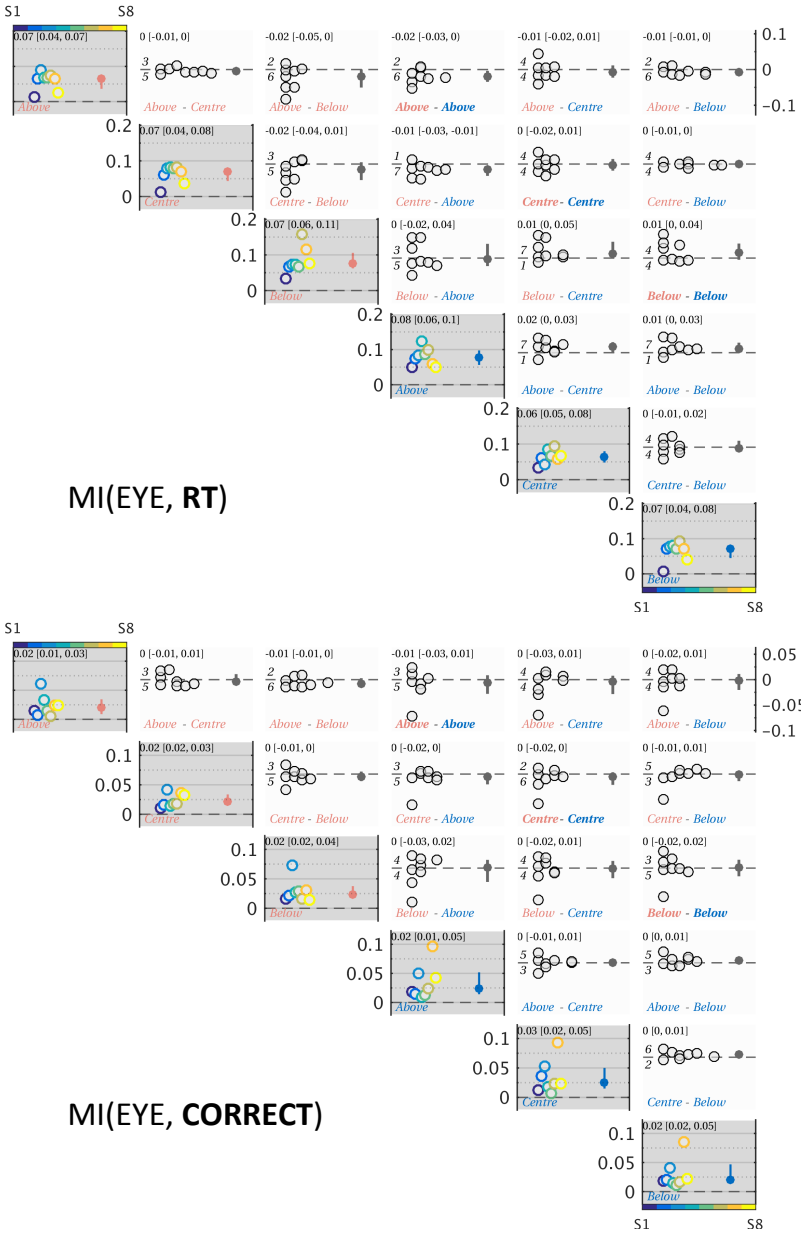

Figure S3.1. MI behavioural results for face trials: all pairwise comparisons. Upper panel is for RT; lower is for correct. In each panel, scatterplot in the grey background shows the distribution of individual MI quantity in behavioural responses (colour-coded circles), separately for each face condition (from left top to right bottom: upright *Above*, *Centre*, *below*; inverted *Above*, *Centre*, *below*). The coloured disks and horizontal bar show the group

medians with their 95% CI that are also detailed in the top. Each scatterplot in the white background shows the distribution of individual differences between pairs of face conditions and their group results. The pair to compare and the direction of differences are illustrated on the bottom. The group results are also detailed on the top. Italic numbers above or below the x-axis show the number of circles above or below the x-axis.

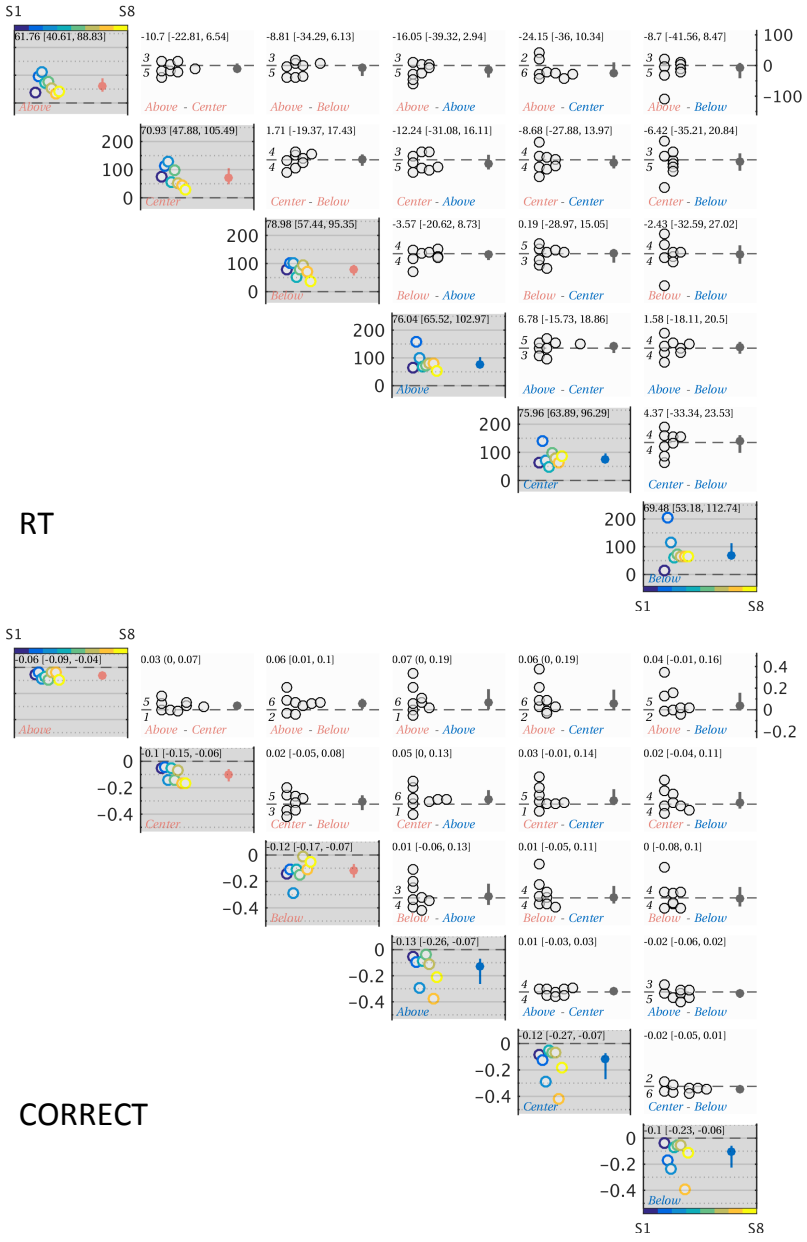

Figure S3.2 Behavioural modulations: all pairwise comparisons. Upper panels are for RT, lower for correct. In each panel, with the grey background, scatterplots show the behavioural performance differences (bin1 - bin10) for participants (colour-coded circles) and group medians with 95% CI (disks and horizontal bar), separately for each face condition. Scatterplots with white background show the distribution of differences of modulations (bin 1

- bin 10) between pairs of face conditions and their group results. The pair to compare and the direction of differences are illustrated on the bottom. The group results are also detailed on the top. Italic numbers above or below the x-axis show the number of circles above or below the x-axis.

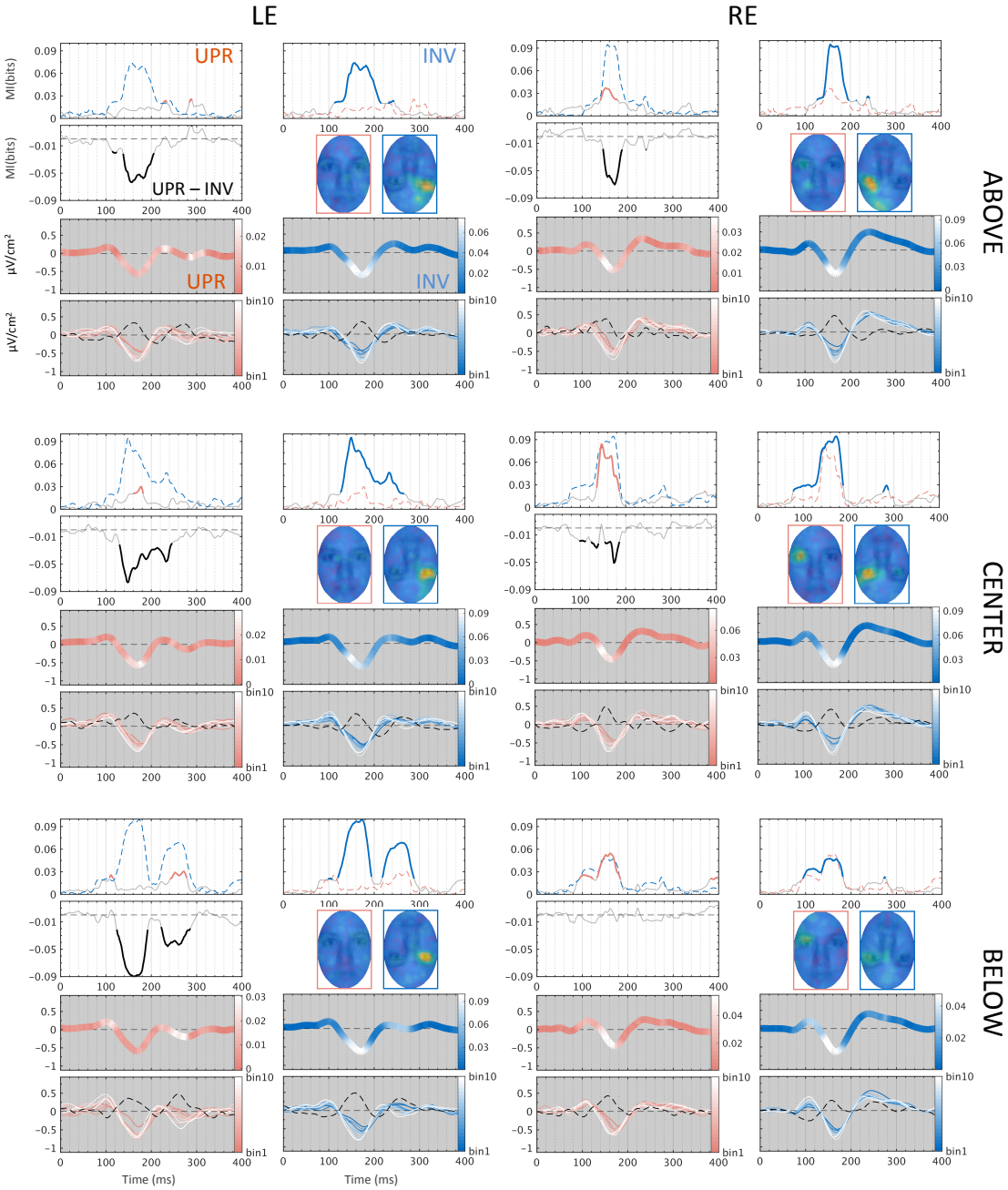

Figure S3.3. Coding of observer 1. First and second columns are for faces with the eyes appeared at *Above*. Second and fourth columns are *Centre*, the last two columns are *Below*. First four rows are for left hemisphere, the lower four rows are for right. First row: Time course of maximum MI(EYE, [ERP, ERPg]) across electrodes of interest are plotted in curves

for each face condition separately. Thicker parts of waves indicate statistical significance. Second row: MI differences are placed on first, third fifth columns. Classification images on the second, fourth and sixth columns indicate that sensors mostly code contralateral eye regions. Third row: the maximum MI curves corresponding to the first row solid lines unfold on the averaged ERPs in Bubble trials. Fourth row: averaged ERPs on Bubble trials are colour-coded at each level of eye visibility. The red and white waves indicate bin1 (lowest eye visibility) and bin10 (highest eye visibility). The black dashed curve represents the differences (bin1 - bin10).

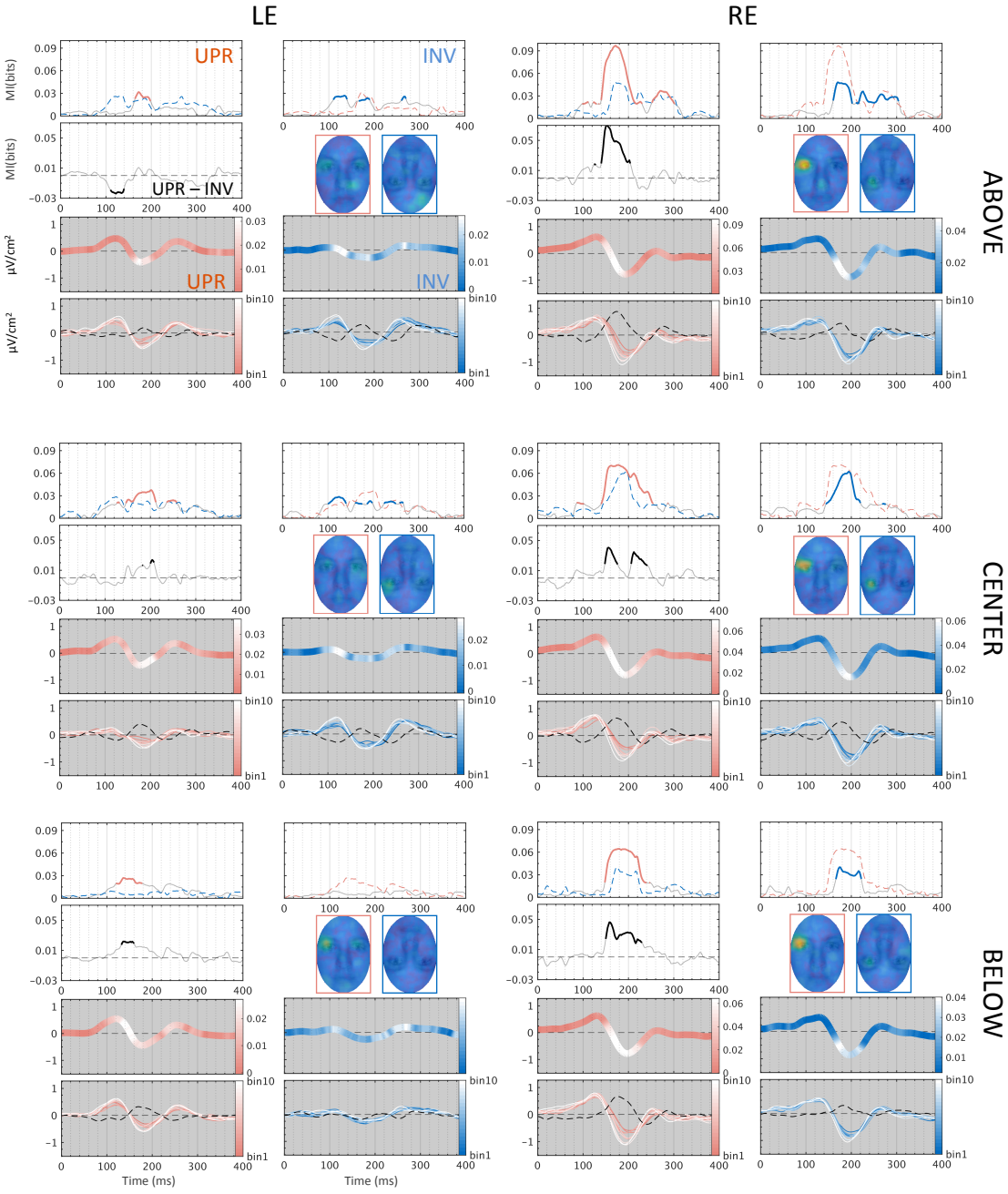

Figure S3.4. Coding of observer 2

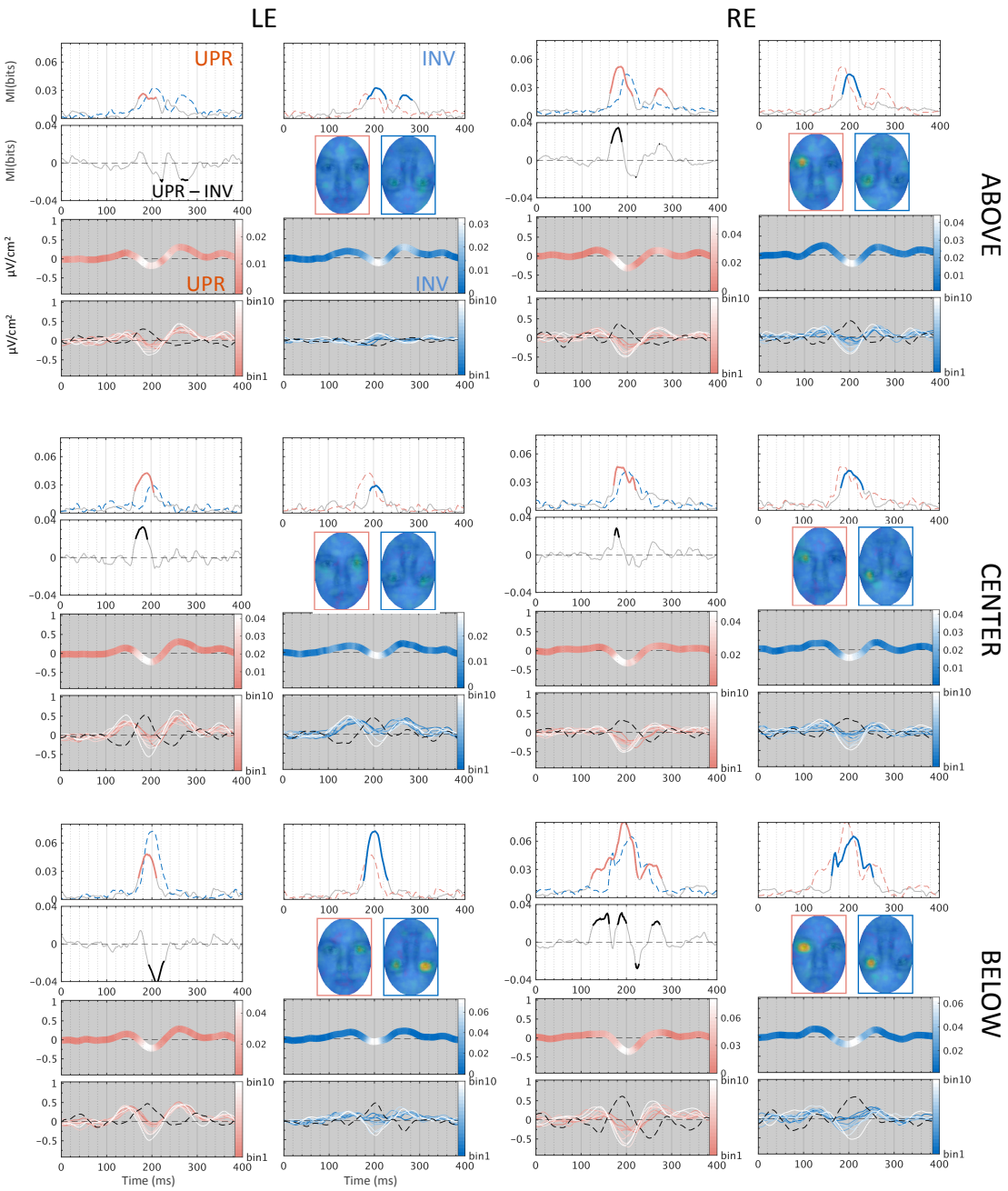

Figure S3.5. Coding of observer 3.

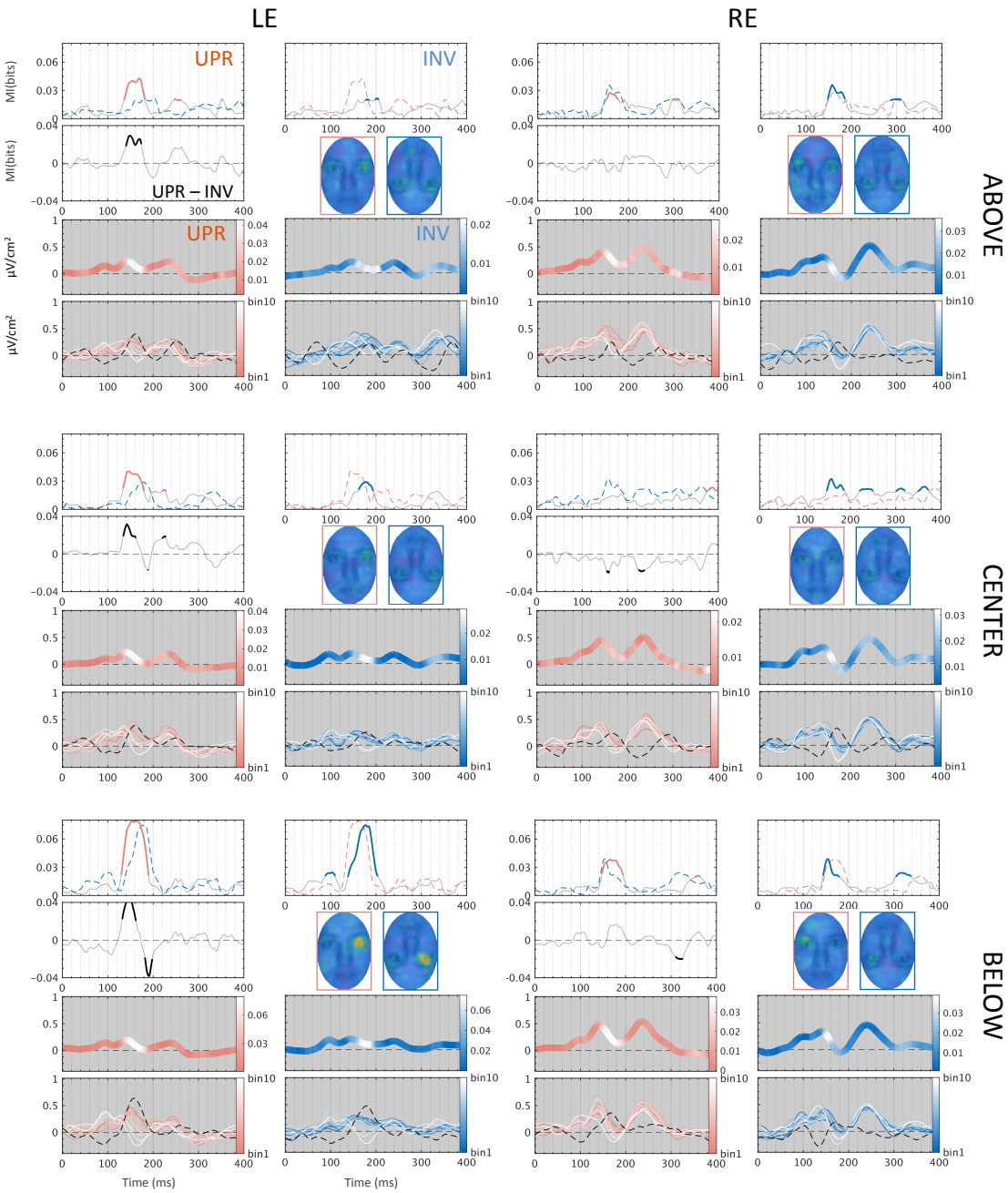

Figure S3.6. Coding of observer 4.

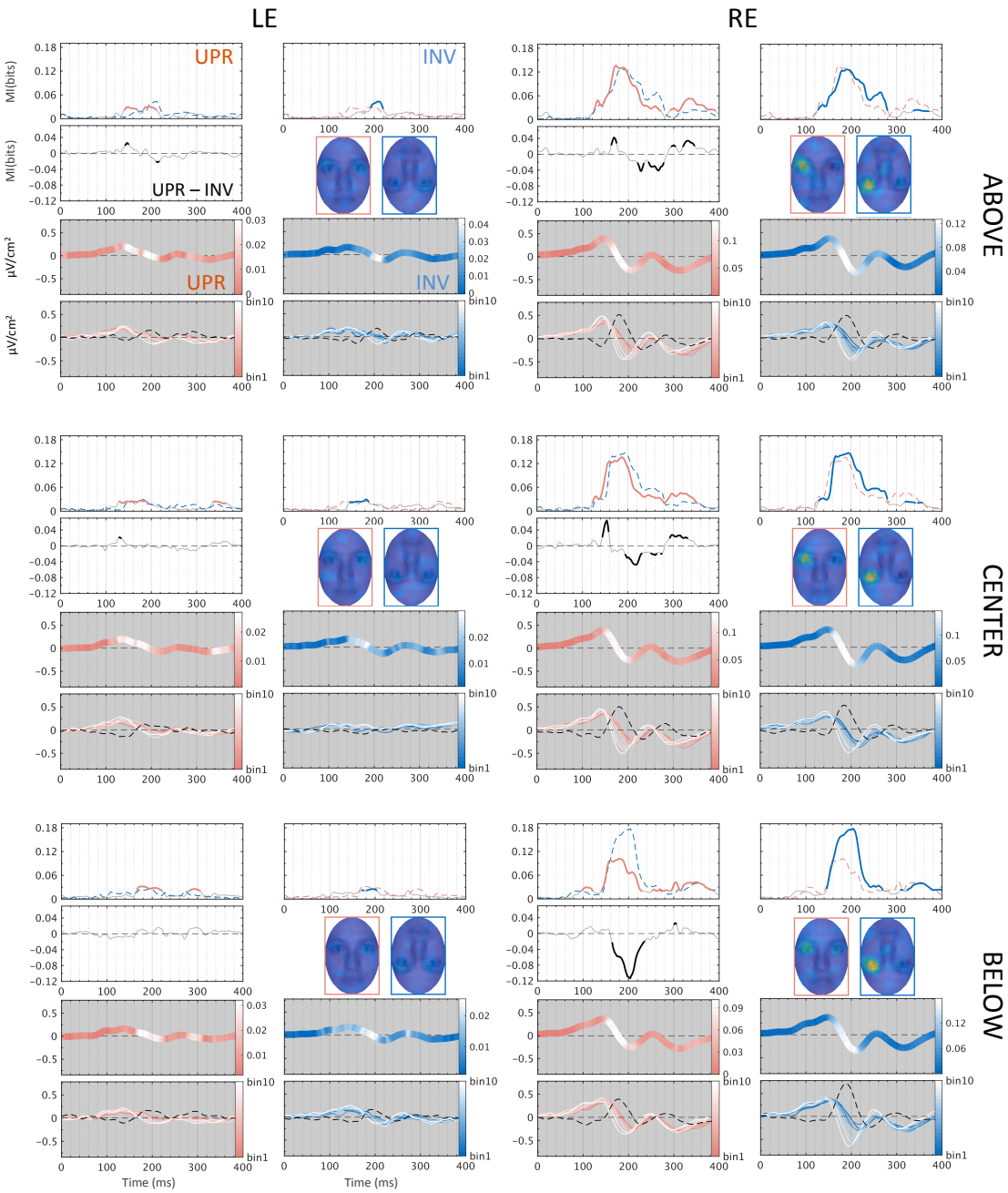

Figure S3.7. Coding of observer 5.

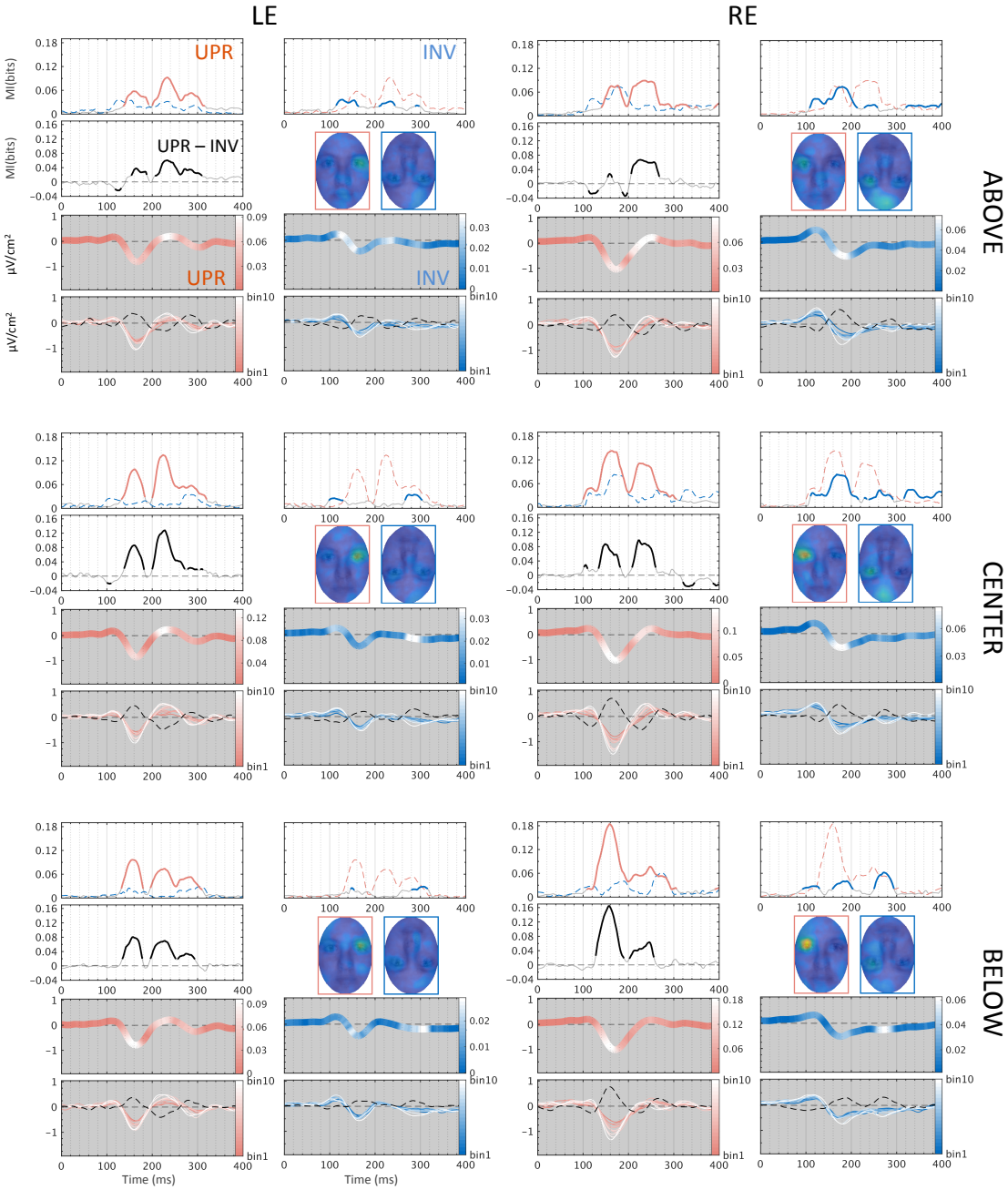

Figure S3.8. Coding of observer 6.

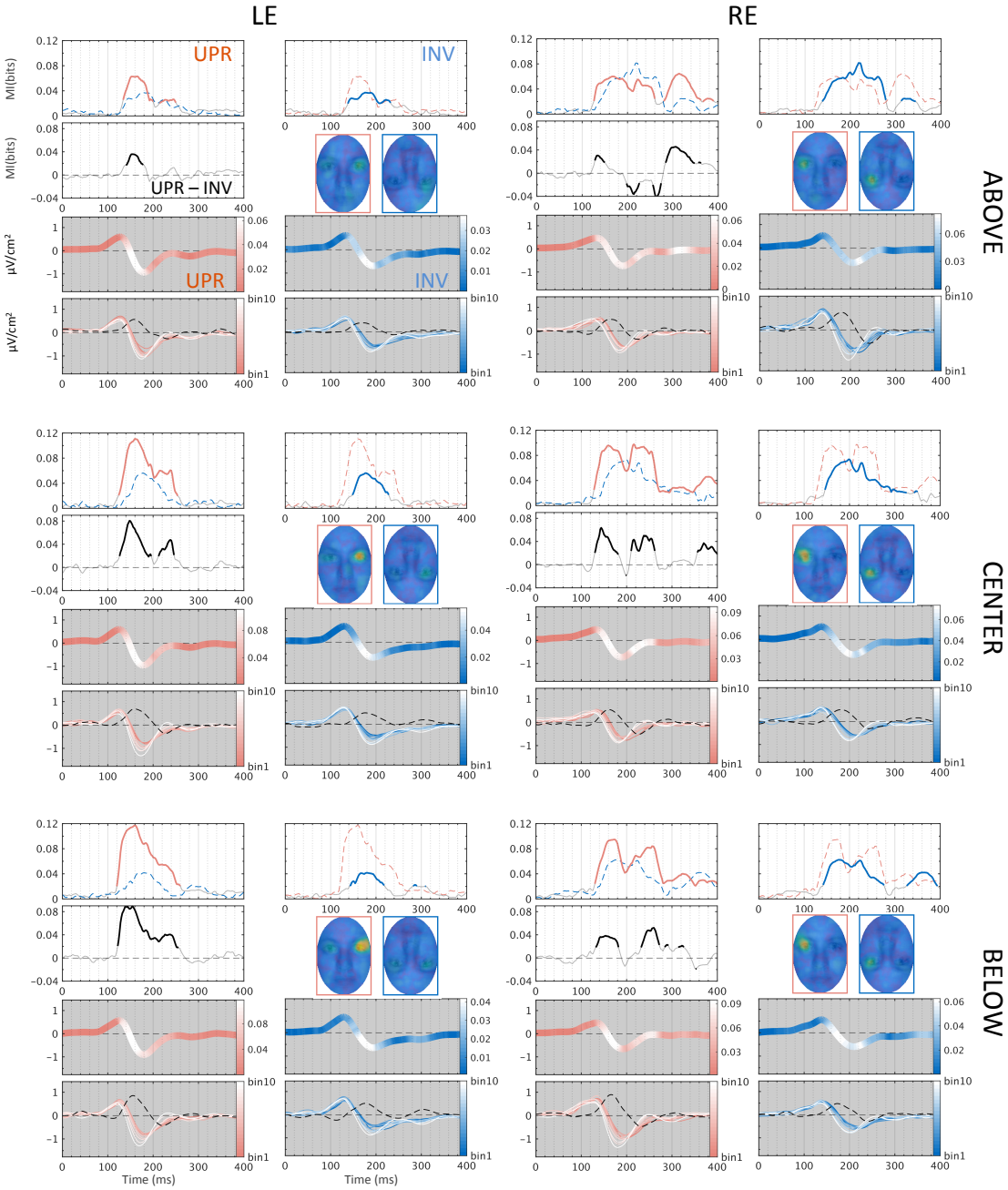

Figure S3.9. Coding of observer 7.

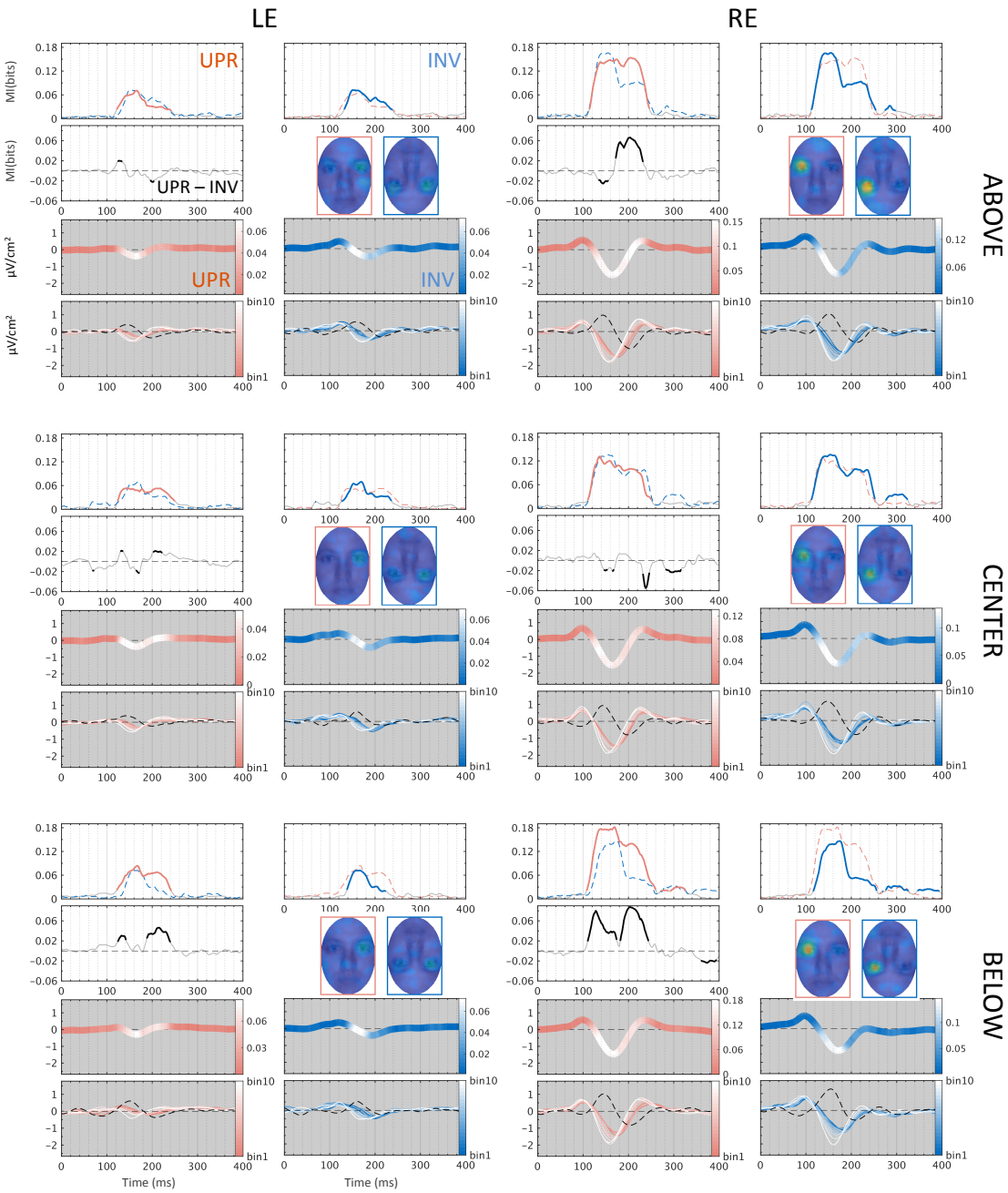

Figure S3.10. Coding of observer 8.

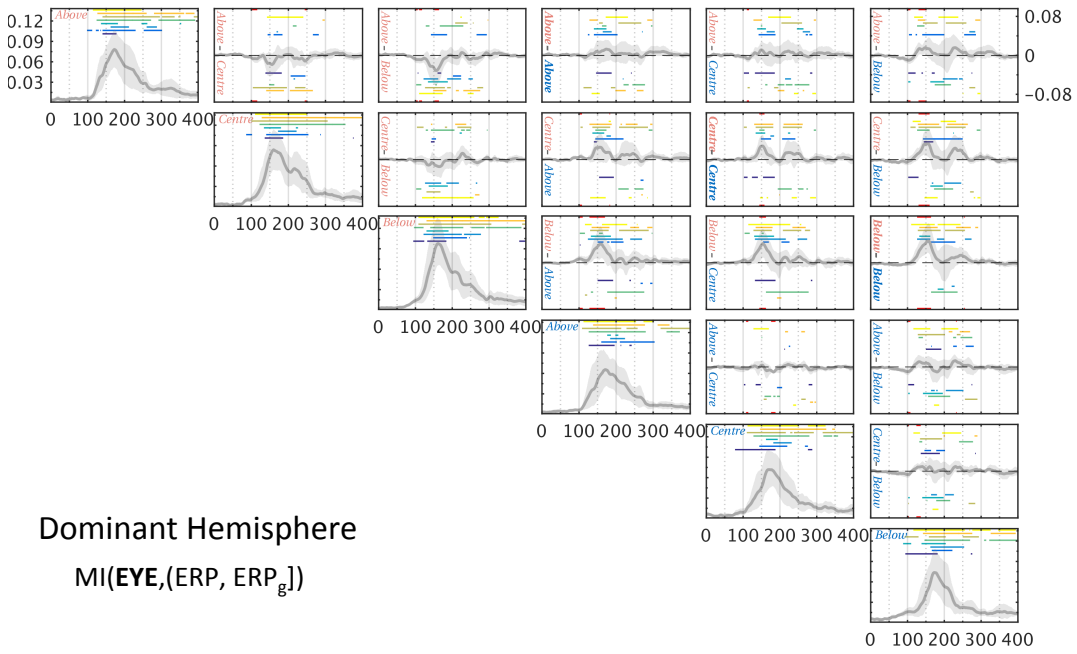

Figure S3.11. MI EEG results for face trials: all pairwise comparisons. Red is for upright faces, blue for inverted. In the far left plots of each row, thick line with the shade shows mean maximum MI across 8 participants with 95% CI for each face condition. Colour-coded horizontal bars indicate statistical significance per participant. The rest plots show mean across participants of the MI differences with 95% CI between upright and inverted. Colour-coded horizontal lines above the x-axis show stronger effects in the condition that illustrated on the upper area. Opposite effects are placed below. The red horizontal bar on the x-axis indicates time points of group-level significant differences.

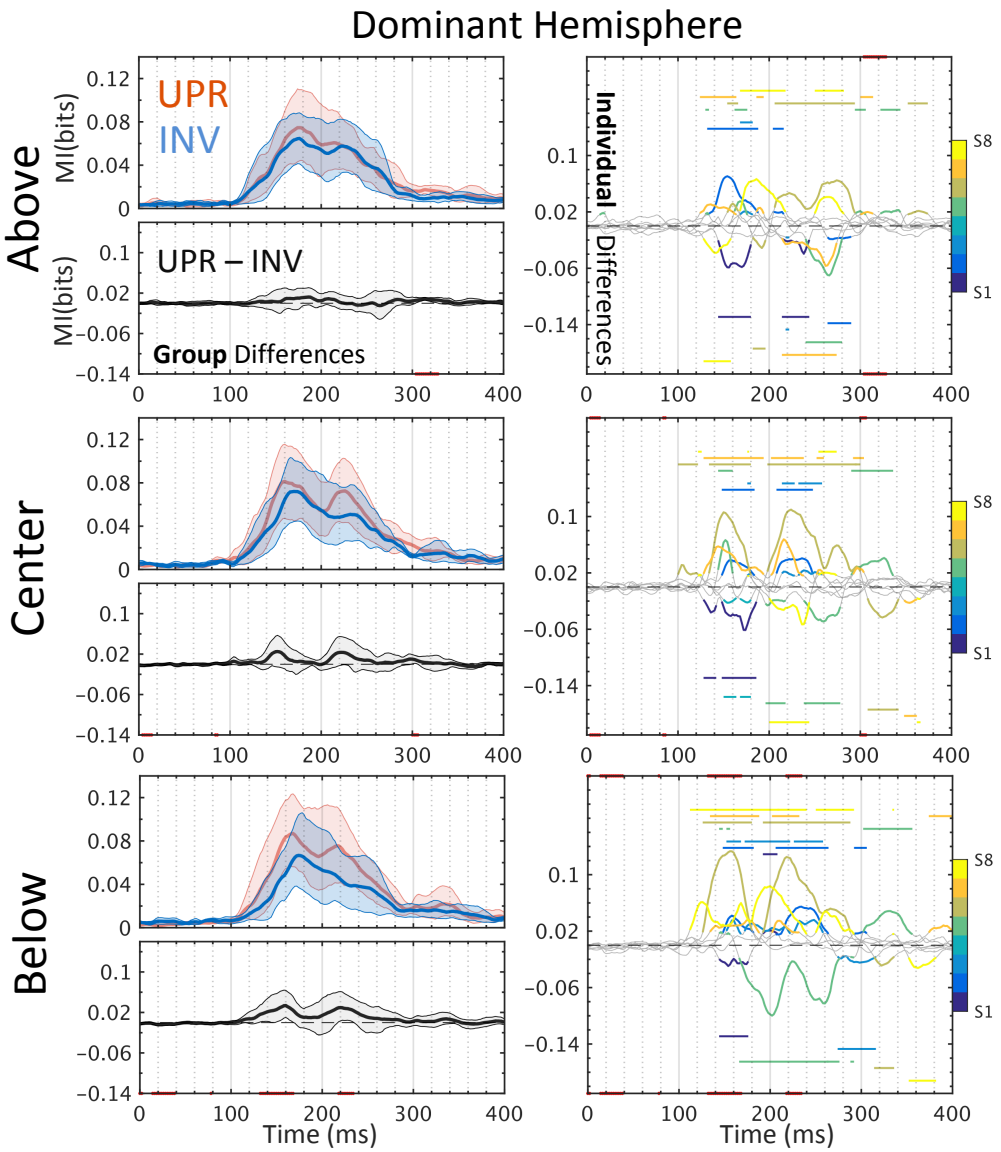

Figure S3.12. MI EEG results from the causal dataset. Group-level results are placed on the left. In the first, third and fifth row, the panels illustrate the time course of group averaged MI for each face condition. Curves with shades show mean maximum MI across 8 participants with 95% CI. In the second, fourth and last row, panels show mean across participants of the MI differences between upright and inverted with 95% CI. The red horizontal bar indicates time points of significant differences. The right panels show individual differences. Colour parts of waves indicate statistically significant differences per participant. Colour-coded horizontal lines above the x-axis show stronger effects in upright versus inverted, and opposite effects are placed below.

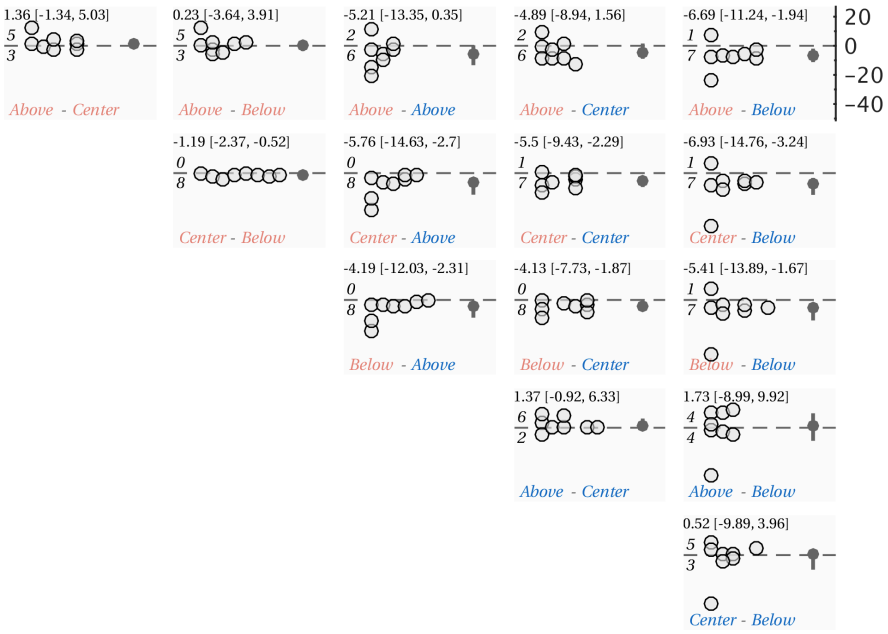

Figure S3.13. Integral latency: all pairwise comparisons. Each scatterplot shows the distribution of individual differences between face conditions (black circles) and group medians with 95% CI (black disk and horizontal bar). The pair to compare and the direction of differences are illustrated on the bottom. The group results are also detailed on the top. Italic numbers above or below the x-axis show the number of circles above or below the x-axis.

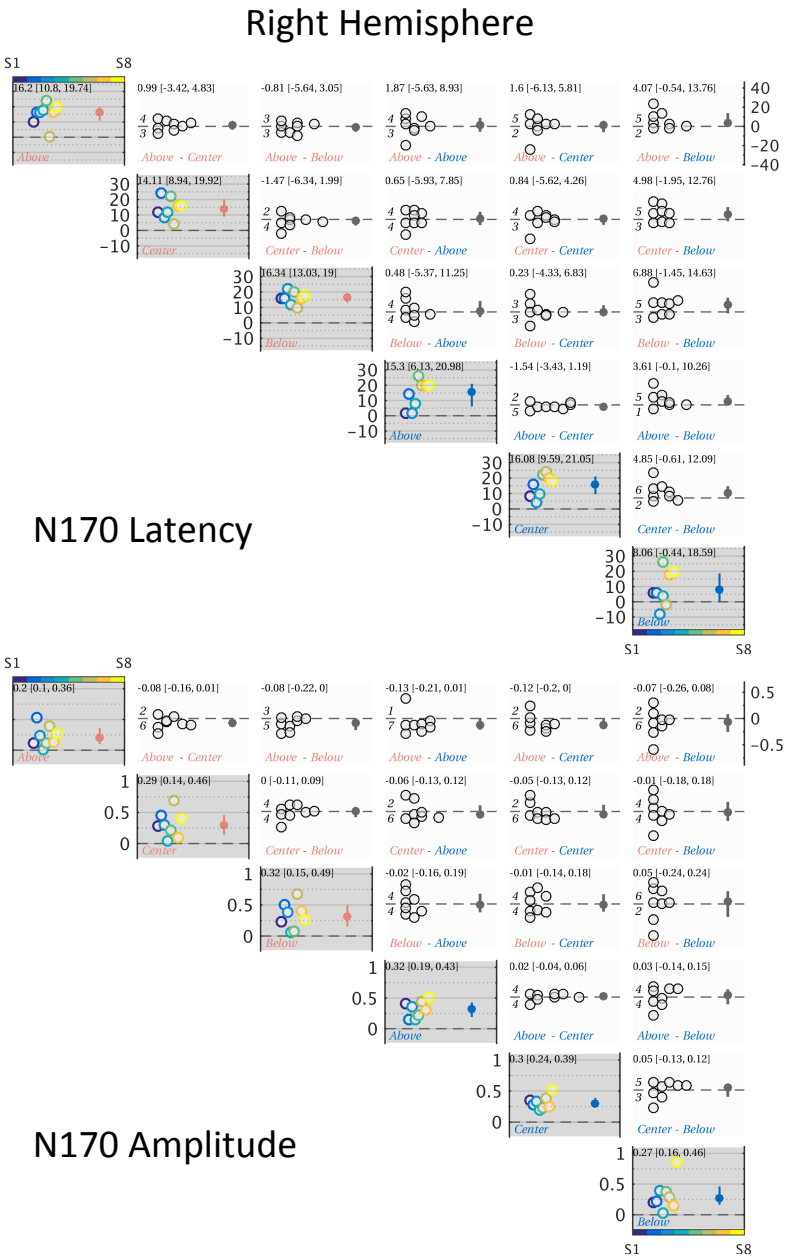

Figure S3.14. ERPs modulations: all pairwise comparisons. Upper for the N170 latency, lower for amplitude. In each panel, with the grey background, scatterplots show the Differences of ERP peak (bin1 - bin10) for participants (colour-coded circles) and group medians with 95% CI (disks and horizontal bar), separately for each face condition. Scatterplots with white background show the distribution of differences of modulations (bin 1 - bin 10) between pairs of face conditions and their group results. The pair to compare and the direction of differences are illustrated on the bottom. The group results are also detailed on the top. Italic numbers above or below the x-axis show the number of circles above or below the x-axis.

Appendix C

Supplementary material for Chapter 4.

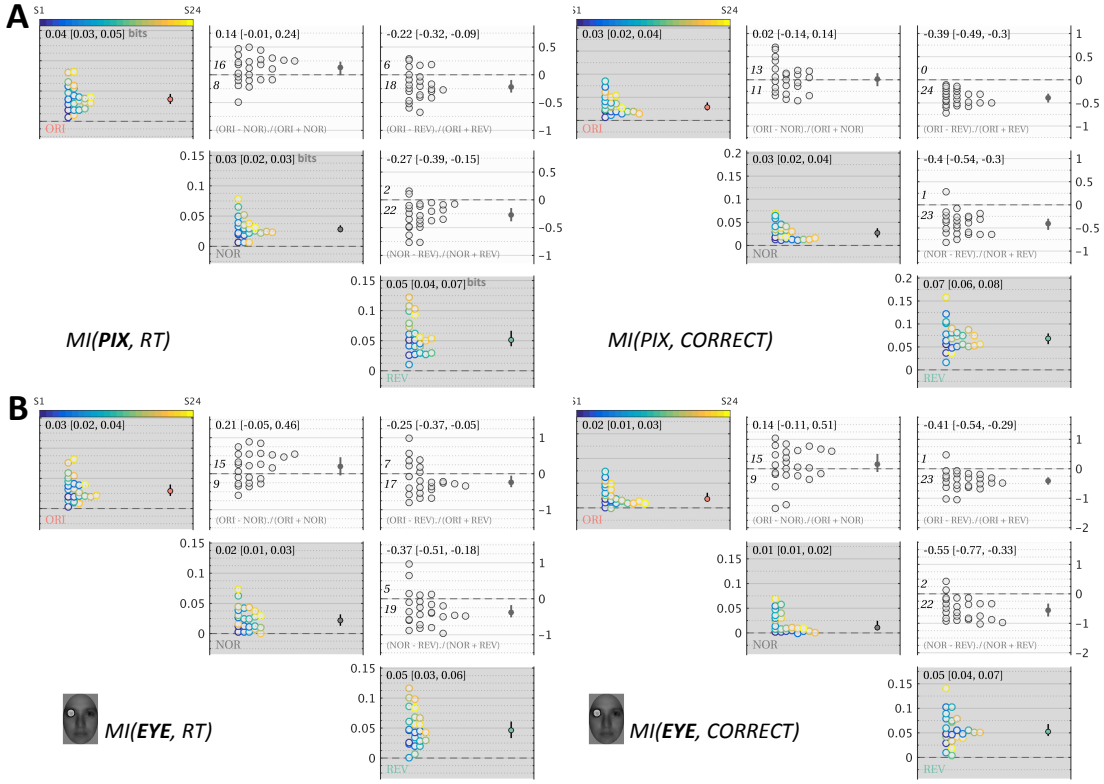

Figure S4.1. MI behavioural results: all pairwise comparisons. In each panel, scatterplot in the grey background shows the distribution of individual MI quantity in behavioural responses (colour-coded circles), separately for each face manipulation (from left top to right bottom: ORI, NOR and REV). The coloured disks show the group medians with their 95% CI that were also detailed in the top. Each scatterplot in the white background shows the distribution of individual differences (Contrast Index Ratio) between pairs from face conditions (ORI vs. NOR, ORI vs. REV, NOR vs. REV) and group results. Italic numbers above the x-axis show how many participants had stronger effects in ORI vs. NOR or ORI vs. REV, or NOR vs. REV, and the number of participants that had opposite effects are placed below. (A) Whole stimulus sampling. Left: RT; Right: Correct or not. There is no difference between ORI and NOR. The maximum MI on REV is stronger than ORI and NOR. (B) Eye mask analysis results are similar to whole stimulus sampling analysis.

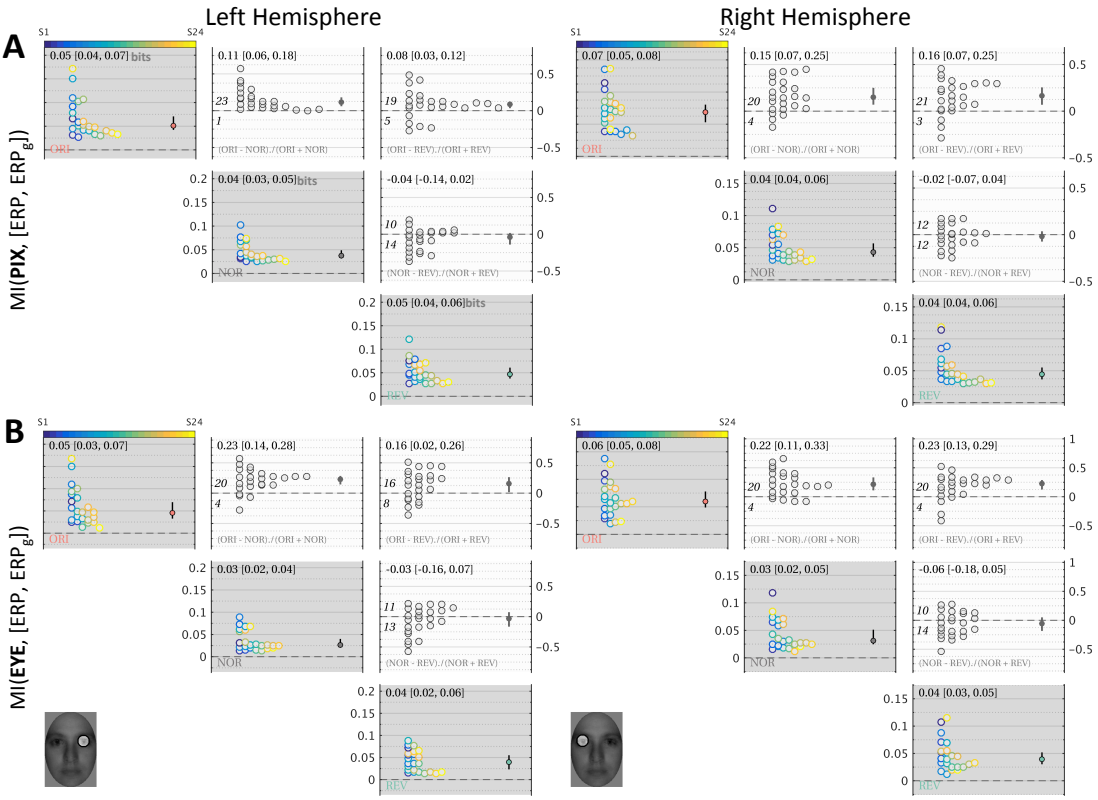

Figure S4.2. Face contrast-related effect on ERPs sensitivity to contralateral eye. Same figure structure as Figure S1. (A) The maximum MI using whole stimulus sampling analysis across pixels, electrodes and frames per hemisphere. In the left hemisphere paired comparison analyses show largest contralateral eye sensitivity on ORI and no statistically significant difference between NOR and REV. Left and right hemisphere show similar results. (B) The maximum MI involving contralateral eye region across frames and electrodes in the right and left hemisphere. The eye sampling result is similar to whole stimulus sampling analysis.

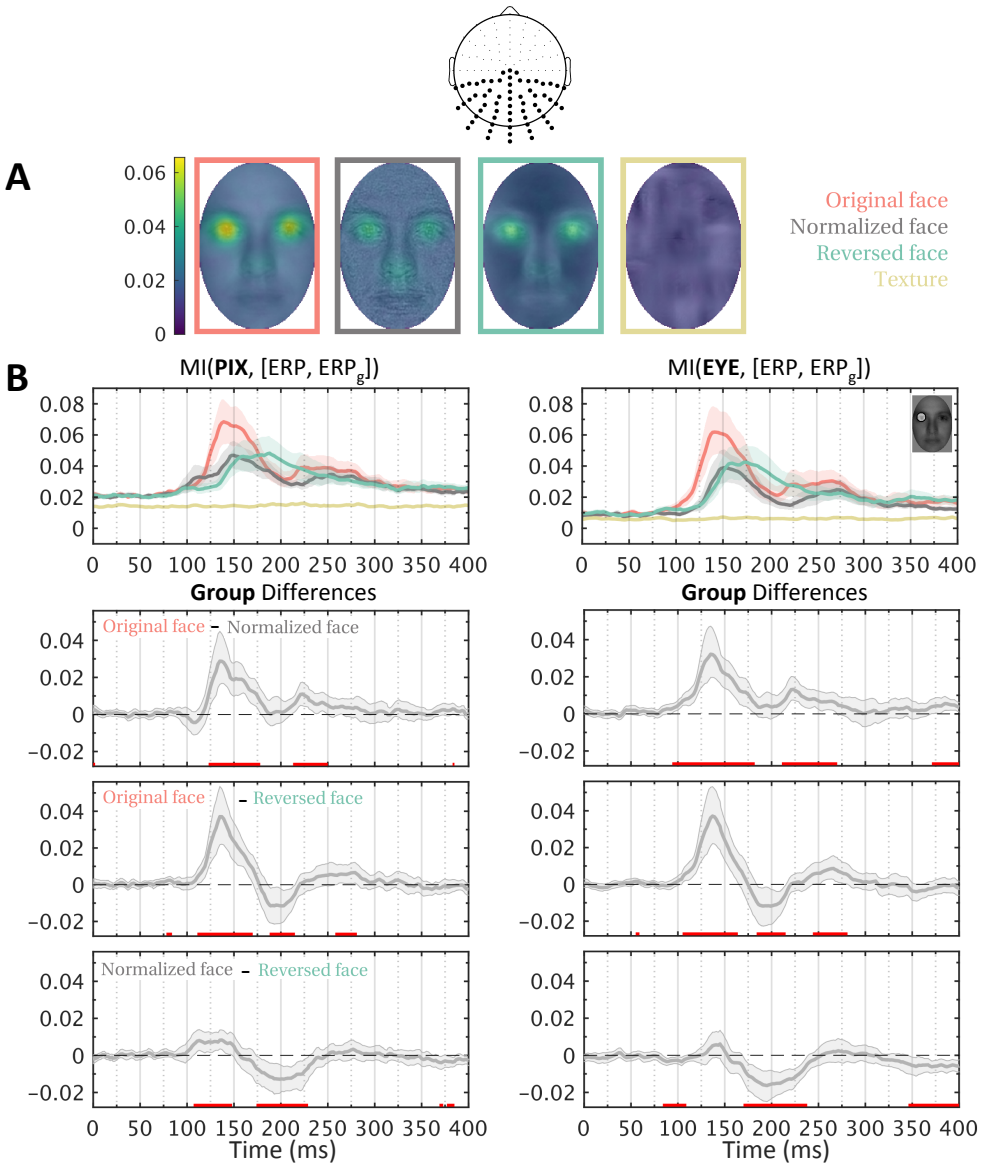

Figure S4.3. Comparison between whole stimulus and eye mask analyses over all posterior electrodes. These electrodes of interest labelled in black disks are shown in the top. (A) The group averaged classification images revealed eye sensitivities in every face condition. (B) The first row shows how MI quantity unfolds over time per each condition. Group differences are placed in the next three rows. Left: Whole stimulus sampling. The time course of maximum MI(PIX, [ERP, ERPg]) across pixels and electrodes. Right: Eye mask analyses. The time course of MI between left eye region and electrodes. MI results between whole stimulus and eye mask analyses are similar.

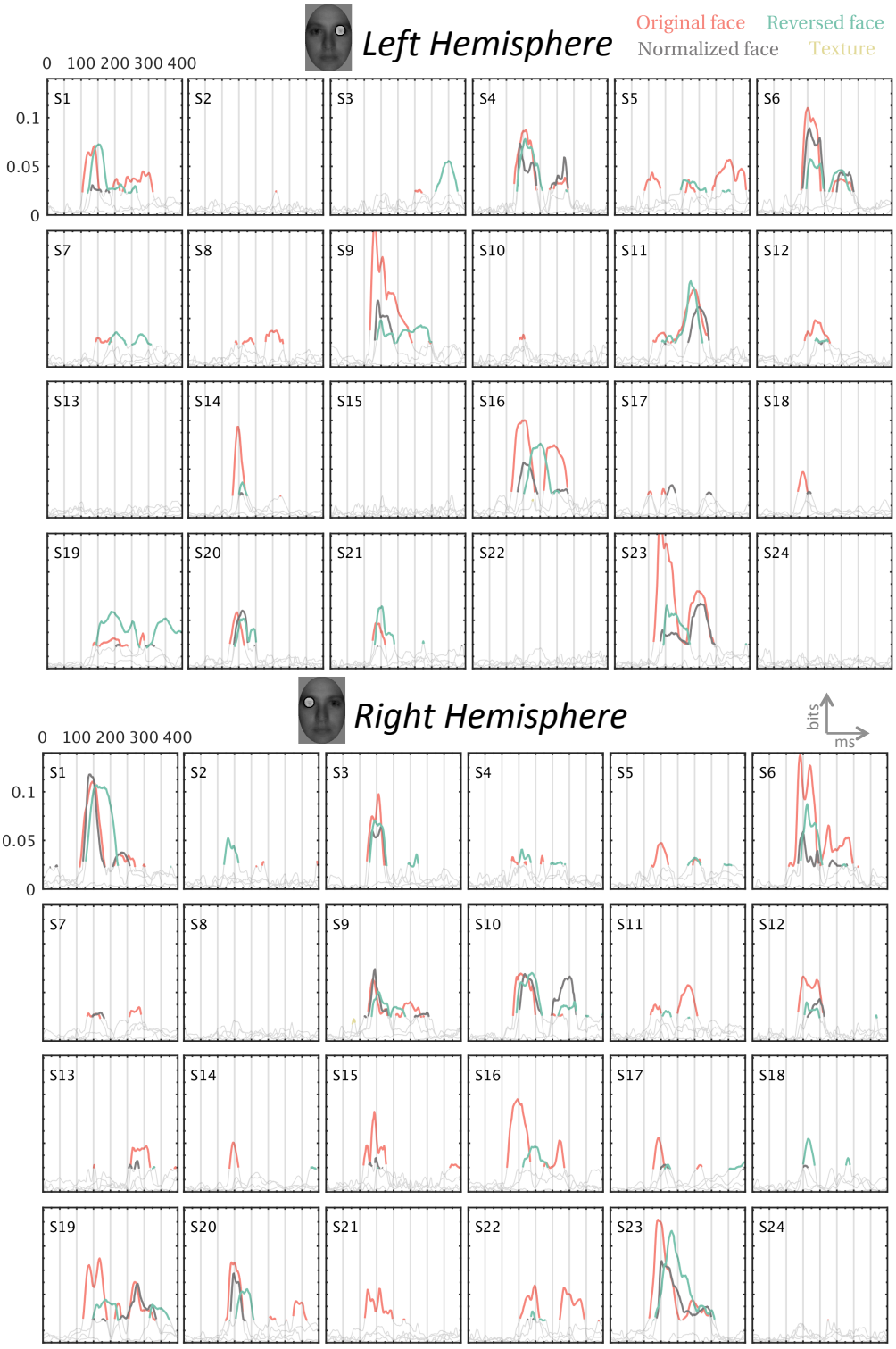

Figure S4.4. Significant MI(EYE, [ERP, ERP_g]) per participant for each condition. The curves show the maximum MI across electrodes per hemisphere and coloured sections indicate statistical significances.

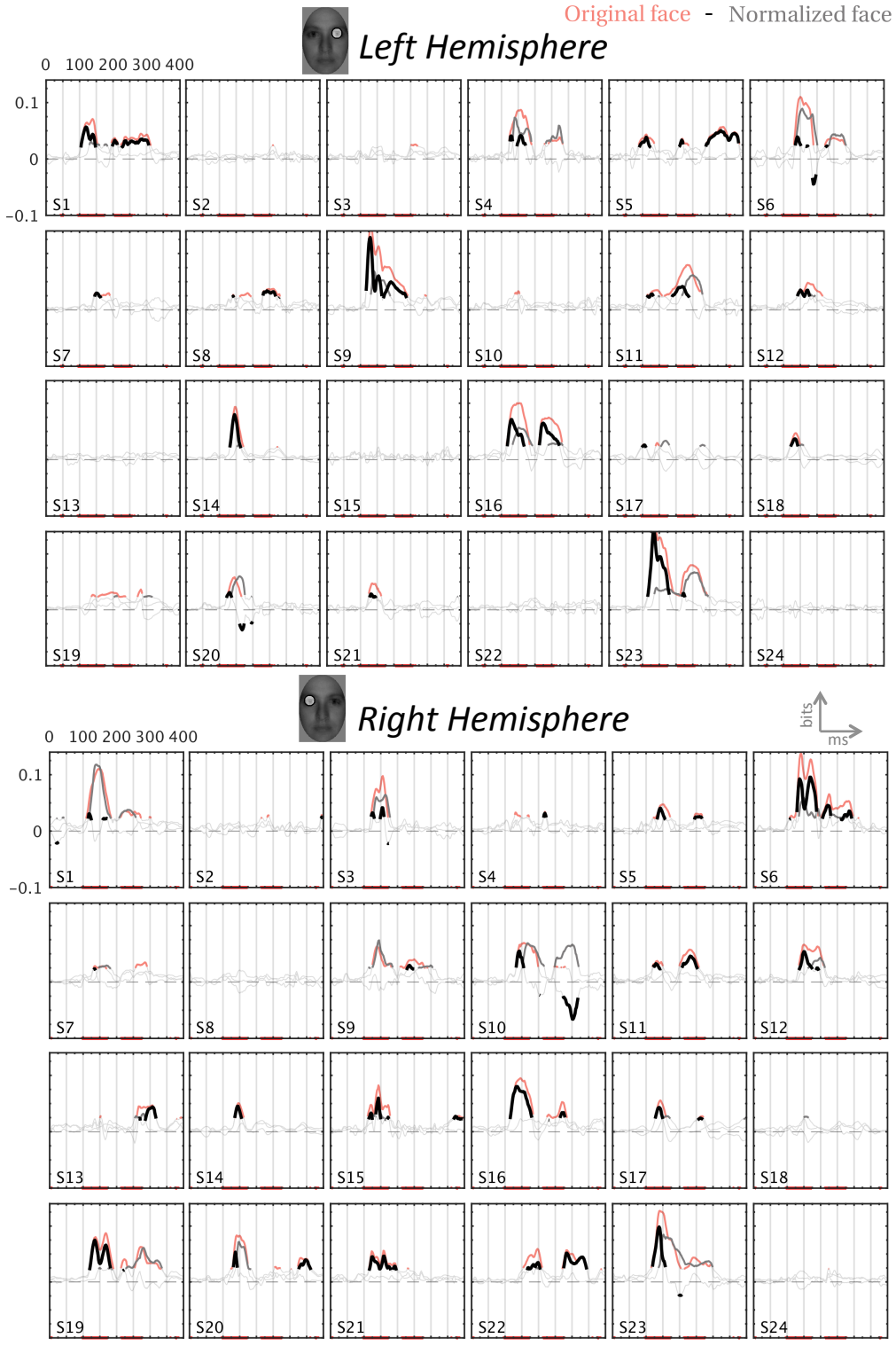

Figure S4.5. Significant differences of MI(EYE, [ERP, ERP_g]) between ORI and NOR per participant. Coloured sections indicate statistical significances for corresponding face condition. Thick black sections indicate statistically significant differences.

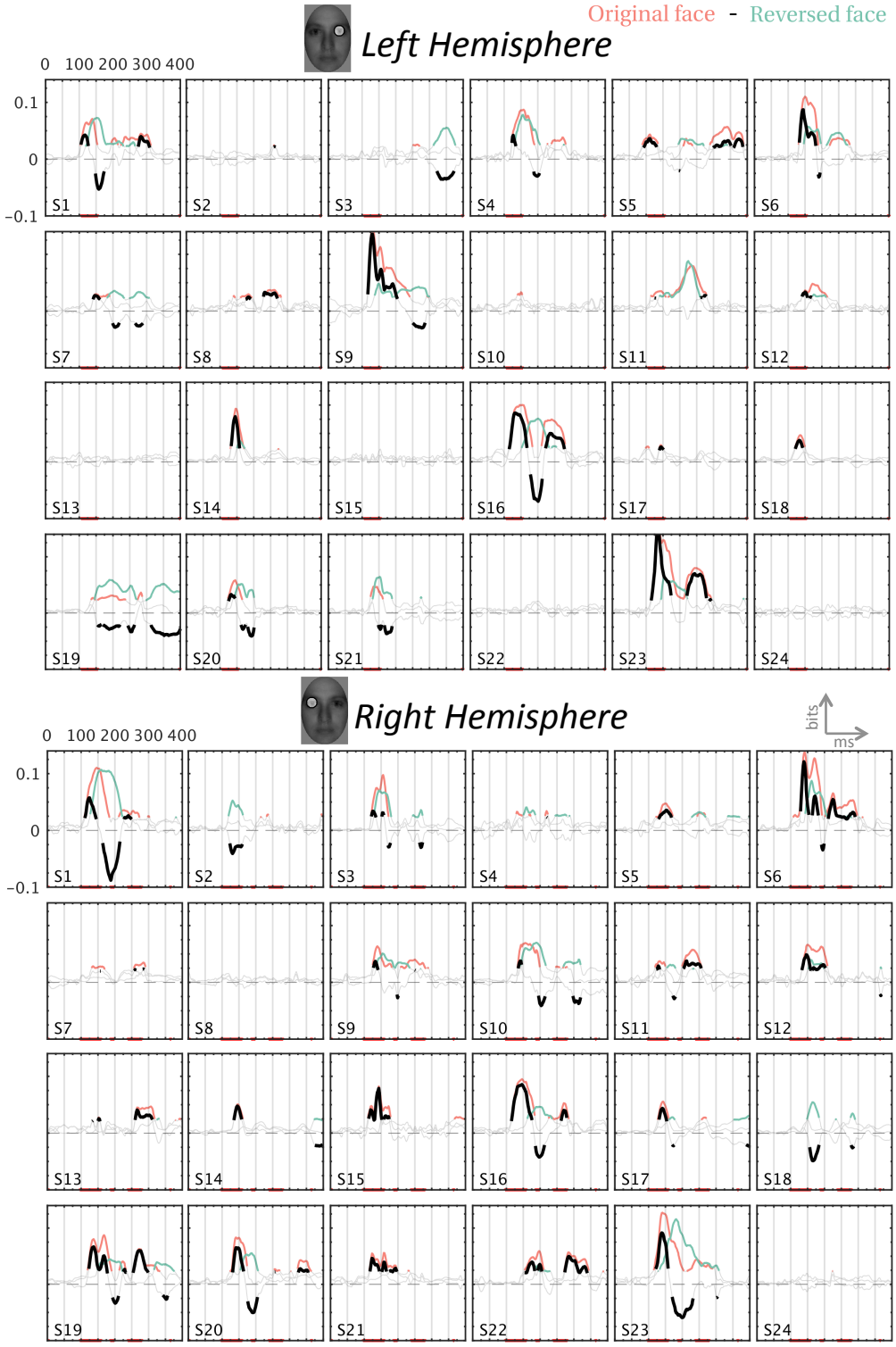

Figure S4.6. Significant differences of MI(EYE, [ERP, ERP_g]) between ORI and REV per participant.

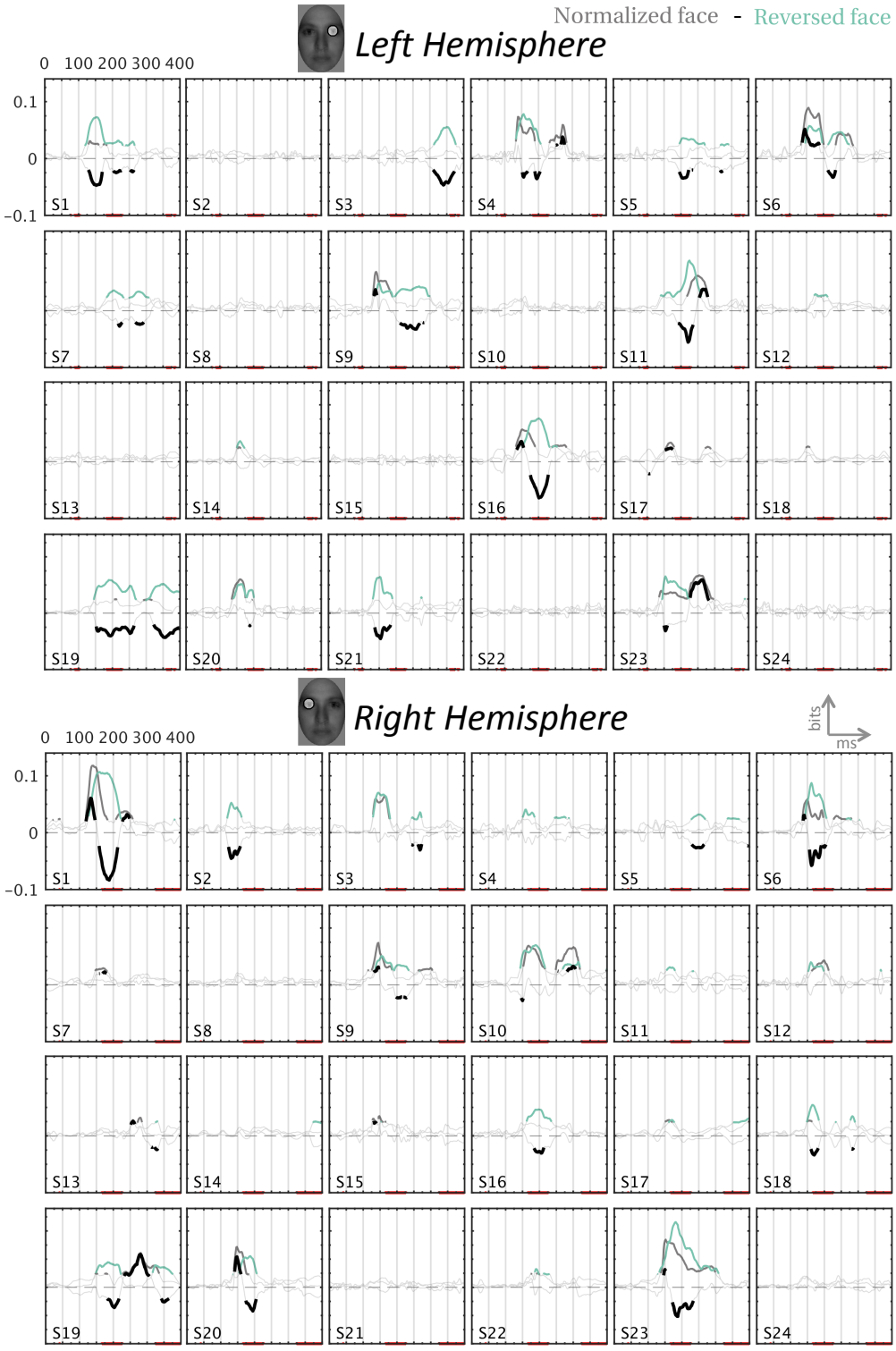

Figure S4.7. Significant differences of MI(EYE, [ERP, ERP_g]) between NOR and REV per participant.

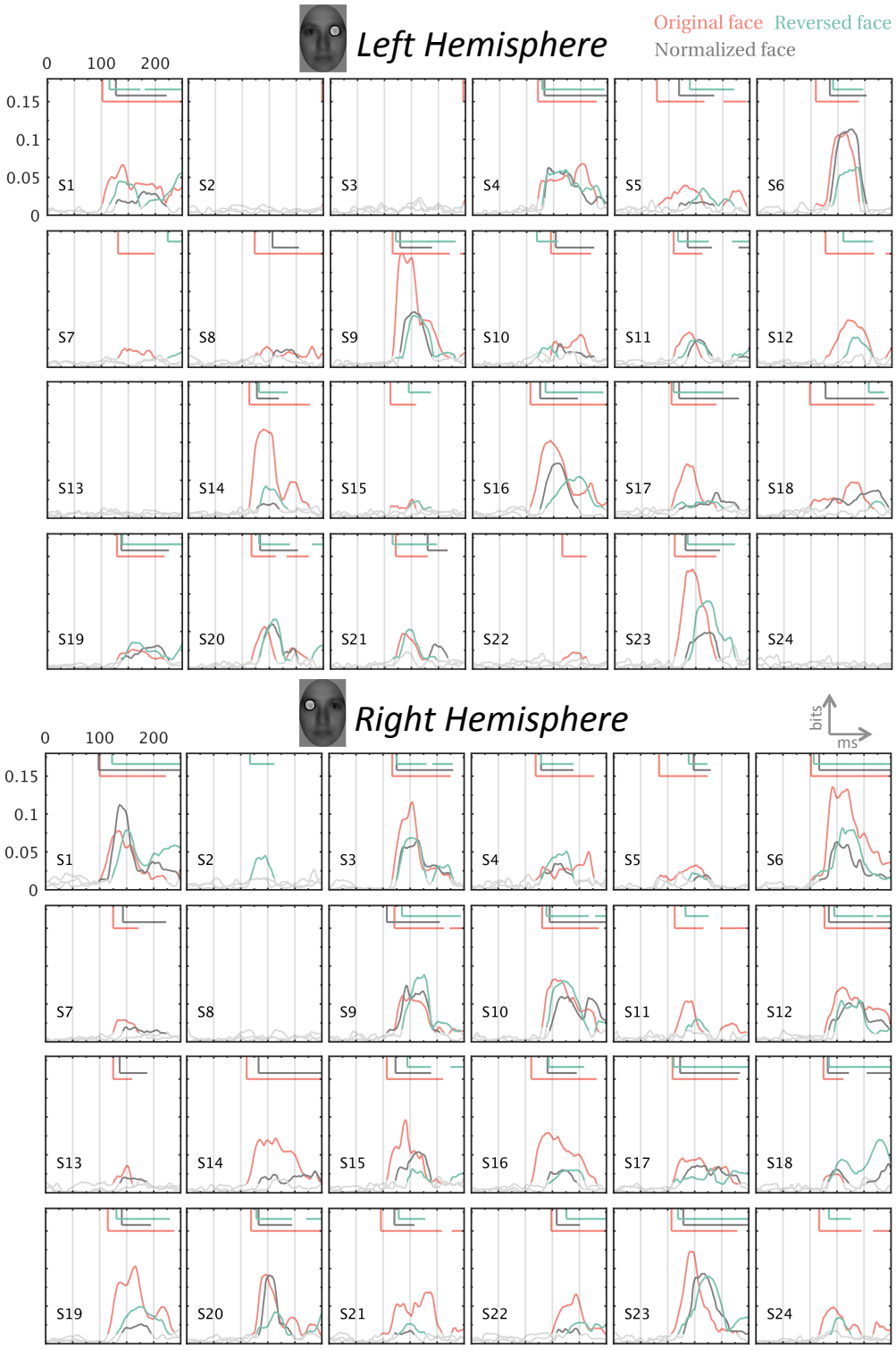

Figure S4.8. MI(EYE, [ERP, ERP$_g$]) onset per participant based on causal dataset. The curves show the maximum MI across electrodes per hemisphere. Coloured horizontal lines and coloured sections of curves mark significant effects for each face condition. The vertical lines mark the onset of these effects.

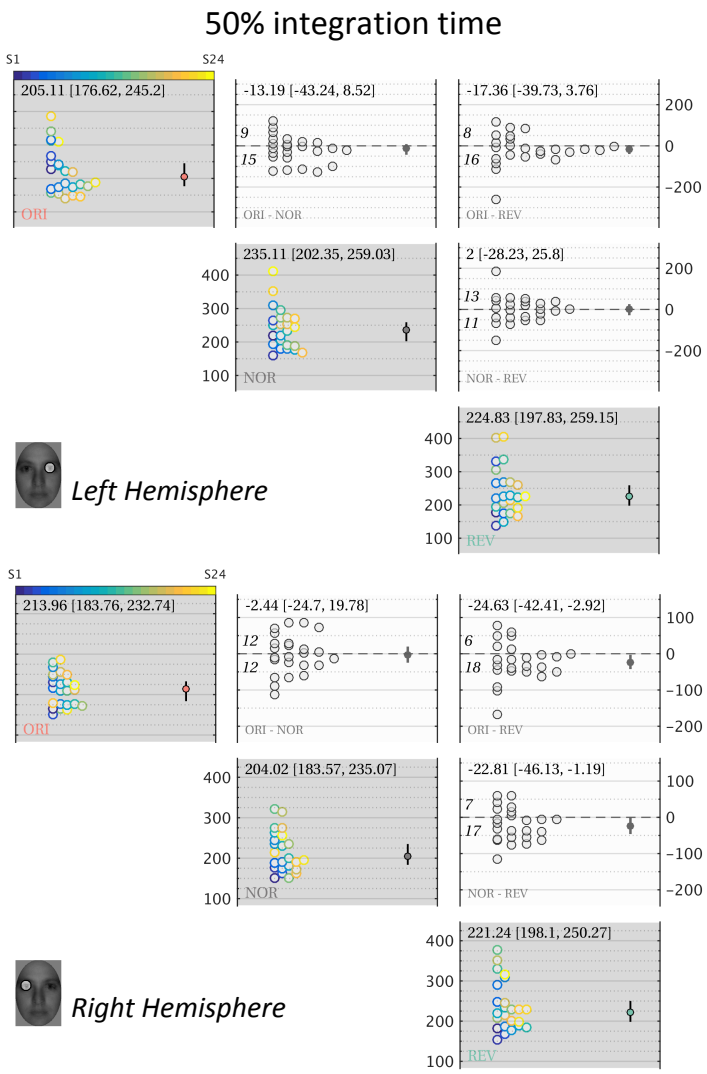

Figure S4.9. Face contrast-related effect on 50IT (in ms). Same panel structure as Figure S1. In the left hemisphere there are no differences between any pair of face conditions. In the right hemisphere pairwise comparison results show a significantly slower processing speed of contralateral eye sensitivity on REV compared with ORI and NOR, and there are no differences between ORI and NOR faces.